# Developing a Method for Digital Twin-Based Geometry Assurance of Sheet Metal Assemblies

Master's Thesis in Product Development

ISAC PALM
DANIEL STRÖBY

DEPARTMENT OF INDUSTRIAL AND MATERIALS SCIENCE
CHALMERS UNIVERSITY OF TECHNOLOGY
Gothenburg, Sweden 2026
www.chalmers.se

MASTER'S THESIS 2026

# Developing a Method for Digital Twin-Based Geometry Assurance of Sheet Metal Assemblies

ISAC PALM
DANIEL STRÖBY

CHALMERS
UNIVERSITY OF TECHNOLOGY

DEPARTMENT OF INDUSTRIAL AND MATERIALS SCIENCE
*Division of Product Development*
Geometry Assurance & Robust Design
CHALMERS UNIVERSITY OF TECHNOLOGY
Gothenburg, Sweden 2026

Developing a Method for Digital Twin-Based Geometry Assurance of Sheet Metal Assemblies
ISAC PALM
DANIEL STRÖBY



Examiner: Prof. Rikard Söderberg, Chalmers University of Technology, Department of Industrial and Materials Science
Supervisor: Dr. Roham Sadeghi Tabar, Chalmers University of Technology, Department of Industrial and Materials Science
Industry Supervisor: Dr. Frank Litwa, Mercedes-Benz AG, Tolerance Management BiW & Exterior

Master's Thesis 2026
Department of Industrial and Materials Science
Division of Product Development
Geometry Assurance & Robust Design
Chalmers University of Technology
SE-412 96 Gothenburg
Telephone +46 31 772 1000

Cover: Mercedes-Benz E-class estate wagon, copyright Mercedes-Benz AG 2024 [1].

Printed by Chalmers Reproservice
Gothenburg, Sweden 2026

Developing a Method for Digital Twin-Based Geometry Assurance of Sheet Metal Assemblies
ISAC PALM
DANIEL STRÖBY
Department of Industrial and Materials Science
Chalmers University of Technology

# Abstract

This thesis investigates how a digital twin-based geometry assurance workflow can be developed for compliant sheet metal assemblies. Current industrial workflows are limited by fragmented data, insufficient traceability between physical and virtual processes, and process adjustments that are not consistently stored or reused in simulation models.

The study was conducted in collaboration with Mercedes-Benz AG and combined an exploratory case study, data mapping, compliant variation simulation, sensitivity analyses, machine-learning-based calibration, and a case-based evaluation of the proposed workflow. A rear roof frame assembly was used to identify the information required for non-rigid simulation and to investigate the influence of process parameters.

The study identified data breaks related particularly to shimming and welding sequence. The investigated assembly showed a shimming sensitivity of 80.07% and a welding-sequence sensitivity of 31.58% for the scan-based model. A quantile-based regression model was selected for simulation-to-measurement calibration because the available simulation and measurement datasets lacked one-to-one case traceability. The model improved the agreement between distributions by an average of 90.22% and reduced the RMSE of the evaluated scanned case by 29.66%. Applying shimming optimization reproduced a deformation pattern similar to that observed in the physical assembly, although differences in magnitude remained.

The results indicate that the proposed workflow can provide a foundation for digital twin-based geometry assurance. However, stronger evaluation and case-specific prediction require additional traceable physical cases, recorded process parameters, and reusable data formats.

Keywords: Digital Twin, Geometry Assurance, Compliant Variation Simulation, Sheet Metal Assembly, Machine Learning, Shimming, Weld Sequence

# Acknowledgements

We would like to express gratitude to all including parties who has supported and contributed to this master's thesis.

First, we would like to thank our academic supervisor, Dr. Roham Sadeghi Tabar, for his guidance, feedback, and support throughout the project. Without his support this would not have been possible. We would also like to thank our examiner, Prof. Rikard Söderberg, for his input and feedback throughout the thesis.

We would also like to thank our industrial supervisors Dr. Frank Litwa and Alina Sachsenweger, and Mercedes-Benz AG for giving us the opportunity to conduct this thesis in an industrial context. The access to data, tools, and process acknowledgment has been invaluable for the thesis and for understanding the practical challenges related to digital twin-based geometry assurance within the automotive industry. Furthermore, they made the process of integrating into the workspace of Mercedes-Benz a pleasant experience and made us feel welcomed. Which was truly appreciated.

Finally, we would like to thank the engineers and employees at Mercedes-Benz who have supported us with technical discussions and support with technical aspects of the thesis.

Isac Palm & Daniel Ströby, Gothenburg, June 23, 2026

# Disclosure of AI Use

AI tools were utilized to assist with the writing process, specifically for spelling and grammatical improvement. Furthermore, AI was used to generate and troubleshoot code for data formatting and the plotting of results. However, all ideas, analyses, and conclusions presented in the thesis are original. AI was not used to generate concepts or scientific content. The authors have reviewed AI-assisted materials and take responsibility for the final content of this thesis.

# List of Acronyms

Below is the list of acronyms that have been used throughout this thesis listed in alphabetical order:

| | |
|---|---|
| AI | Artificial Intelligence |
| BiW | Body-in-White |
| CAD | Computer-Aided Design |
| CAE | Computer-Aided Engineering |
| CAT | Computer-Aided Tolerancing |
| Cp | Process Capability |
| Cpk | Process Capability Index |
| DOF | Degrees of Freedom |
| DT | Digital Twin |
| FE | Finite Element |
| FEA | Finite Element Analysis |
| FEM | Finite Element Method |
| GD&T | Geometric Dimensioning and Tolerancing |
| GEO | Geometry Station |
| HLM | High-Low-Median |
| KPC | Key Product Characteristic |
| MAE | Mean Absolute Error |
| MBD | Model-Based Definition |
| MC | Monte Carlo |
| MCS | Monte Carlo Simulation |
| MDS | Mercedes-Benz Development System |
| MIC | Method of Influence Coefficients |
| ML | Machine Learning |
| PCA | Principal Component Analysis |
| PCFR | Place-Clamp-Fasten-Release |
| PDM | Product Data Management |
| PLM | Product Lifecycle Management |
| PMI | Product Manufacturing Information |
| QIF | Quality Information Framework |
| RCA | Root Cause Analysis |
| RE | Re-spot Station |
| RMS | Root Mean Square |

| | |
|---|---|
| RMSE | Root Mean Square Error |
| RSS | Root-Sum-Square |
| SST | Single Source of Truth |
| STL | Standard Tessellation Language |
| SVM | Support Vector Machine |
| XML | Extensible Markup Language |

# Contents

# List of Figures

# List of Tables

# 1
# Introduction

This chapter introduces the concept of geometry assurance and a digital twin-based geometry assurance. It outlines the background and context of the thesis, defines the problem description and purpose, the research questions, the scope and limitations, and the ethical and sustainable considerations of the thesis.

## 1.1 Background

When parts or components are created, no matter which manufacturing technique, some amount of geometric variation will occur [2]. Geometric variation can also occur during the assembly processes, this variation can source from different things, such as the earlier mentioned manufacturing, assembly sequence, and location of fixtures [3]. This geometric variation can cause trouble in the stages of assembly and afterwards where parts might not fit together, they can lose their function or the appearance of the product might be affected. Removing geometric variation completely is not possible and would be an expensive task, hence tolerances are applied to regulate the amount of geometric variation that is allowed. However, the tighter the tolerances, the more expensive the manufacturing and assembly process becomes. At this stage, the usual process is to perform a trade-off calculation, to see what level of tolerance is required in order to achieve the set "*performance*" or "*goal*". However, the Geometric Dimensioning and Tolerancing (GD&T) process can be used from the early concept stages, all the way to the late serial production stage, either to evaluate or compare different assembly concepts.

Today, cars are complex and contain a large amount of different components that needs to fit together, all affected by geometric variation in some way. This can cause tolerance chains which can escalate and cause detrimental effects at later stages.

Digital tools are used to simulate the geometric variation and tolerance chains in complex assemblies [4]. These tools are called Computer-Aided Tolerancing (CAT) software, e.g. 3DCS and RD&T. These software take the aforementioned variations and tolerances into account and most commonly performs a stochastic simulation, called Monte-Carlo (MC). Running several iterations of an assembly with random values distributed along a standard deviation curve, based on set tolerance ranges. These simulations can then be coupled to external software to perform FE analyses with non-rigid bodies, or in some cases use an internal FE-solver, for example RD&T's internal FE solver.

The data needed to run the simulations can be collected directly from measurement points and fed back through a bi-directional data flow to a digital representation of the physical assembly process, a so called Digital Twin (DT) [5]. If this simulation data is then fed back into the physical process with the same bi-directional data flow, the concept of a DT is fulfilled. This makes it possible for the physical process to compensate for errors found in the simulations in and iteratively improve the process.

### 1.1.1 Context

Sheet metal assemblies in the automotive industry, especially Body-in-White (BiW) are inherently compliant, which means that the sheet metal will deform during assembly. This deformation occurs due to clamping forces [4], welding sequence [6], welding heat [7], gravity and spring-back effects [8]. Because of this, the geometric variations becomes complex and require non-rigid (compliant) simulations based on finite element methods (FEM). The compliant simulation are time consuming and complex rather than rigid assembly simulations.

Currently, to setup a non-rigid assembly model in a CAT tool is largely manual and time consuming. In order to set up a non-rigid model, locating schemes, joining conditions, contact interactions, and simulation parameters are needed. Information about these parameters is often scattered across different data-sets, data-bases or standards/guides.

The data that is scattered is needed, both from the physical system processes, but also from the virtual simulations. When this data is then gathered, it can be used to optimize the assembly in real time with a bi-directional loop, as a DT.

Assembly parameters are adjusted by trial and error in the physical assembly cell. The variation simulation model is often setup through gathering all the relevant data, i.e., geometries, specifications and tolerances, which can be tedious. However, research shows that the use of machine learning (ML) shows potential in improving the prediction of the outcomes [9]. But, ML integration into industrial geometry assurance workflows is limited

The ML limitation is relevant at Mercedes-Benz, since it is a world leading automotive manufacturer both in quality, performance, and standard. Mastering the geometric variation with the help of tolerance management is key. The tolerance analysis workflow at Mercedes-Benz is tedious with data points scattered, which makes it inefficient. Setting the foundation of the companies problem statement, which creates an opportunity of developing a new method for a digital-twin based geometry assurance of sheet metal assemblies.

## 1.2 Problem Description

Advanced CAT and computer aided engineering (CAE) tools are available. However, the current geometry assurance process for compliant sheet metal assemblies remains inefficient due to the fragmentation of data and information systems. While the tools themselves are capable, the virtual simulations can fail to reflect physical reality because they are disconnected from the physical process.

To achieve accurate simulations, specific data is required, data such as tolerances, measurement points, welding sequences, locating schemes, and physical process adjustments. Currently, this data is distributed across different product data management (PDM) systems, documents, files, and tacit knowledge from the operators of the physical process. Most prominent, physical optimizations like shimming are conducted without information storage or information relay.

While the data is generated by both the physical process and the digital representation, the way it is stored and integrated creates "data breaks". Without a system to trace physical adjustments and feed them back into the digital representation, the process remains inaccurate. This creates a clear gap for a digital twin-based geometry assurance of sheet metal assemblies method.

## 1.3 Purpose

The purpose of the project, is to develop a method for geometry assurance of sheet metal assemblies in a DT. The method should allow for fast and accurate assembly simulations and be integrated into industrial scaled product development. Furthermore, it should be able to be coupled with a Machine Learning (ML) model, to optimize the prediction of the outcomes.

## 1.4 Research Questions

To address the aim of the thesis, four research questions were formulated. These questions define the main areas of investigation and provide the structure for the analysis conducted throughout the study.

- Research question 1
  - What tools and data are needed for a sheet metal geometry assurance assembly simulation?
- Research question 2
  - How can simulation, measure and process data be integrated into different product development phases?
- Research question 3
  - What verification and evaluation processes are required to ensure that the simulation outcome is relevant and sufficient?
- Research question 4
  - How can the simulation accuracy be improved with the help of ML approaches?

## 1.5 Scope and Limitations

The thesis focus is to develop a method for a digital twin-based geometry assurance of compliant sheet metal assemblies, in collaboration with Mercedes-Benz AG. The thesis is limited to BiW, due to the assemblies in BiW are of non-rigid behavior and its influence is significant. Additionally, the industry supervisor is well integrated into the BiW process, which makes it more accessible. The method will be limited to the CAT software RD&T, due to licensing. Furthermore, the scope includes the automation of a compliant model setup or partially automated and optimizing the outcome by using ML-based calibration models trained using available historical simulation and measurement data. Evaluation is performed through a single case study of a rear roof frame assembly, and the method is designed to be generalizable, but it is not fully verifiable since it is tested on a single case. The results are constrained by available data, the limited time frame of the study during the spring of 2026 and the resources supplied by Chalmers University of Technology and Mercedes-Benz AG. If the thesis is to be published and results shown, then it is limited to non-classified data, screened material, and released parts.

## 1.6 Ethical and Sustainable Considerations

The master's thesis is conducted at Chalmers University of Technology at the department of industrial and materials science in collaboration with Mercedes-Benz AG. This means that it involves the use of industrial data and methodologies related to the Tolerancing Management division of Mercedes-Benz R&D branch. This leads to that ethical aspects must be considered.

Data confidentiality and intellectual property is important in every industry. The data used in this project, including CAD models, measurement data and simulation setups can contain sensitive information. Therefore, all data and content that will be included in the thesis and published has to be in accordance with company guidelines. Meaning that the thesis will have to be approved by Mercedes-Benz AG before publishing.

The thesis contributes to sustainability primarily through improvements in product development efficiency and manufacturing quality. If a fully working digital twin-based system is established, with a machine learning feature that can use old and current that to predict future outcomes, then the need to prototype and produce concepts in the same extent lessens. Leading to a lower material consumption and reduced waste during the product development process.

The thesis can further contribute to sustainability through sustainable product development practices. By increasing the decision making power in the early stages of the product life cycle. Together with the possibility to identify and solve geometry problems earlier in the development process, it reduces the costly and resource heavy changes in the later stages.

# 2
# Theory

This chapter outlines the theory, research, and the current state of the art related to the topic. It is divided into five different sections to establish a stable ground of knowledge to answer the research questions stated in 1.4. The areas of interest is: product life cycle, geometry assurance, assembly process applied in automotive industries, DTs, and ML methods. They are presented below in the same order.

## 2.1 Product Life Cycle

The product life cycle refers to the total lifespan of a product, beginning with the initial perception of a market opportunity and extending through development, manufacturing, use, and finally disposal or recycling [10]. This section covers the development phase of the products life cycle, since it is the most relevant with regards to the scope of the thesis.

### 2.1.1 The Product Development Process

A product development process can be described as the sequence of steps and activities that a company use to conceive, design, and commercialize a product. The type of product development process differs depending on the company, where some have a strict plan that they follow and others aren't able to describe their plan. However, the generic product development process according to Ulrich et al. [11], includes six phases. The general six phases are illustrated in Figure 2.1. The phases according to this model is: planning, concept development, system-level design, detail design, testing, and mass production.

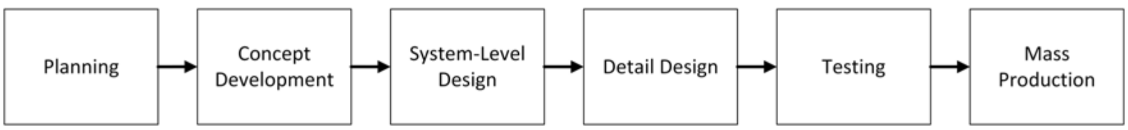


**Figure 2.1:** Generic product development process, reconstructed from [11].

The planning phase is the first phase that initiates the project approval and the actual start of the product development process. This step mainly includes opportunity identification. This is done through assessment of technology development and market objectives, and outputs the mission statement for the project. The concept development phase is where the concept starts to form. This step includes identification of market needs, concept generation, and evaluation. In the system-level design phase the product architecture is defined, the product is divided into subsystems and components, a first design of the preliminary components are set and the allocation of detail design responsibility is set. In the detail design phase the complete specification of the geometry, materials, and tolerances of all parts, is conducted. In the specification the intended tooling, supply chain, and assembly for each component is also specified. Furthermore, the material selection, production cost, and robust performance is finalized during this phase. The testing and refinements phase is where early prototypes are made and evaluated by testing. This phase identifies if the design will work or not. If not, refinements can be done. Lastly in the production ramp-up phase the product is produced with its intended components. This step is done to ensure the production capability by identifying the potential issues in the production line. The products produced in this phase can also be handed out to trusted customers for final evaluations.

#### 2.1.1.1 Example of Mercedes-Benz Product Development Processes

As aforementioned, the product development process differs depending on factors such as company or sector. Mercedes-Benz is an example of a world leading automotive company, that uses a strict product development process to realize high quality products with a high number of functions. The process can be described as a master plan [12], which is a detailed plan that consists of the development time frame and its quality gates. The quality gates serve as checkpoints to control the quality of the product during the process. A hypothetical example of a master plan is illustrated in Figure 2.2

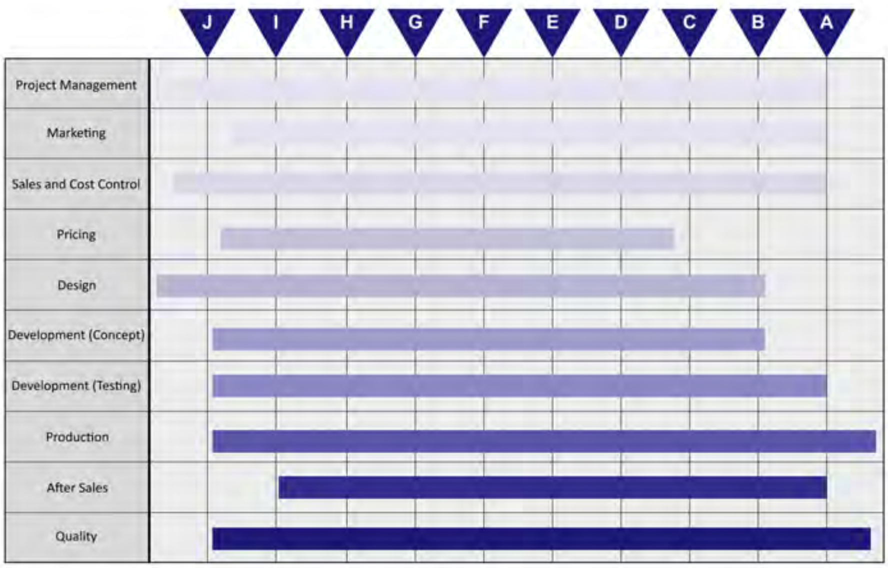


**Figure 2.2:** Mercedes-Benz master plan, reconstructed from[13].

This is a part of Mercedes-Benz Development System (MDS). As the process goes through the quality gates, the involved departments synchronizes and evaluates the status according to defined standards. This leads to an assessment of the maturity level and project process. In between each quality gates are individual milestones for the different departments in order to meet the intended standards for each gate. The quality gates are illustrated in figure 2.2, at the top of the timeline, ranging from A to J.

A brief description of every quality gate is presented below to describe where in the development process deliverables takes place, and the maturity level of the product. The information provided is based on Mercedes-Benz's internal product development quality gates [13][12]. However, the names are changed due to confidentiality.

During the first phase (definition phase), two quality gates occur. Quality gate J and I. Quality gate J will include requirement definitions of the vehicle (brand values, desired innovations, module strategy for the vehicle) with initial design proposals [13].

The definition phase ends with quality gate I which is concluded with a concept booklet. After this the different departments carry out the respective target elements and through several iterations, initial dimensional concepts are available in CAD.

For quality gate H, the concept booklet has evolved into a vehicle specification sheet which is presented during this gate. From here, a 1:1 model of the vehicle is created to determine interior and exterior design which results in the joint and radius plan where the joints, radius and offset dimensions are defined.

For the quality gate G an initial mathematical validation of the digital prototype test (DPT-V) is done to pass. This validation focuses on vehicle structure, powertrain and chassis. The output will be a mathematically precise surface description (Strak data) for the first test vehicle (E-vehicle) and the start of the pre-development phase.

In the quality gate F the final vehicle specifications are approved and the design freezes for exterior and interior. This wraps up the pre-development phase and starts the series development phase.

To get the product approved for quality gate E, the Strak data is revised and optimized.

Up to quality gate D, a complete constructed phase 1 E-vehicle must be done. This is to be able to get information about test drives and crash tests into the series design. Further, the first evaluations of the digital confirmation vehicle (B-vehicle) is done.

The construction of phase 2 E-vehicle then marks the beginning of the pre-series phase and to quality gate C, these vehicles contains series-production components. These components makes it possible to optimize the production tools and involved components.

In quality gate B, all the requirements in the vehicle specifications, undergoes a reconfirmation with the B-vehicle and a final optimization of the series-production parts is done.

Quality gate A is the last gate and for the product to go through this gate, all involved departments must approve the product.

### 2.1.2 Product Life Cycle Management

Product Life cycle Management (PLM) provides a framework for managing product related information across the entire product life cycle, from early development to later downstream phases. Product information in a PLM context includes both structured data and electronic documents, which need to be integrated in order to create a coherent and usable information environment [10]. Within this broader context, product information is organized through information models that define the relevant entities, relationships, and structures needed to represent the product consistently [14]. This makes PLM not only a matter of storing files or data, but also to ensure accessibility, traceability, and continuity of product information across functions and lifecycle stages. Against this background, it becomes relevant to focus on the specific engineering information that defines and communicates the product in practice. The following section therefore introduces product manufacturing information (PMI) as a more specific part of product-related information within a PLM context.

#### 2.1.2.1 Product Manufacturing Information

PMI refers to the manufacturing related information describing a geometry. It includes essential specifications such as dimensions, GD&T, datum definitions, surface finishes, material requirements, and other annotations necessary to manufacture and inspect a part [15]. Within a model-based definition (MBD) framework, the 3D CAD model serves as the single "authority model", where PMI is linked to the geometric features instead of being communicated solely through traditional 2D drawings [16].

The main purpose of PMI is to create a clear link between the design phase and downstream activities [16], such as manufacturing, simulation, assembly, and inspection. By storing tolerances and other engineering requirements directly in the CAD model, the product definition becomes more consistent and easier to reuse throughout the product life cycle [15]. This improves communication of design, reduces documentation, and supports a more continuous digital thread between different engineering functions. Furthermore, it eliminates the time-consuming and error-prone manual copying of specifications from drawings to manufacturing and inspection machine controls [17].

#### 2.1.2.2 Data Exchange Standards for Product and Quality Information

To maintain the information flow without manual intervention or data loss, neutral industry standards are required to ensure interoperability between software systems. In the context of geometry assurance and carrying model-based product information, there are three primary standards. STEP (standard for the exchange of product model data) AP242, JT (jupiter tesselation), QIF (quality information framework).

STEP AP242 (ISO 10303-242) is extensively established in modern CAD systems and supports the MBD of PMI, including dimensional and geometrical tolerance data [18]. STEP AP242 is also capable of carrying complex engineering information such as simulation data for kinematic analysis and composite design specifications, including stacking sequences and ply orientations [18]. According to Roth et al. [16], the exchange of specification information through STEP AP242 is mainly sufficient to automate variation simulation for tolerance analysis and synthesis during the design phase. Thus, STEP AP242 is an enabler for communicating the "as-designed" product definition in a computer interpretable form. [16].

JT, standardized as ISO 14306:2017, is an information rich format that compromises both geometry representation and the storage of PMI [18]. In the context of geometry assurance, JT is not used as much as the STEP AP242 when it comes to direct input or first feed knowledge bases for subsequent activities [16]. For example, JT is a common way to transfer geometric dimensioning and tolerancing (GD&T) information from CAD to downstream tools, such as Siemens Teamcenter [16].

In contrast to STEP and JT, QIF (ISO 23952:2020) has its roots primarily in the measurement and quality assurance domain [16]. QIF is an XML-based framework composed of several schema definitions that are both human-readable and machine-interpretable [16]. Its unique strength lies in its ability to combine both "as-designed" specifications and "as-inspected" measurement results within a single information container [16]. Using a decoupled normalized relationship model, QIF employs unique identification designators (ids) to create associative relationships between objects, such as linking verification data back to specific nominal features. This capability makes QIF an enabler for closing gaps in the digital thread, allowing real manufacturing information to be fed directly into digital twins to optimize assembly processes in real-time [16].

## 2.2 Geometry Assurance

This subsection will introduce the concept of geometry assurance, what it is and why it is important for ensuring the quality and function of a product.

### 2.2.1 Geometric Variation

In manufacturing processes there will always be geometric variation. No product or component can be produced exactly the same, or exactly as the nominal geometry, every time. This is due to many different factors such as process limitations, material behavior, tooling imperfections, environmental influences, and measurement uncertainties. From this, all parts will deviate slightly from each other and the intended geometry. Though these geometric variations can be managed through tolerances which defines the acceptable range of variation in certain areas and features of the manufactured product. Thus, the tolerances allows for manufacturability of components but does not eliminate the variation, only allowing a certain degree of variation around the nominal values. When the term deviation is used it refers to the difference between the ideal and actual geometry for a single part, whereas variation describes the variability of the deviation, which happens when a part is manufactured several times in the same process [15].

#### 2.2.1.1 Variation Propagation in Assemblies

In an assembly, these geometric variations do not just increase linearly. They have a tendency to depend on each other and therefore lead to variation propagation [2]. It propagates through the locations, constraints and contacts between the included components. This means that the geometry variation problem cannot solely be observed from the perspective of a single component, but instead from a system level perspective where the components depend on each other.

#### 2.2.1.2 Impact of Geometric Variation

The geometric variations have different types of consequences on the product, such as functionality, perceived quality and economical [17]. From a functional perspective the geometric variation can lead to misalignment in the final product, causing performance issues. This could be closing- or position functionalities [19], where a misalignment of e.g. a door hinge can lead to problems when when closing the door [12]. This will also affect the perceived quality of the product which refers to the customers visual assessment of a products quality. In the automotive industry, this is often judged by the split lines [2] which refers to the gaps and flushness between body and panels. Hence, the same misalignment that can cause poor performance can also create inconsistent gaps and flushes which symbolizes low quality for the customer. From an economical point of view, the consequences can be costly if the geometric variations are not taken into considerations. Throughout the product development process, cost for changes to the product increases the further into the process [13]. With the inability to account for variation, problems might occur late into the process which demands for these costly changes. Though accounting for variation can also have economical consequences where tightening the tolerances will increase the cost exponentially [20], which is further detailed in 2.2.4.4.

### 2.2.2 Geometry Assurance - Framework and Life Cycle Perspective

Geometry assurance is defined as the set of activities performed to secure geometric quality [5]. Geometric variation in the final product are unavoidable because of the process variations in manufacturing, assembly and joining. To prevent these variations to cause negative impacts on the functionality, aesthetics and cost, they must be systematically managed throughout the process [17]. Geometry assurance act as a bridge between quality requirements and the physical production.

#### 2.2.2.1 Geometry Assurance Across the Product Life Cycle

The geometry assurance process is often divided into three different sections of the product development process. These sections are the concept phase, verification phase and production phase [2]. Together they can be described as a product realization loop as seen in Figure 2.3.

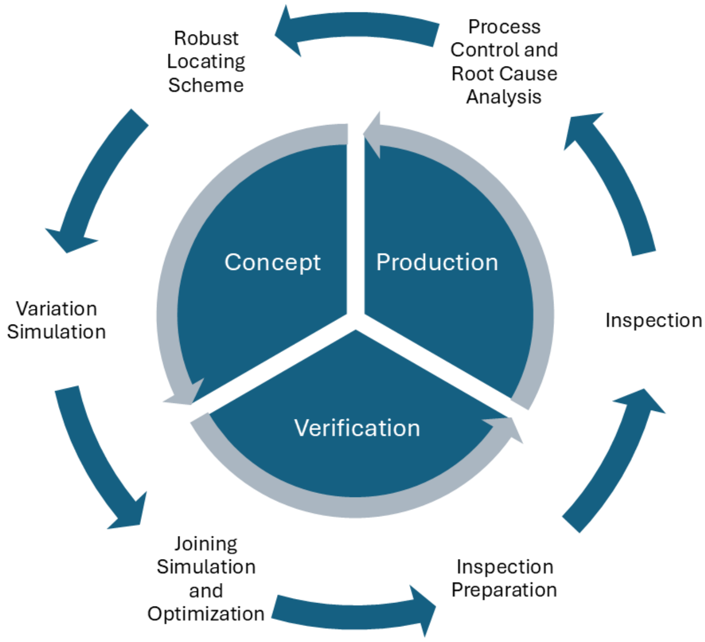


**Figure 2.3:** Product realization loop, reconstructed from [2].

During the concept phase the product and its production concept are developed by analyzing and optimizing them. The role of geometry assurance in this phase is the following tasks:

- Definition of split-lines
- Defining product tolerances
- Defining part tolerances
- Definition of locator positions

In the verification phase the focus is to test and verify the product and production system [2]. During this phase the following activities are usually carried out by the geometry assurance team:

- FEM-based variation simulation
- Inspection preparation
- Virtual trimming

In the production phase the product is in full production. The virtual assembly model together with the inspection data is used here to control production and detect and correct errors. The following tasks are done during this phase:

- Root Cause Analysis (RCA)
- Six Sigma

#### 2.2.2.2 Model-Based Variation Management

Due to the complexity of the geometry in modern products and assemblies, the help from digital tools are needed to perform geometry assurance analyses [4]. These tools are referred to as computer aided tolerancing (CAT) tools which are used to create virtual assembly models that can simulate how input tolerances and part deviations propagate into variation in the final assembly. The CAT programs work hand in hand with computer-aided design (CAD) tools. The CAD tools provides the CAT tools with the 3D models of the products geometry [15].

### 2.2.3 Sources of Variation and Locating Schemes in Assemblies

Geometric variation in final assemblies is a result of the stack-up of deviations originating from multiple stages of the manufacturing and assembly process. Managing these variations requires a deep understanding of their sources and the physical mechanisms through which they propagate, primarily defined by the locating schemes used to position parts in space.

#### 2.2.3.1 Sources of Geometric Variation

The variation that affects the final assembly can be categorized into three different segments: part variation, fixture variation, and joining tool variation [12].

**Part variation** describes the deviation of an individual component from its nominal model. Deviation that will occur during the design or manufacturing process of the component, such as machining, casting or metal forming [3], depending on the material properties and geometry.

**Fixture variation** is the variation that forms from the construction of the joining station and from each fixtures in the station.

**Joining tool variation** is the variation from joining tools, which comes from wrong joint parameters and tool wear.

#### 2.2.3.2 Rigid vs. Non-Rigid Assemblies

In geometry assurance there are mainly two different models to use for analyses. Rigid and non-rigid (compliant) models. A rigid model is where all the included components are assumed to maintain their ideal nominal shape. This means that the deformation of the component is disregarded [12]. This implies that the only deviation from a rigid model will be the displacement from the whole component. Thus, any deformation caused by outside forces like clamping, welding or bolting will be omitted.

A compliant model, do however, allow for deformation of the individual components. To be able to model a compliant part, Finite Element Analysis (FEA) is introduced. FEA uses the Finite Element Method (FEM) which is a numerical method used to solve complex mathematical models. Often used in engineering to investigate structural and thermal properties in assemblies or structures [21]. The method divides the "real" linear model into smaller parts (discretize) called elements which are connected with nodes. The elements together form a mesh which describes the whole part but as a linear simplified model. By applying material properties and boundary conditions a system of linear equations that describes the model's behavior, can be created. The general FEM equation can be seen in Equation 2.1 where F is the load vector and describes the applied loads. K is the stiffness matrix which includes element information, material properties and boundary conditions. Lastly, u is the unknown vector of nodal displacement [21].

$$F = Ku \tag{2.1}$$

By using FEA it is possible to approximately calculate non-linear problems as linear, making it far less computationally dependent.

#### 2.2.3.3 Degrees of Freedom and Locating Schemes

In geometry assurance it is important to define the position of the included components of the assembly. A body in space can move in six degrees of freedom (DOF), three rotational movements and three translational movements [19]. The movements occurs along or around axes, one rotation and translation per axis. To lock the body in space six contact points is needed, where three points coincides in the primary plane, two points in the secondary plane and one point in the tertiary plane. This creates a complete datum system [19]. The datum system is known as the 3-2-1 scheme and is used within GD&T. As an example of this, looking at Figure 2.4, points A1, A2 and A3 are used as the three points in the primary plane which constraints the body's translation in Z and its rotation in around X and Y. Points B1 and B2 are used as the points in the secondary plane and constrain the body's translation in X and rotation around Z. Point C1 is set in the tertiary plane and constrain the body's translation in Y, making the body completely constrained in all DOFs.

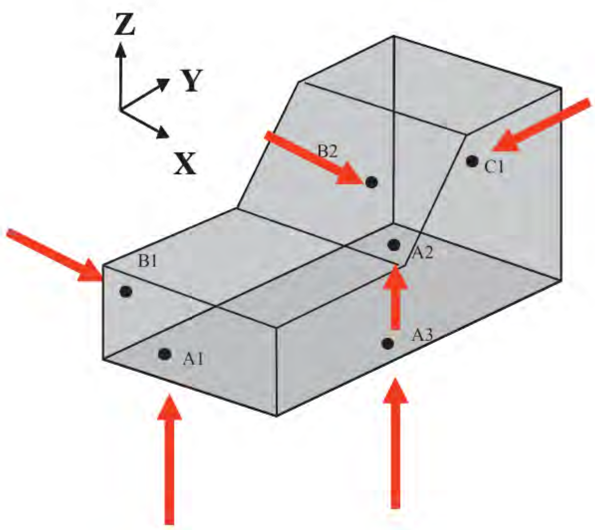


**Figure 2.4:** 3-2-1 locating scheme [2].

For compliant parts, such as sheet metal parts, the 3-2-1 locating scheme is often insufficient because it might not prevent the part from deforming due to gravity or process forces. Therefore, over constraining the body with additional support points is usually needed [2] to set the model to its nominal geometry.

In CAT tools the locating points of the locating scheme is referred to as datum targets illustrated in Figure 2.5 (b). Datum targets are used as references when describing tolerances. Furthermore, there is also datum features illustrated in Figure 2.5 (a), which references an entire geometric feature of a component, instead of a small part of the surface as for the datum target [22].

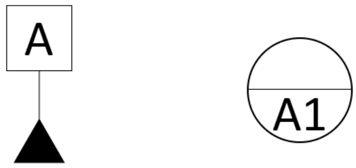


**(a)** Datum feature.

**(b)** Datum target.

**Figure 2.5:** Left; Datum feature. Right; Datum target.

#### 2.2.3.4 The Position-Clamp-Fasten-Release (PCFR) Concept

The assembly process for compliant parts is typically modeled through the PCFR (Position, Clamp, Fasten, Release) cycle [12]:

- Position: Parts are loaded onto the fixture and aligned on the locators.
- Clamp: Clamps are closed, forcing parts toward their nominal position and building up internal stresses.
- Fasten: Parts are joined (e.g., via welding or clinching), often inducing further deformation.
- Release: The assembly is released from the fixture, and spring-back occurs as internal stresses are redistributed.

### 2.2.4 Tolerance Management and Statistical Foundations

A tolerance can be defined as the permissible limit or limits of variation in a physical dimension or in a physical property of a material [23]. Meaning that tolerances define the permitted range of deviation for geometric features such as shape, dimension and position [23]. By complying with these functional dimensions, the intended technical and aesthetic functions of the assembly are ensured. Functionally appropriate tolerancing also ensures the interchangeability of components in mass production [23]. Without a consistent allocation of tolerances and reference points, the quality of a product cannot be accurately assessed or controlled during the product realization process [23].

**Table 2.1:** Reconstructed table based on [24], showing selected tolerances.

| Tolerance | Characteristic | Symbol |
|---|---|---|
| Form | | |
| | Profile of a line | ⌒ |
| | Profile of a surface | ⌓ |
| Orientation | | |
| | Profile of a line | ⌒ |
| | Profile of a surface | ⌓ |
| Location | | |
| | Position | ⌖ |
| | Profile of a line | ⌒ |
| | Profile of a surface | ⌓ |

**Form tolerance** controls the shape of a feature without considering its position or orientation in relation to another object or surface [24]. Profile of a line controls the shape of a feature in a single cross section, curve or edge [24]. Profile of a surface controls the shape of a surface, meaning that the surface variation must lie within the tolerance range [24].

**Orientation tolerance** controls how the feature is angled in relation to a datum target. Controlling the tilt, angle or alignment. Profile of a line describes how a profile line is angled in relation to a datum target. Profile of a surface describes the surface profile in relation to a datum target.

**Location tolerance** controls the exact position of a feature in relation to datum targets. Profile of a line describes how it should be positioned in relation to the datum targets. Profile of a surface describes how the surface should be positioned in relation to the datum targets.

#### 2.2.4.1 Geometric Dimensioning and Tolerancing

GD&T is a graphical language used to define the geometry of a part and to specify the permissible variation of its features, particularly with respect to size and position [25]. It provides a systematic way of describing the intended geometric relationships between features, defining their shape, and annotating their dimensions. In this sense, GD&T serves as a structured means of communicating design intent in a precise and clear way. This is important because the geometric relationships between part features must be clearly defined in order to support consistent interpretation throughout design and manufacturing. Thus, GD&T contributes to improving product quality by improving the communication [26] and clarity of technical specifications.

#### 2.2.4.2 Tolerancing Calculation Methods

To determine if an assembly will meet the requirements, there are different methods used which are based on the analysis of the tolerances. Mathematical methods to see how the tolerances stack up together.

**Analytical Worst-Case Tolerancing** is the first method where the most critical values of all the individual tolerances are observed. The maximum and minimum tolerance values. These are then summed together between all the involved components to calculate the worst case scenarios. The Worst-Case tolerancing method guarantees to a 100% that the requirements will be met if the tolerances are managed accordingly [19]. However, the risk of all the parts in a chain reaching their extreme values at the same time is very small. The method will at the same time lead to tight tolerances which increases the manufacturing cost and therefore not used as much [12]. It also requires the model to be of simple geometry. The equation for this is seen below in Equation 2.2.

$$T = \sum_{i=1}^{n} t_i \tag{2.2}$$

**Analytical Statistical Tolerancing** is another analytical tolerancing method which is based on the Root-Sum-Square (RSS) method. Instead of summing together the extremes, this method will assume that the part tolerances are normally distributed [19]. This leads to lower requirements for tolerances but won't guarantee 100% accuracy. It also requires the model to be of simple geometry. The equation for Statistical Tolerancing can be seen in Equation 2.3

$$T = \sqrt{\sum_{i=1}^{n} t_i^2} \tag{2.3}$$

**Numerical Statistical Tolerancing** are used for more complex 3-dimensional geometries using CAT tools. The calculations are most often based on Monte Carlo (MC) simulations. These simulations generates randomized values for each individual tolerance which is then iterated several thousands times. This will stack up the tolerances and derive a statistical distributions of the assembly outcome which can then be analyzed.

#### 2.2.4.3 Covariance Propagation and Sensitivity Coefficients

The relationship between input variation and output response is often described with sensitivity coefficients. The coefficient act as function that will tell if the input variation will be suppressed or amplified in the output. The calculation can be seen in Equation 2.4 below.

$$Y = Y_0 + \sum_{i=1}^{n} S_i X_i \tag{2.4}$$

#### 2.2.4.4 Top-Down Tolerance Allocation

Ideally the tolerance allocation should be performed top-down which means that product-level requirements are broken down into part tolerances. These tolerances are based on sensitivities and costs. This involves looking at the conflicts in the manufacturing costs where tighter tolerances lead to increased costs, and scrap/quality loss costs which decreases with tighter tolerances [12]. An optimal solution takes both these perspective into account.

### 2.2.5 Analytical Methods in Geometry Assurance

Analytical methods in geometry assurance are the mathematical and computational tools used to predict, analyze, and optimize the geometric quality of products. These methods allow for the evaluation of design concepts and production processes long before physical prototypes are built, significantly reducing the need for costly late-stage changes. By utilizing virtual assembly models, engineers can simulate how variations from parts, fixtures, and joining tools accumulate and propagate through the assembly.

#### 2.2.5.1 The Method of Influence Coefficients (MIC)

MIC is a method of building linear relationships between the part deviation, represented as the scanned geometries, and acting forces on the assembly. This method is used to replace the sensitivity matrix in the heavy computational FEM calculations, with a less computational heavy linearized matrix which will lead to a less computational heavy calculation when applied.

$$Ku = f_d + f_c + f_w \tag{2.5}$$

K is the global stiffness matrix, u is the displacement vector and f is the forces: d for clamping, c for contact, and w for welding [5].

#### 2.2.5.2 Variation Analysis

Variation analysis is used to predict the statistical distribution of the critical dimensional variation which is referred to as Key Product Characteristics (KPCs) [12] in the final assembly. The primary purpose of a variation analysis is to ensure the robustness of the assembly. This is to meet the functional and aesthetic requirements even when unavoidable variation in the manufacturing process happens. Depending on if the model is rigid or compliant the simulations will differ.

To model a variation simulation in a CAT tool, the first step is to have a geometry of the components and the assembly. This model can either be rigid or compliant. For the rigid model, all the components are assumed to keep their nominal shape and will therefore not be able to account for deformations inside the single parts. Thus, a CAD model of the parts and the assembly is solely needed. For a compliant model, these deformations are accounted for and a CAD model is not enough to run the simulations. Instead, FEA is introduced [2] as described earlier in 2.2.3.2. A compliant model will require more computational power and is therefore used in cases where it's needed, such as sheet metal assemblies.

Next, the locating scheme is defined as described in section 2.2.3.3. A rigid model is commonly positioned using a 3-2-1 locating scheme. For a compliant model, however, this scheme is often insufficient because the individual parts may deform under gravity and process forces. Additional support points are therefore introduced through an N-2-1 locating scheme, resulting in an over-constrained model [4].

Key Product Characteristics (KPCs) is then defined to evaluate the simulated assembly outcome. The KPCs represent geometrical features or dimensions that are critical to the function or quality of the assembly, such as gaps, flushness, or selected measurement-point deviations. The simulation results are evaluated at these locations to determine how input variation and assembly conditions affect the final geometrical quality. For compliant models, the PCFR sequence described in section 2.2.3.4 is also considered, since positioning, clamping, fastening, and release can deform the individual parts and influence the final assembly outcome [27].

To be able to determine the variation in the simulation, all the tolerances need to be applied to the model. These tolerances are delivered by a statistical distribution, most often normal distribution. If measured data from real manufactured parts are available, these can also be used as a distribution.

When it comes to executing the variation simulation, Monte Carlo simulation is the most commonly used method. As described in 2.2.4.2, MC generates random tolerance values for all the single parts and calculates the outcome of the final assembly. The process iterates thousands of times. For a rigid assembly, only the geometric and kinematic connections are calculated. For a compliant model the single part deformation is also included in each iteration.

The result of a variation simulation will most often consist of a histogram of all the iterations made and their variation compared to the nominal. The histograms are created for each measurement.

In the result there are different values that are crucial for a variation analysis. Optimization of the system will later be carried out based on the help from these key values.

**Mean** tells the mean value after all the iterations, for the inspected measurement.

**Mean shift** tells how much the calculated mean differs from the nominal value for the measure.

**Range** is the total range of values, from the minimal calculated value to the maximum.

**Standard deviation** ($\sigma$) is the parameter that describes the normal distribution [19]. There is also $6\sigma$ which translates to $\pm 3\sigma$. $99.99966\%$ of all the calculated cases end up in the range of $6\sigma$ [19], and it is developed to secure the geometric outcome of the produced assemblies without tight and costly tolerances [28].

**Process capability** ($C_p$) is used to measure how well a process performs between its upper and lower tolerance limits (USL and LSL) [20]. The value from this tells how much space the process natural distribution takes in comparison to the allowed tolerance space. The equation for $C_p$ can be seen below in Equation 2.6.

$$C_p = \frac{USL - LSL}{6\sigma} \tag{2.6}$$

The equation does not account for mean shifts, only for a perfectly centered graph. If the $C_p$ value is 1, it means that the process is within the $6\sigma$ limits to $100\%$ and takes up the whole tolerance space exactly [19]. If it exceeds 1, it's narrower than the $6\sigma$ space width. If it's below 1 the process distribution spreads outside the limits.

**Process capability index** ($C_{pk}$) is similar to the process capability. The difference is that $C_{pk}$ allows for mean shifts when calculating the process capability. How to calculate this can be seen below in Equation 2.7.

$$C_{pk} = min[\frac{USL - \mu}{3\sigma}, \frac{\mu - LSL}{3\sigma}] \tag{2.7}$$

The $C_{pk}$ values can be interpreted the same way as for $C_p$. For companies, the standard target value for $C_{pk}$ is 1.33 or above [19].

#### 2.2.5.3 Stability analysis

The core purpose of a stability analysis is to evaluate the locating scheme which relates to the geometric robustness [2]. In a stability simulation, a unit disturbance is often used and applied one at the time, on the fixed points of the model. It is not necessary to use the real tolerances in this case [29]. The result is often presented as a stability matrix or as a color map on the model itself [2] which is illustrated in Figure 2.6. The red areas represents a sensitive design where small deviations in the fixture points leads to big propagation. Whereas the blue areas represents a robust design. By changing the fixture points of the locating scheme, a more robust design can be achieved [2].

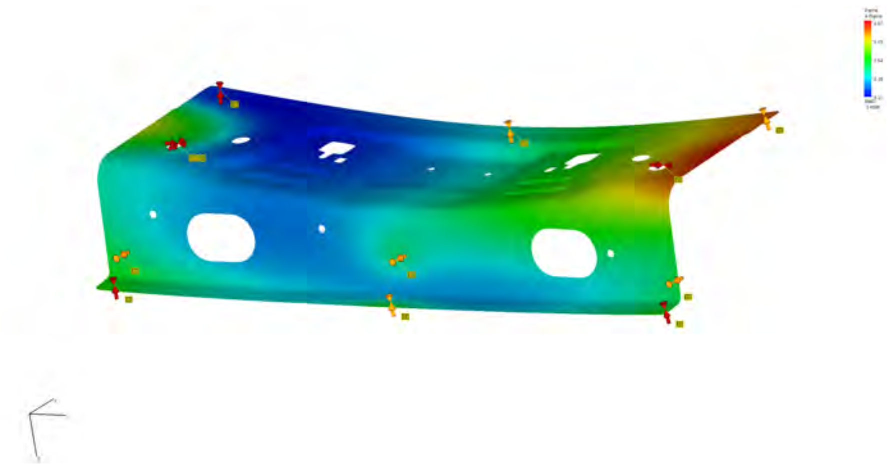

**Figure 2.6:** Stability analysis performed in RD&T.

#### 2.2.5.4 Contribution Analysis

Contribution analysis is another analytical method within geometry assurance that is used to identify and rank the different sources that contributes to the measured variations [29][30]. The purpose of the contribution analysis is to pin point the most critical tolerances to be able to either optimize these or trouble shoot in the production [29].

#### 2.2.5.5 Root Cause Analysis (RCA)

Root cause analysis (RCA) is a systematic process used to identify the cause of geometric variations, which lies outside the given tolerances [2]. "The aim of root cause analysis is to give diagnostic support for the effort to reduce dimensional variation in assembled products in the automotive and other industries." [31].

## 2.3 Assembly Processes Applied in Automotive Industries

In assembly variation an important contributor is tooling variation, which can be dissected into two sources: weld gun variation and fixture variation, (clamps and locators) [3].
Welding gun variation has a large impact on the final assembly variation [3], this variation can stem from for example, using two different spot welding robots during the same Place Clamp Fasten and Release (PCFR) operation. The variation can also depend on the type of weld gun used, the three most standard types are: position-controlled weld gun, equalized weld gun, and forced-controlled weld gun [3].

### 2.3.1 Body in White

Cars consists of a structural frame to keep its components in place. This frame is called the body-in-white (BiW). Depending on the car brand and model this BiW is made from sheet metal consisting of either steel, aluminum, or both.

### 2.3.2 Sheet Metal Assemblies

Sheet metal assemblies are considered compliant, which means that they experience deformation during external forces, forces which occur during joining processes [20]. These deformations creates a geometric variation.

The sheet metal assembly process of the BiW can be described with the PCFR method. The first one is the placement of the parts. Here the sheet metal parts that are included in the assembly are placed in a fixture that is rigid and stable which allows for repeatability and automation of the assembly process [20].

Next step is the clamping of the parts. In this step the involved parts are forced into their nominal position by the clamps, which also constraints the parts from moving in each direction. Due to the force from the clamps, bending and internal stress occurs for the involved parts.

Geometric deviation occurs from welding which is due to the exerted heat and forces during the operation [7]. The PCFR also creates geometric deviation since it is an external force, and also causes a spring-back mechanism [7].

When joining sheet metal parts into assemblies or subassemblies with spot-welding in the automotive industry, the spot-welding is categorized into two different categories: geometry stations (GEO-station) and re-spot stations (RE-station) [20]. The GEO-station is considered to perform the important spot-welds that has the most influence on the assembly, where the geometrical quality of the assembly is determined. After the GEO-station it moves on to RE-station where a larger number of welds are set to reinforce it [20].

### 2.3.3 Inspection

In the automotive industry, controlling the quality and outcome of parts is essential. It is usually performed with either tactile measuring systems or optical coordinate scanning systems [12]. There is a clear advantage using optical, such as more flexible measurement results, correction, and optimization of the component parts, assemblies, and final product [12].

When using optical measuring a detailed surface description of an object can be obtained, through scanning several million points in a single scan [12]. Where small circular stickers are placed on the surfaces as measuring points for the optical tool. With the help of the scan data, a 3D mesh can be created which can be used in simulations [12].

## 2.4 Digital Twins

A digital twin (DT) consists of three main components, a physical system or process, a virtual representation of the system, and a continuous information exchange between the systems that ties them together [32]. The physical system is the assembly station or process that is being modeled. The virtual representation is tied to a specific physical system or assembly step. It is updated to track exactly how the system behaves at certain points, and over time [32]. The information exchange is continuous, from sensors, measuring instruments, or inspections to update the virtual representation (physical to virtual) [32]. The outcome from the simulations in the virtual representations is then fed back to improve the physical system (virtual to physical) [32].

### 2.4.1 Digital Twins in Geometry Assurance

Within the area of geometry assurance and tolerance management, DTs are mainly used to control and minimize the geometrical variation which occurs during assembly processes [17]. In the modern automotive industry, DTs are used to update self compensating assembly lines, which means that the production is adjusted in real time to avoid variations outside the allowed limits [5] [17].

The real time adjustments can be performed with different methods. Part matching or selective assembly is the method within DTs that matches parts with variations that cancel each other out partly, which will reduce the total variation after assembly [16] [5]. Locator adjustments is when the DT calculates and optimizes the layout of the clamps, to minimize geometrical variation [5]. Last, joining sequence optimization is when the sequence of the clamps and welds are evaluated [5]. The DT calculates the effects of the clamping- and welding sequence and what effect it will have when the assembly is released (spring-back mechanics), and optimizes it and feeds the information back to the physical system [5].

## 2.5 Machine Learning Methods

Machine learning methods are relevant when data can be used to learn relationships between inputs and outputs. In this thesis, they are used to support simulation calibration and to connect the work to digital twin-based geometry assurance, where measured data and learning models can improve prediction and adjustment capabilities [33, 5].

### 2.5.1 Machine Learning and Regression Models

Machine learning is generally categorized into two main types: supervised and unsupervised learning [33]. In supervised learning, the goal is to predict an outcome based on a set of input features. In an unsupervised learning, the goal is to describe patterns or associations within data without a target [33]. Regression models are a part of supervised learning, often used when the target output is a quantitative measurement [33]. These models assume a relationship where the inputs have a measurable influence on the output [33].

### 2.5.2 Distribution-Based Calibration and Quantiles

Quantile mapping is a distribution-based correction method where quantiles of a simulated source distribution are mapped to corresponding quantiles of an observed target dis-

tribution. This makes it possible to compare and correct datasets based on distributional position rather than direct one-to-one sample correspondence [34].
Standard quantile mapping is usually applied to individual variables, while multivariate quantile mapping extends the method by correcting several variables simultaneously. Cannon describes this as a way to transfer properties of a multivariate target distribution to a multivariate source distribution [34].

### 2.5.3 Principal Component Analysis

Principal Component Analysis (PCA) is a widely used multivariate statistical technique for analyzing data tables where observations are described by multiple inter-correlated variables [35]. The primary objective of PCA is to extract the most important information, compress the size of the dataset and simplify its description by identifying underlying patterns [35]. PCA can do this by transforming the original variables into a new set of orthogonal variables called principal components [35].

The components are calculated so that the first principal components explains the largest possible variance in the data. Each component coming after is then calculated to explain the largest remaining variance, while remaining uncorrelated (orthogonal) to the previous principal component [35].

PCA has also been applied in sheet metal assembly research. Sadeghi Tabar et al. used PCA together with Support Vector Machine (SVM) models to identify the number of critical weld points contributing to the majority of variation in assembly deviation after joining [6]. In geometry assurance, PCA can be a tool for managing geometrical variation in manufacturing and assembly processes. It is used to identify features that contributes to the majority of the variation [6].

### 2.5.4 Machine Learning in Geometry Assurance

Since using real time scan data to constantly improve the assembly through DTs is computationally heavy for larger batches, there is a possibility to utilize and train deep networks with the help of the data and recursive optimization loops which will reduce the computational need [5].

Sadeghi Tabar et al. [5] conducted a study where they utilized physics based incremental learning in a DT for an assembly to predict outcomes. The DT consisted of a process model, part model, neural network, and a real life assembly. By first training the network on old datasets and then using physics based incremental learning to update the process model and part model. It resulted in an outcome that showed that the network could adapt parameters and reduce the variation and increase the geometrical quality.

# 3
# Methodology

This chapter presents the methodology used to conduct the thesis and develop the proposed method. It includes the literature review, an exploratory study consisting of; a study of the development process carried out at Mercedes-Benz, data collection and data mapping, model building and simulation, and lastly ML-based calibration and process optimization. The exploratory case study was used to formulate requirements on the proposed method which was lastly evaluated.

The framework of the methodology is structured into four main phases:

**Phase 1, Theoretical Foundation and Process Mapping (Sections 3.1 - 3.5):** A theoretical base is established through a literature review. Furthermore, an exploratory case study of the internal Mercedes-Benz development process to identify gaps with the help of current research and state of the art within the context. The case study continues throughout the methodology with data collection and mapping then define the information- required and available across the development process.

**Phase 2, Simulation Models and Verification (Sections 3.6 - 3.8):** Using the mapped data, a series of simulation models is constructed. These models act as the analytical tool, and their accuracy is verified by testing the influence of external factors, gravity, and heat influence. Furthermore, contact point limit testing is performed to evaluate the influence of contact points.

**Phase 3, Analysis and ML Calibration (Sections 3.9 - 3.11):** Sensitivity analyses are conducted on the simulation models to understand the influence off different processes. In this case welding sequence and shimming. In order to calibrate the model an ML calibration regression model is introduced. It learns from historical measurement data to correct and optimize the simulated geometric offsets.

**Phase 4, Method Development and Case Study (Section 3.12 - 3.13):** The method is formulated from the insights gained from the exploratory cases study. The formulated method is then evaluated with a final case study if it enables the integration of a digital twin-based geometry assurance of sheet metal assemblies.

## 3.1 Literature Review

Literature was gathered by conducting searches using the databases Google, Scopus (Elsevier), and Google Scholar. Frequent keywords used when searching included: GD&T, Geometry Assurance, Digital Twin, Sheet Metal Assemblies. The literature search was also complemented by recommended publications from the academic supervisors, and by receiving internal documents from the industry supervisors.

The literature was screened using the CRAAP method [36]. The CRAAP method screens sources for currency, relevance, authority, accuracy, and purpose [36]. If the source passes the screening then it is considered relevant for the thesis.

## 3.2 Development Process Study Mercedes-Benz

The development process at Mercedes-Benz was studied in order to gather insights into how geometry assurance is integrated into the process at Mercedes-Benz. With the goal to identify at which stages in the development process geometry assurance is taking place and what data is generated, stored and used throughout the process. With a specific focus to compliant sheet metal assemblies.

The study was conducted through reading internal documents, informal meetings and discussions with engineers and supervisors, and observations of existing workflows. The main focus was within tolerance management and how the process for tolerance management affected the whole process.

The study covered the overall development process, it included quality gates and the different development stages. To identify where CAT simulations are used, how the data is created and stored surrounding CAT simulations, what information is required at the different stages.

## 3.3 Case Study Assembly

The selected assembly is part of the rear roof frame of the Mercedes-Benz E-Class estate wagon, illustrated in figure 3.1. It consists of four different parts constructed out of sheet metal. The assembly illustrated in figure 3.2.

The single parts of the assembly are identified with the following indices: 1. 600 3.3, 2. 700 3.4, 3. 300 3.5, and 400 3.6.

**Figure 3.1:** Mercedes-Benz E-Class estate wagon. Copyright 2024 by Mercedes-Benz AG [1].

**Figure 3.2:** Assembly visualized in Siemens NX.

**Figure 3.3:** Part identified as 600.

**Figure 3.4:** Part identified as 700.

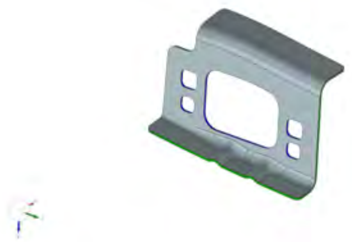

**Figure 3.5:** Part identified as 300.

**Figure 3.6:** Part identified as 400.

## 3.4 Exploratory Case Study

In order to gain an understanding of the current geometry assurance limitations at Mercedes-Benz, an exploratory case study was conducted using the rear roof frame assembly, introduced in Section 3.3. The purpose of the exploratory case study was to evaluate the existing workflow to establish a foundation for developing a new method that supports a workflow that enables a digital twin-based geometry assurance process.

This was done by analyzing the data flow and workflow, alongside iterative simulation model building, simulation verification and validation, and ML model construction.

## 3.5 Data Collection and Data Mapping

The data collection was performed on the selected case study assembly. The data collection and mapping had two main goals. The first was to collect current data, positioning system (clamps and fixtures), weld points, tolerances, and measurement data for the simulations and simulation models. The second goal was to collect and map how the data changes and proceeds between the different stages in the process and through the different quality gates. The data was collected through internal documents and Mercedes-Benz AG and through internal PLM software. When the PMI data was insufficient, supplementary information was gathered from internal guidelines and standards.

The data was then mapped, in order to get a clear overview of the data that is needed and produced in the different stages and quality gates. To create illustrations of the data mapping, Figma and Microsoft Visio was used.

## 3.6 Simulation Model Building

The simulation model is based on the case study assembly showcased earlier in Figure 3.2. The four parts has their own locating schemes. The three parts, 400, 300, and the 600 are spot welded to the 700 part. The simulation models was built using the CAT software RD&T.

First a rigid model was built to establish a baseline model. The purpose of this was to enable a direct comparison with the compliant models. In order to demonstrate the necessity and more accurate compliant simulations for sheet metal assemblies. Afterwards, a compliant model was set up manually to serve as a baseline for the compliant models. Finally, a compliant model was setup semi-automatically using a created python script that formatted the collected data into a .txt file. The .txt filed could be used to generate a model with RD&T and refined manually.

To gather results and verify the simulation models, ten measurement points were defined. These correspond to physical measurement locations on the actual assembly. Allowing the simulated outcomes to be validated against existing measurements. The ten measurement points are numbered as followed and illustrated in the figure 3.7:

- 1. X
- 2. Y
- 3. X
- 4. Y
- 5. N
- 6. N
- 7. Y
- 8. Z
- 9. Y
- 10. Z

The letter after each measurement point, e.g. x indicates the direction of the measurement in relation to the assemblies coordinate system,

**Figure 3.7:** Measurement points visualized on the assembly.

### 3.6.1 Rigid Model

In the rigid model the 400, 300, and the 600 part was positioned separately to the 700 part using a 3-2-1 positioning scheme. With tolerances applied in the target points according to either a standardized company-wide guideline or through 3D-PMI depending on availability. If the 3D-PMI lacks information about a target point, then the tolerance is extracted from the guideline. The 700 part was positioned onto a local ground without tolerances assuming that the fixture is always ideal for this case.

Measure points are created at relevant points following the existing measure points on the real world counterpart, in order to be able to validate the simulations. The measure points can be seen in 3.7.

The measurement point 8. was given a tolerance because the tolerance from the flange is translated in the Z direction. This is because the small 300 part had a single part tolerance that needed to be accounted for.

### 3.6.2 Compliant Model (non-rigid)

In the compliant model, parts 400 and 300 was positioned separately onto the 700 part using a 3-2-1 positioning scheme. For the 600 part a N-2-1 positioning scheme was used. The 700 part was located onto a fixture using a N-2-1 positioning scheme. The N-2-1 positioning system was used to over-constrain the assembly, in order to limit deformations from external sources. Tolerances was applied to the target points according to the standardized company guideline or through the 3D-PMI.

The model was then converted into a supertpart using a superpart feature in RD&T. Creating a single part out of all the parts, with a single N-2-1 positioning system. The weld spots was defined as a local-target pair based on the 3D-PMI. The weld sequence was configured according to the real assembly process, illustrated in Figure 4.24 and GEO points was also configured according to the real assembly process.

Lastly, contact points were calculated using a feature in the software RD&T for locating contact points. If the number of contact points exceeds 1000, they will be reduced down to around 1000 in order to maintain computational efficiency, whilst still providing an accurate result.

### 3.6.3 Compliant Model Variants

To simulate the assembly process and account for the different phases with different data availability, three compliant model variants were constructed. The models range from nominal CAD geometry to synthesized data, representing a real world scenario with non synthesized data in ideal cases. The following section details how the models were constructed.

#### 3.6.3.1 Nominal Model with Tolerances

The nominal model with tolerances is based on nominal CAD geometry, with positioning system, and tolerances on information available in internal PLM systems and standards, through PDM and 3D PMI. The weld spots and sequence was configured according to the real process. Since this represents an early stage in the development process no welding optimization or shimming was used as inputs in the model.

#### 3.6.3.2 Model with Scan Data as Input (Verification Model)

The model with scan data as input is a derivative of the nominal model, using the same positioning system, weld points, and sequence. However, tolerances are applied by using single-part scan data as an input into the simulation model. This generates an offset in each node (the distance between the nominal CAD data and the 3D scanned geometry). The scanned geometry is significant to account for variation that the nominal CAD geometry does not, increasing the accuracy of the simulation and allowing for a digital twin connection.

#### 3.6.3.3 Model with Synthesized Data as Input

The model with synthesized data is a derivative of the nominal model. However, the input data was in the form of 1000 simulated parts for each single part. The 1000 simulated parts creates a range for each node which applies as the tolerance.

**3.6.3.3.1 Synthesized Data** The goal is trying to replicate the tooling process by modifying the positioning system of each part separately and disturbing the target points locally with single part tolerances, within the range of $\pm$ 0.4 - 1 mm.

The deformed single parts prints 1000 shapes (mesh) that can be used as input data, simulating 1000 physical parts.

### 3.6.4 Model Building Through Script

To build a model semi-automatically a function within the software RD&T can be used. The function reads a script in .txt format with information about part id, assembly hierarchy/sequence, positioning system and support points, and weld points. Together with the .txt file a folder with the meshes for the parts is loaded. When the model is created in RD&T, it is mostly complete, however it still needs manual engineering verification. Making sure that the positioning system and weld spots are correctly set up and connected to mesh nodes. Furthermore, measurement points, tolerances and welding sequence needs to be applied manually after the model is generated.

## 3.7 Simulation

The following section presents the simulations conducted. Covering how distribution tests was conducted, and how the simulation model was setup.

### 3.7.1 Simulation Setup

The simulation model used a mid-surface mesh with an element size of 6 mm, as per Mercedes-Benz Standard. The mesh was refined around the weld points, to improve the calculation of local effects.

Material properties are set to the following:

- Poisson's ratio 0.3
- Young's Modulus 210 GPA
- Thickness of part 600 0.9 mm
- Thickness of part 700 1.5 mm
- Thickness of part 300 2.0 mm
- Thickness of part 400 2.0 mm

The simulations were performed using 1000 iterations in order to ensure statistical convergence. Providing a stable estimate of the standard deviations, variation, mean values / mean shift, and RMS.

## 3.8 Simulation Influences

To understand what impacts the simulation results and in what way, different influences was tested on the simulation models. Three influences was tested, gravity-, heat-, and contact point influence which will be detailed in this section.

### 3.8.1 Gravity Influence

To determine the relevance of gravity induced variation in the simulation, the verification model was ran an extra time with gravity force induced in the Z-axis. The simulation was then compared to the one without gravity influence.

### 3.8.2 Heat Influence

To determine the relevance of heat induced influence in the variation simulation, a single iteration simulation with heat influence was ran and compared to the verification model.

When setting up the model for heat influence, it is based on the model from the non-rigid simulations but the weld points are modified. Instead of being nodal connections (represented in a single node) the weld points are defined with a radius allowing them to have impact on a greater area of the mesh. This enables the introduction of thermal effects, closer to reality.

The weld gun efficiency was set to 100% and the power was set to 1 with the duration of 0.5 seconds. The type of weld gun was a balanced gun. The weld sequence is illustrated in the figure 3.8.

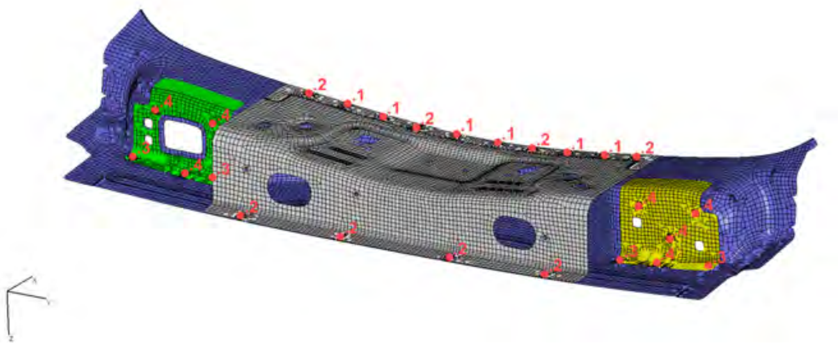

**Figure 3.8:** Welding sequence according to current assembly procedure.

### 3.8.3 Contact Point Influence

To determine the influence of contact points, a test was run without altering the amount of contact points when identifying contact points. The increase of contact points increases the accuracy of the simulation but also drastically increases the computational power needed. The test was conducted on the verification model.

## 3.9 Sensitivity Analysis

In order to identify what sources influence the model the most, two different sensitivity analyses were ran. First one was on shimming and the second one was on weld sequence. These two will be detailed in the following section.

### 3.9.1 Shimming Sensitivity

To identify the impact of shimming, a shimming sensitivity study was conducted, where in each positioning point a shimming operation of -2mm, -1mm, 0mm, 1mm and 2mm was tested. The influence of the shimming adjustment was shown through the 10 defined measurement points.

#### 3.9.1.1 Choosing shimming locations

The shimming locations for the used assembly were unknown and therefore, the locations of the shims had to be chosen based on the locating points and support points of the model. This means that the sensitivity will be conceptional and not based on real shimming locations. As this model contains 31 individual locating and support points, evaluating all the possible combinations of shims are infeasible due to problem size. With the range -2mm to 2mm with a 1mm step it would create $5^{31}$ unique combinations. Therefore, a screening process of the shimming points had to be done.

The screening process started with obtaining the offset values for each measurement point based of the shimming combinations. The model used, was the nominal model with the tolerances. For this screening process, all shimming points was given two values; -2 and 2. These values represented the amount of shimming in that point in millimeters. A variation simulation was then run for each point with the given values, while the other shimming points were set to zero. This was done by creating a script that created a text file that RD&T read in and ran the variation analysis and exported the results containing the offset value for each measurement point based on the given shim. The script then generated a new text file and iterated this process for every shimming point.

After the screening simulations had been completed, a second script was used to evaluate which shimming points had the highest potential to improve the assembly outcome. The purpose of this script was not only to identify which shimming points caused the largest change in the measurement results, but also which points improved the overall result of the assembly the most.

To evaluate the overall influence of a shimming point, a global deviation measure was calculated from the measurement point offsets. This score was defined as the sum of the squared offset values of all measurement points as seen in Equation 3.1, where $y$ is the offset value of the measurement point $i$ and $n$ is the total number of measurement points. Thus, larger deviations contribute more to the measure than smaller ones, and a lower value represents a better geometrical outcome.

$$J = \sum_{i=1}^{n} y_i^2 \tag{3.1}$$

In addition to the global deviation measure, the Matlab script also examined the local influence on the measurement points. This sensitivity was calculated using Equation 3.2, where $S$ is the local impact from shim $j$ on measurement point $i$, $y^{(+2)}$ is the offset value on measurement point $i$ when shim $j$ is +2mm and $y^{(-2)}$ is the offset value on measurement point $i$ when shim $j$ is -2mm. Because the total range between these is 4mm they are divided by 4 to generate the score. This sensitivity describes how much a specific measurement point changes per millimeter of shim change in a specific shimming location.

$$S_{ij} = \frac{y_{ij}^{(+2)} - y_{ij}^{(-2)}}{4} \tag{3.2}$$

For each shimming point, the global deviation measure from the $-2$ mm case and the $+2$ mm case was compared, and the direction that gave the lowest value of $J$ was defined as the best direction. The improvement potential of each shimming point was then calculated as the difference between the baseline value and the best obtained value, as shown in Equation 3.3, where $J_0$ is the baseline global deviation measure and $J_{\text{best},j}$ is the lowest obtained value for shimming point $j$. A positive value of $I_j$ therefore indicates that the shimming point improved the overall assembly outcome compared to the baseline case.

$$I_j = J_0 - J_{\text{best},j} \tag{3.3}$$

To support the interpretation further, the number of improved and worsened measurement points was also examined for each shimming point, by comparing whether the absolute offset of each measurement point decreased or increased compared to the baseline case.

Based on this analysis, all 31 shimming points were ranked. The ranking was mainly based on how much each shimming point improved the global score, while the local influence was used as supporting information during the interpretation. From this ranking, the five shimming points with the highest positive influence on the assembly outcome were selected. These points were considered the most relevant candidates for further study, since they showed the greatest potential to improve the measurement results.

#### 3.9.1.2 Evaluating Shimming Sensitivity

As for investigating the shimming sensitivity of the assembly, new data had to be acquired. This time only the 5 most relevant shimming points from before, were used to gather this data. The same text file used in section 3.9.1.1 to get the offset values from RD&T, was used here. However, only 5 shimming points were considered and the range was changed to -2 to 2 with 1 step in between, so [-2, -1, 0, 1, 2]. This was to increase the amount of variations of the shimming to get a more nuanced result. Based on this, a new Matlab script was created to generate new text files as in section 3.9.1.1, but with every possible combination of shimming by the 5 shimming points. This created a total of $5^5 = 3125$ different offset outcomes.

To calculate the shimming sensitivity, RMS is used. From all the offset values acquired, the RMS is calculated individually to find the highest and the lowest value. These are then used to calculate the total shimming sensitivity of the assembly using Equation 3.4, which gives the result in percentage.

$$S = \frac{RMS_{max} - RMS_{min}}{RMS_{max}} \cdot 100 \tag{3.4}$$

Using the result, it is then possible to analyze whether changing the shimming is a feasible optimization way to go or not.

#### 3.9.1.3 Choosing shimming values

The target case was used as the starting point, and the effect of each shimming combination was added to the measurement values to estimate the corrected result. The corrected values were then checked against the lower and upper limits. The best shimming combination was selected by first minimizing the number of measurement points outside the limits, then minimizing the remaining violation, and finally choosing the combination that placed the measurement points best within the allowed interval.

### 3.9.2 Weld Sequence Sensitivity

To identify the sensitivity to the welding sequence, a weld spot optimization was conducted. Each GEO spot was tried in each possible sequence, for the model we had ten GEO spots, meaning that it became 55 possible sequences. To calculate the sensitivity the model has to welding the equation 3.4 is used. The optimization is done through a feature within RD&T.

## 3.10 Simulation Verification

To validate the simulation, the individual parts used for the verification model were welded at the process station. The resulting assembly was then 3D scanned and measured according to the measurement points. To accurately track the influence of the manufacturing process, it was ensured that the initially scanned single parts were the exact ones used in the final assembly. This approach resulted in a complete scanned assembly that served as a comparative baseline to evaluate the simulation and the case study. Furthermore, establishing this direct link between the individual parts before and after assembly serves as a foundational step toward a digital twin-based methodology.

## 3.11 Machine Learning Model

The following section discloses the approach in order to integrate ML into the geometry assurance workflow. The structured approach to create the ML model was divided into several steps: establishing the end goal of the ML application, defining the necessary inputs and outputs, selecting the model architecture, gathering and preprocessing training data, and finally developing the scripts to train and test the models. The following subsections detail how each of these steps was executed.

### 3.11.1 Aim and scope of the ML Study

The aim of the ML part of this thesis was to investigate wether data-driven methods could be used to improve the results between simulation and real world assembly outcomes. The work was therefore formulated as a simulation to measurement calibration problem, where the objective was to use available measurement data to correct or adjust simulated geometric offset values.

The ML model was not intended to replace the geometry assurance simulation model. Instead, it was developed as an additional calibration on top of the workflow. The purpose of this was to learn the differences between simulated and measured results and use this knowledge to generate a more measurement like prediction from new simulated data.

This scope was chosen because the available project data did not contain all information required for a complete case-based digital twin model. In particular, the available data did not include a large number of traceable physical assembly cases with scanned part geometry before assembly, corresponding process settings, and measured assembly outcome after assembly. Therefore, the ML work focused on what could be achieved with the available simulation and measurement data, while also evaluating how the approach could be extended toward a more complete digital twin framework in the future.

### 3.11.2 Available Data and Data Preparation

Two main types of data were used in the ML workflow: simulated geometric offset data and measured geometric offset data. The simulated data were obtained from a variation analysis using CAT software and the model built earlier. The measured data was obtained through an internal data base and represented physical assembly outcomes from the same assembly. Both the simulated and measured data included offset values located in measure points on the assembly.

The simulated data was gathered through single run variation simulations in RD&T. The results from each run was shown as offset values for each measurement point that could be downloaded in csv or txt format.

Before the ML models were developed, the simulation and measurement datasets were rearranged into a common structure. Each row in the structure represented a measurement point and each column represented one value of simulated or measured offset. A representation of the structured data can be seen in Table 3.1. This format made it possible to compare the distribution of simulated and measured values for each measurement point. To be able to structure such a table, a script was created in Matlab that took the downloaded files and structured the offset values in an xlsx format for later use.

**Table 3.1:** Representation of structured measurement data table

| Measure | Value 1 | Value 2 | Value 3 | Value 4 |
|---|---|---|---|---|
| Measure 1 | X | X | X | X |
| Measure 2 | X | X | X | X |
| Measure 3 | X | X | X | X |

After structuring the data, a data matching step was performed. This was to identify each measurement points in both the simulated and measured datasets. Only the common measurement points were included in the ML workflow. This was necessary to ensure that the model was trained and evaluated on comparable data.

In addition to the original simulation input tables, a preprocessing script was developed to handle newly exported RD&T result files. These files contained measurement point names and corresponding offset values for individual simulation runs. The script extracted the measurement point names and values from each text file and compiled them into the same table format as the original simulation dataset. This allowed newly generated simulation data to be used in the same ML workflow without changing the model structure.

### 3.11.3 Model Candidates

Based on the available data and the aim of improving the simulation outcome with ML methods, three model formulations were considered. These formulations represent different levels of data availability and different degrees of connection to a future digital twin workflow.

The first considered model was a quantile-based regression model. This model was developed to handle the lack of direct one to one mapping between the simulated and the measured data. Instead of matching individual simulation and measured cases, this model instead maps the representative quantile for the datasets and maps them towards each other. This model was therefore suitable for the available data structure where several simulated and measured values existed for each measurement point, but no traceability between them. Thus, no opportunity for a case mapping.

The second model candidate was a PCA-based state calibration model. In this model, the measurement points were treated as one combined geometric state of the assembly rather than as separate individual outputs. Principal Component Analysis (PCA) was used to represent the main variation patterns in this state with a smaller number of principal components.

The purpose of using PCA was not to remove measurement points, but to investigate whether the shared variation between the measurement points could be described more compactly. This makes the approach relevant from a digital twin perspective, since a digital twin should ideally describe the condition of the assembly as a combined state rather than only as independent measurement point deviations.

The third model was a conceptual case-based digital twin model. This model was not fully implemented due to the limited data available. It was instead used to define and show the direction of the ML workflow in the future state. This model was a case-based model which would require scanned geometry of each individual part before assembly, measured assembly geometry after assembly and traceability between these. Thus, what the parts look like before and after assembled. Furthermore, traceable process inputs such as shimming, locator settings, clamping sequence or welding sequence would also be required as controllable inputs. With this data, the model could be trained to predict the outcome of a specific physical assembly instance and support process decisions accordingly to minimize potential variation.

The purpose of considering these three models was to identify which approach that was reasonable with the available data and fit to the overall workflow of the thesis. It was also done to clarify what additional data that would be required for a more advanced digital twin implementation.

### 3.11.4 Training, Testing and Evaluation

This subsection mentions the procedure behind how the models were trained, tested and evaluated.

#### 3.11.4.1 Quantile-based model

The quantile-based model was trained using a supervised regression approach. Since the simulation values and measured values were not paired as cases, a common quantile grid was used to create comparable positions in the two distributions. For each measurement point, the simulated and measured values were sampled at the same quantile levels. This created paired observations based on distribution position rather than the instance order of the simulated and measured values.

Each row in the training dataset represented one measurement point at one quantile level. The input variables were then generated from the simulated distribution. These were, the quantile level, the simulated value at that quantile, the mean of the simulated distribution and the deviation of the simulated distribution. The target variable was the measured value at the corresponding quantile level.

The regression model was trained to learn the relationship between simulated distribution values and measured values. The dataset was divided into a training set and a testing set, where 80% was training and 20% testing to keep the balance between training and testing.

The trained regression model could then be applied to new simulation data. For a new set of simulated distribution, the quantile positions, simulated values, mean and standard deviation were calculated and used as input to the trained model. The model then predicted calibrated values intended to represent similarities to the real measured outcome.

#### 3.11.4.2 PCA-based model

For the PCA-based model, the simulation data were first rearranged into the same format as for the quantile-based model, where each row represented one simulated case and each column represented one measurement point. PCA was then applied to the simulated data to define a reduced state space based on the main variation patterns in the simulation results.

The measured data were projected into the same PCA space, using the PCA basis defined from the simulation data. This allowed the simulated and measured assembly states to be compared in the same space. Since the simulated and measured cases were not traceable one-to-one, the model was trained using the same distribution-based principle as the quantile model, but applied to the principal component scores instead of directly to the measurement point values.

A separate regression model was trained for each retained principal component. The input variables were the quantile level, the simulated PC score at that quantile, the mean of the simulated PC score distribution, and the standard deviation of the simulated PC score distribution. The target variable was the measured PC score at the corresponding quantile level.

After prediction, the calibrated PC scores were reconstructed back to the original measurement point space. This allowed the PCA-based model to be evaluated using the same measurement points and error metrics as the quantile-based model.

#### 3.11.4.3 Evaluation

The models were evaluated using both numerical and visual methods. Root Mean Square Error (RMSE) and Mean Absolute Error (MAE) were used to quantify the prediction error during training and testing. In addition, the original simulated values, the calibrated predicted values, and the measured values were compared for each measurement point.

Histogram plots with smoothed distribution curves were used to visualize the distribution-level behavior. The histograms show the percentage of values within each interval, while the smoothed curves were included to make the distribution shapes easier to compare. These plots were used to assess whether the ML-calibrated predictions moved the simulation results closer to the measured data.

The trained model was also applied to a new simulation result based on scanned input data. The predicted values were then compared with the scanned assembly measurement values. This was used as a practical demonstration of model application, not as a complete statistical validation.

### 3.11.5 Model Selection

The models were compared using both quantitative and qualitative criteria. The quantitative evaluation focused on prediction accuracy, using RMSE and MAE as the main error metrics. In addition, the improvement between the original simulated values and the calibrated predictions relative to measured data was evaluated for each measurement point.

The qualitative evaluation focused on methodological suitability and practical applicability. Since the available data did not contain traceable case information, compatibility with non paired simulation and measurement data was an important criterion. Models requiring traceable cases between scanned geometry were therefore considered less feasible for implementation. Though, they remained relevant as future digital twin concepts. Practical integration was another criterion, since the selected model needed to be applicable to CAT software simulation data without requiring too much manual restructuring. Finally, the models were assessed based on their ability to be able to support geometry assurance improvement.

## 3.12 Development of the Method

The culmination of the exploratory case study is the formulation of a proposed method. This proposed workflow integrates the data acquisition, non-rigid simulation building, ML-driven calibration, data feedback loops, and storing the data into a digital twin-based geometry assurance framework for sheet metal assemblies.

To facilitate implementation and future use, the finalized method was structured and visualized as a flowchart. This flowchart outlines the necessary sequence of actions. Where necessary, individual steps within the flowchart are detailed to assist decision making, based on different scenarios.

## 3.13 Case Study

The finalized method was tested and evaluated through a case study on the rear roof frame assembly, previously introduced in section 3.3 and illustrated in figure 3.2. This subassembly was selected for the case study because it provided a sufficient level of complexity and corresponding measurement data available. Furthermore, its manufacturing process included all the necessary steps for the process: fastening, clamping, spot welding, and spring-back release.

The execution of the case study served to evaluate the methods detailed earlier in this chapter. The process consisted of semi-automatically generating a simulation model using 3D scanned data as input, running verification and sensitivity analyses, and finally applying the selected ML calibration model to predict both virtual and physical outcomes. These predicted outcomes were then compared to the physical 3D scanned assembly and evaluated. By conducting these steps, the case study asses the feasibility of a digital twin-based geometry assurance workflow for sheet metal assemblies.

The case study was executed by applying the developed method to the rear roof frame assembly. Where each step in the method was evaluated with the help of the selected assembly.

# 4

# Results

## 4.1 Geometry Assurance in Development Phases

A product development process is complex and has many phases. While the specific requirements for each quality gate can vary depending on the industry, the framework presented is generalized from a study conducted at Mercedes-Benz. The process is broken down and simplified into three distinct processes, concept phase, development and production, see figure 4.1. During the process several quality gates exists, to evaluate the work incrementally and decide wether it is good enough to continue or to be revised. For this case, the most important quality gates for the data flow, work flow, and geometry assurance process was extracted and shown in figure 4.1. The quality gates A1 and A2 occurs during the concept phase and the Aa gate determines if it passes to the development phase. In the development phase B1 and B2 exists and Bb determines if it passes on to the production phase. In production phase the quality gates C1 and C2 exists.


**Figure 4.1:** General product development phases, with quality gates.

The A1 quality gate releases the concept and initial CAD files are ready and available. This starts the project timeline and divides work to all the individual departments. Similar to the master layout plan shown in Figure 2.2.

The A2 quality gate releases a concept booklet, this booklet includes a gap and radii plan to provide engineers with GD&T and defining joints.

The Aa gate requires mathematical validation of a digital prototype in order to pass. This starts the pre-development phase.

To pass the quality gate B1 a exterior design freeze is required. Meaning that larger changes cannot take place after this gate. The complete serial production will be verified digitally. This also means that proper data is accessible, with early scan and measure data of parts from part concept production. Leading to better simulation inputs.

The B2 quality gate requires that a decision that decides how the manufacturing is going to be laid out. Meaning that after B1 has passed, the tools for series production will be in production. The digital level of maturity is optimized.

The quality gate Bb determines if the project is ready to move into series production. For this gate a first concept vehicle is fully built, the manufacturability has to be confirmed and parts will be checked for functionality and approved.

For quality gate C1 the first optimized concept vehicle is required, where minor geometrical changes has been optimized to reach the quality requirements. The full BiW is ready for series production and assured. Meaning that passing quality gate C1 puts the vehicle in series production.

Quality gate C2 is the last one, to pass this quality gate all departments involved in the product has to approve it, and the full design freezes. Production is ramped up.

The different quality gates and phases also implies that the amount of available data is going to increase as you progress. Furthermore, the data will mature and be more correct. With this information, a figure, see figure 4.2 was constructed that showcases what simulation could be ran throughout the process based on the maturity- and available data.


**Figure 4.2:** Flowchart showing which simulation that can be run during different phases of the development process.

## 4.2 Data Mapping

The data available during the product development phases were collected and mapped to their respective quality gates, as illustrated in figure 4.3. In this context, legacy data is available if the project is a derivative project, meaning that it is based on an earlier project with similar geometry.

During the early concept phase (quality gate A1 through Aa), the available data is theoretical and conceptual, using initial CAD concepts with early releases of GD&T plans. As the project advances into the development phase (quality gate Aa through Bb), the early conceptual data gets evaluated, revised and confirmed. New data points are also introduced that gives the project a higher fidelity enabling more robust simulations. Finally, as the project enters the production phase (quality gate Bb through C2), the data reaches maximum maturity. The data is confirmed and frozen ready for series production with large data sets of measured or scanned data.

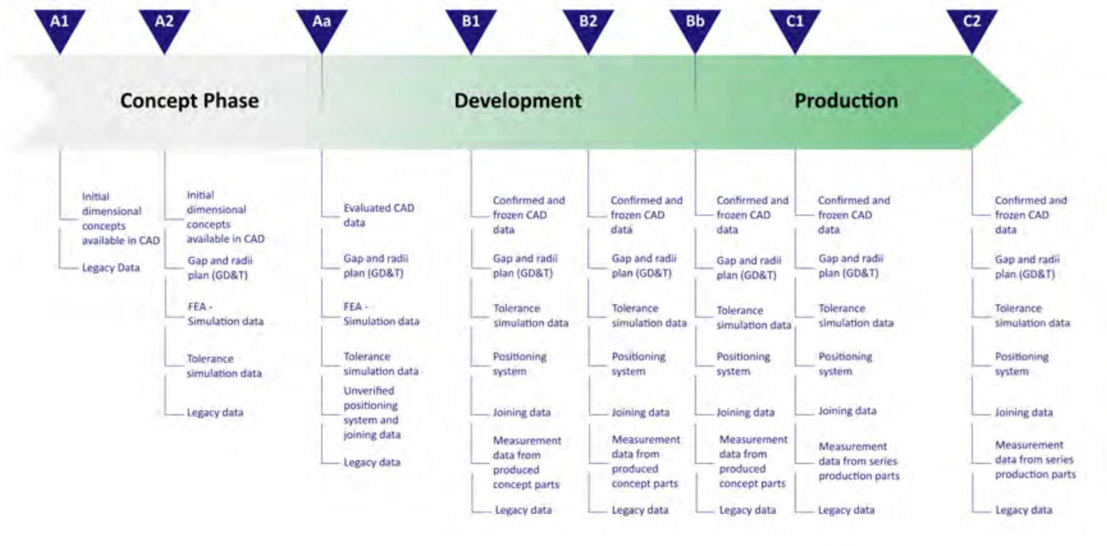


**Figure 4.3:** General product development process with available data shown in each quality gate.

### 4.2.1 Data Needed for Non-Rigid Sheet Metal Assemblies

To identify what data was necessary to build a non-rigid sheet metal variation simulation, a model was built and updated iteratively. Through this the necessary input- and output data was identified and shown in Figure 4.4. The figure is a black-box model, showing the input- and output data but the process is hidden.

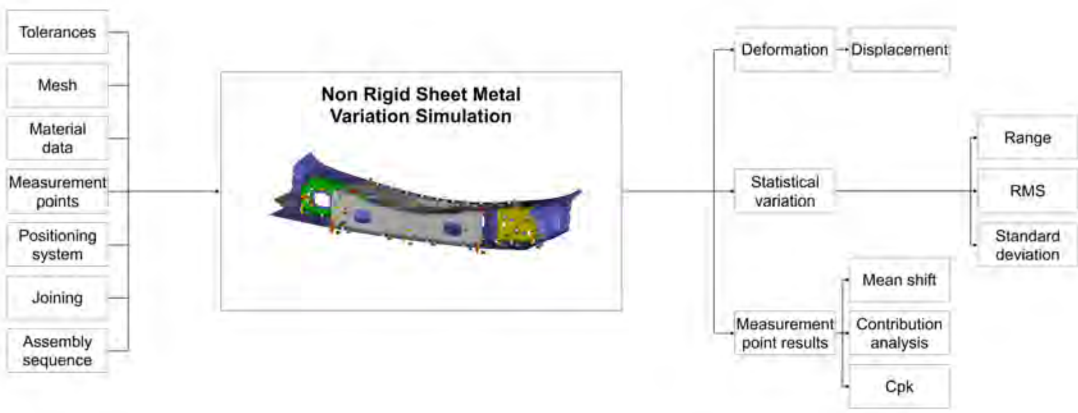


**Figure 4.4:** Black box model of non-rigid sheet metal variation simulation.

The input- and output data are presented below, with elaboration if needed for certain data points. The standard file formats for the simulation input data were mapped, see Appendix A.1.

**Required Input Data:**

- **Tolerances:** Both single part and fixture tolerances.
- **Material Data:** Young's modulus, Poisson's ratio, density, and thermal properties.
- **Joining Data:** The joining sequence alongside specific methods such as weld spots, laser welds, or structural adhesives.
- **Geometric and Process Data:** The physical mesh, measurement points, locating scheme, and the overall assembly sequence.

**Simulation Outputs**

- **Deformation:** Primarily tracking physical displacement.
- **Statistical Variation:** Including the range, root mean square (RMS), and standard deviation.
- **Measurement Point Results:** Yielding data on mean shifts, contribution analysis, and the process capability index (Cpk).

### 4.2.2 Data Flow and Transformation in the Work Flow

The data flow containing vital simulation parameters was mapped and evaluated, as illustrated by the swimlane diagram in Figure 4.5. The diagram is organized by general development phases along the top, while the left column categorizes the three distinct work and data flows: Product Data Management (PDM), Real Process (physical product creation), and Simulation. Black arrows indicate the interactions and data transfer between these domains, whereas breaks in data continuity are highlighted with a red line and a lightning bolt icon.

A key observation from this study is that critical feedback loops, which provides necessary input parameters for the simulations, are frequently broken. Specifically, these data breaks occur when the production optimizes the shimming and welding in order to meet assembly requirements. The optimizations, together with the initial position is not stored or fed back into the PDM system, meaning that the simulation uses outdated information.

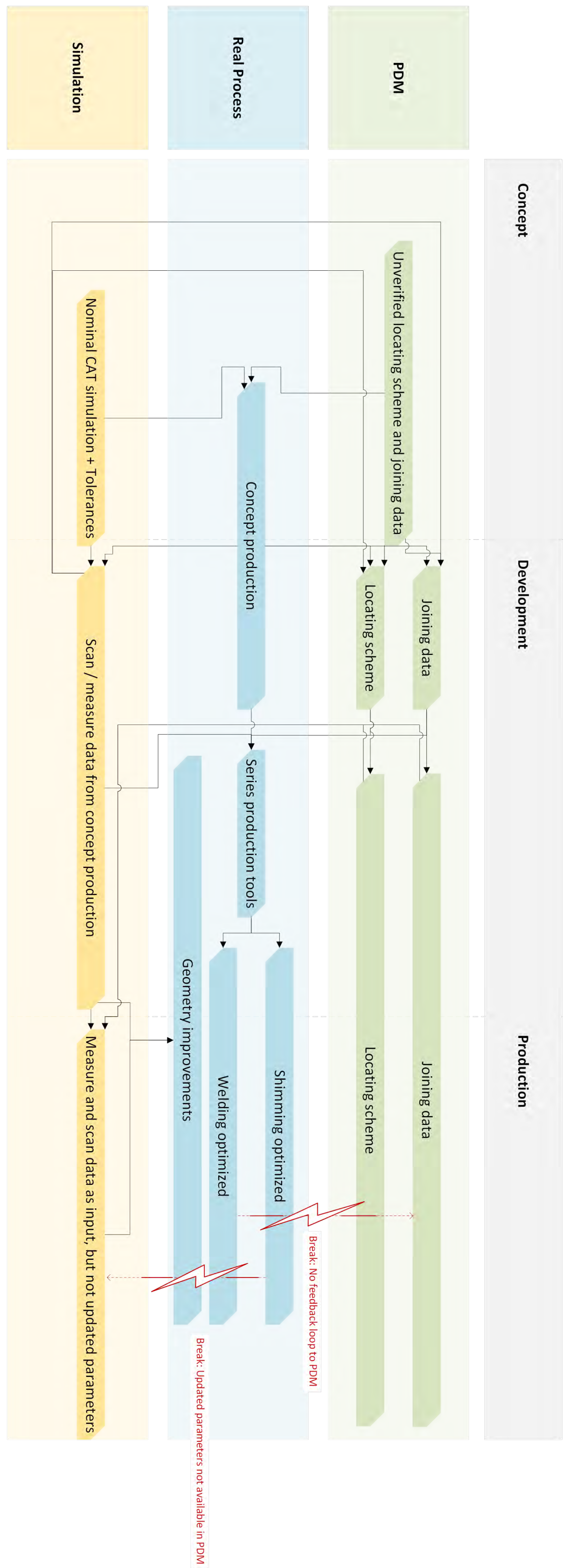


**Figure 4.5:** Swimlane diagram displaying the data- and workflow for selected parameters.

## 4.3 Transfer of Data

This section addresses the transfer of data within the data and workflows, specifically its movement from PLM systems through CAT software and ultimately to data storage. Table A.1 outlines the various formats of the input data. Currently, input parameters (excluding meshes) are provded in .plm, .plmxml, .pdf, and .pptx formats. Research suggests that an emerging file format, QIF, can act as a SST and store these parameters into a single file. Because the QIF format is XML-based, it facilitates compatibility, provided that the parameters currently in .pdf and .pptx formats can be transformed into an XML structure. Which means, both input parameters and output data could be stored in a single QIF file and transferred seamlessly through the workflow. However, this approach relies on software compatibility, which is currently unavailable for RD&T, the specific CAT software used in this thesis. Additionally, it would require a software that can interpret the QIF format to display 3D PMI or an extension to current PDM / PLM visualization software.

## 4.4 Simulation Models

This section covers the various simulation developed for this study. The different simulation models were built in order to simulate the different phases in the development process, reflecting what data is available and its impact on the outcomes. The following subsections present these models in sequence: the nominal model with tolerances (Section 4.4.2), the model based on a single instance of scan data (Section 4.4.3), and finally, the model based on synthesized data (Section 4.4.4).

The results of the simulation outcomes will be shown in color plots, RMS value for the part and through mean shift in the measure points. For the simulation when using a single instance of scan data as an input, it creates no range but only an offset, meaning it creates no standard curve for each measure point. For that case, the mean shift and a mean color coding will be used. The color coding shows geometrical deviation in normal direction. The RMS is the value of each nodes deviation for the entire part.

### 4.4.1 Rigid Model

Since the rigid model is non-compliant, a color plot is not displayed. The deviation for each measure point can be seen in Figure 4.6. The mean shift in each measure point is so small that it cannot be seen on the scale. With the largest deviation being 0.00362 mm. The variation in each measurement point is illustrated in Figure 4.7.

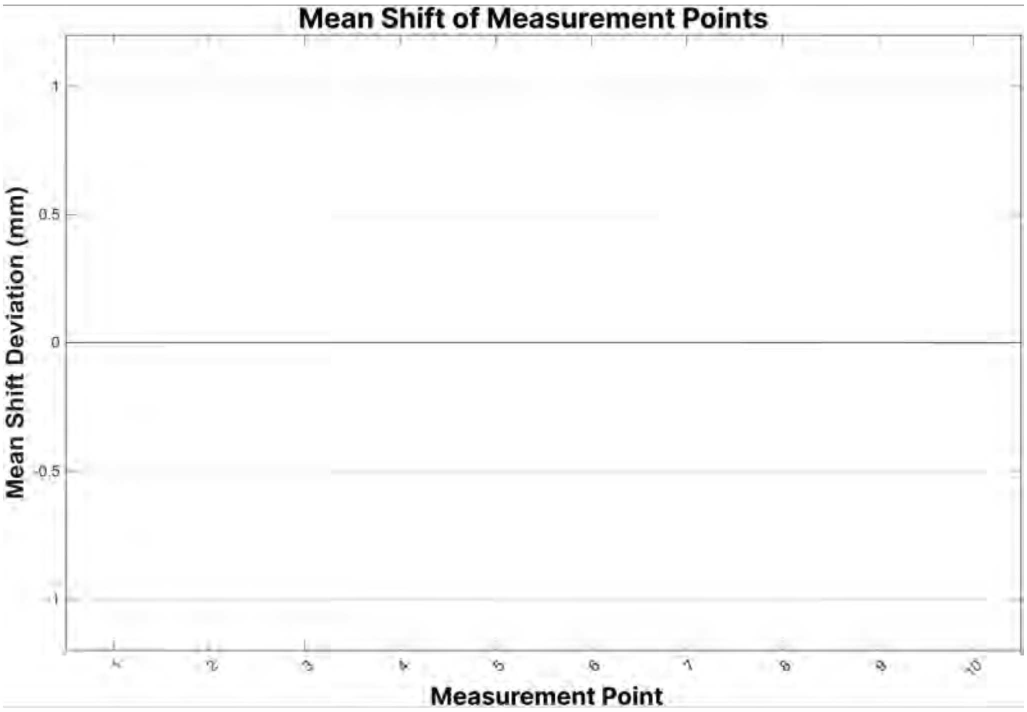


**Figure 4.6:** Mean shift of every measurement point for the rigid model.

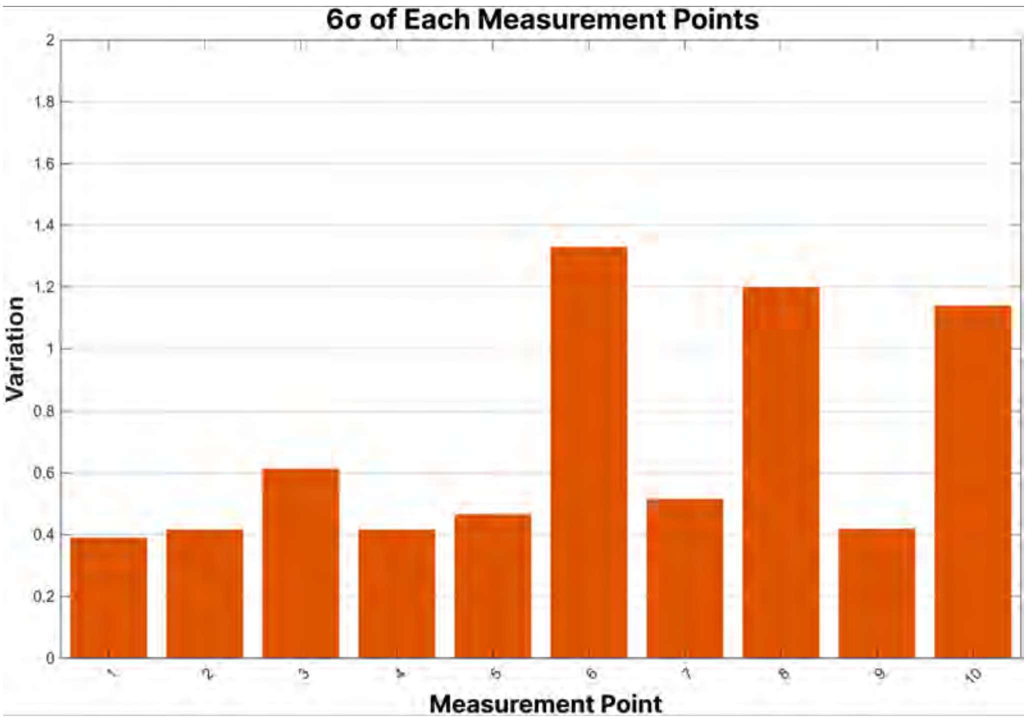


**Figure 4.7:** Variation in each measurement point for the rigid model.

### 4.4.2 Nominal Model with Tolerances

The nominal model based on nominal CAD data with tolerances applied according to 3D PMI and standards showed a part RMS of 0.4873 in normal direction.

Figure 4.8, displays the color plot for the simulation, demonstrating the nodal deviations over the mesh. The most extreme deviation in positive direction is shown as red, and in negative direction as blue. A green color shows results around no deviation.

The results from the measurement points is illustrated in Figure 4.9, where the mean shifts are illustrated, and with the largest shifts in points 6 and 10. The shift in 6 is to be expected, since it is located close to the edge of the assembly, far from any locating point. The same pattern can be seen in Figure 4.10, where the variation is greatest in these points, 6 and 10.

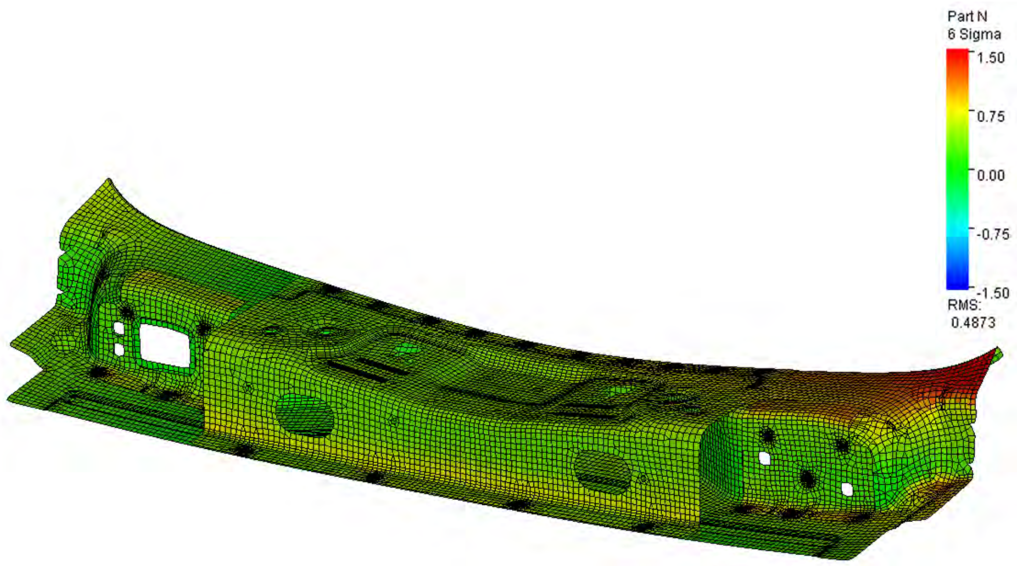


**Figure 4.8:** Deviation plot for the nominal model with tolerances.

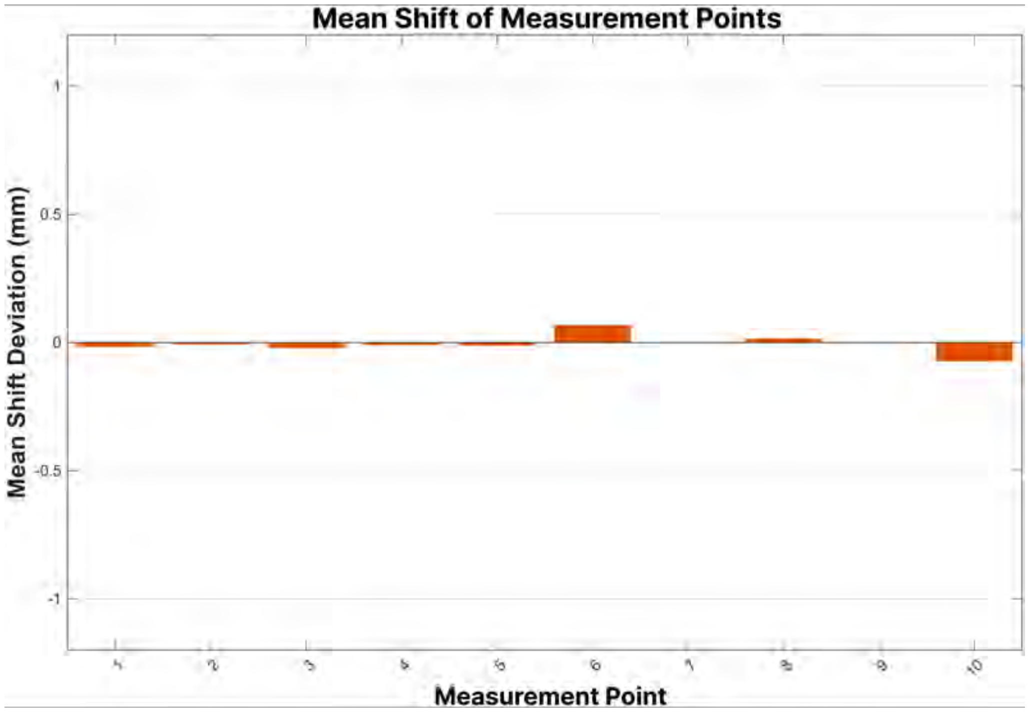


**Figure 4.9:** Mean shift of every measurement point for the nominal model with tolerances.

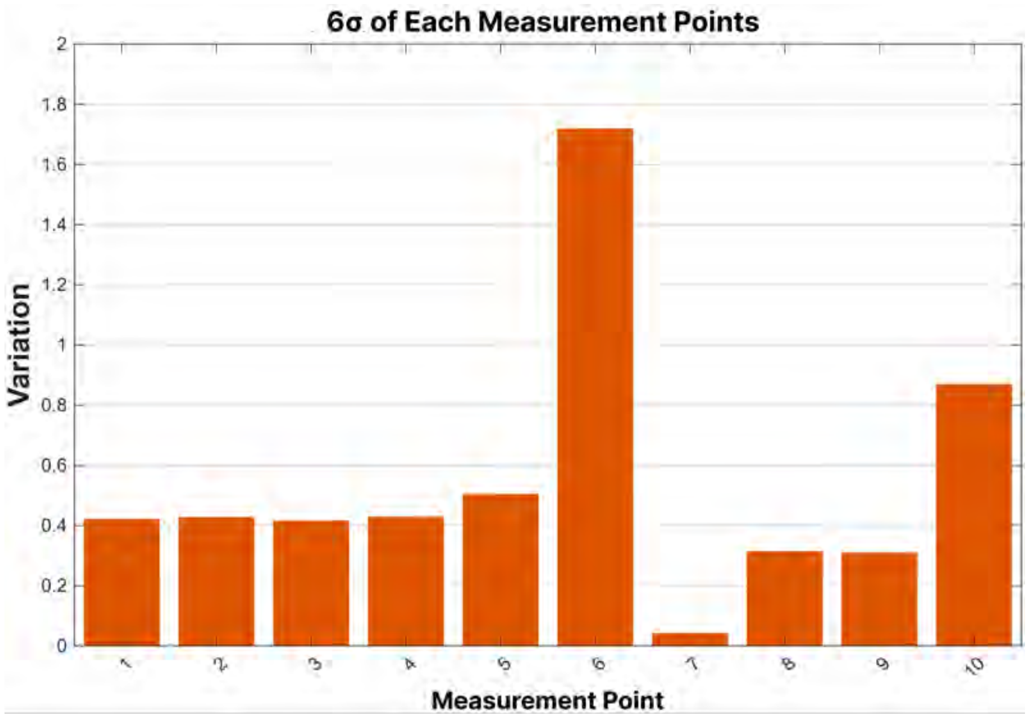


**Figure 4.10:** Variation in each measurement point for the nominal model with tolerances.

### 4.4.3 Model Based with Scan Data as Input (Verification Model)

The model with scan data as input showed a part RMS of 0.2985 in normal direction. Since the input consists of a single instance of data, no variation will be generated. Therefore, no variation plot is generated for this model.

Figure 4.11, displays the color plot for the simulation. Since it is only a single instance of single part scan data as an input, it produces only a single output. Meaning that the color plot shows a part mean in normal direction for a single instance.

The results from the measurement points is illustrated in Figure 4.12, displaying significantly more amplitude in deviation compared to the nominal model. The greatest change can be see in measurement point 5. located at the left edge of the part, followed by point 10. which is located at the left supporting part. The behavior is expected for measurement point 5. and 6., since they are furthest away from the positioning points. Which leads to a bigger amplification in geometric variation.

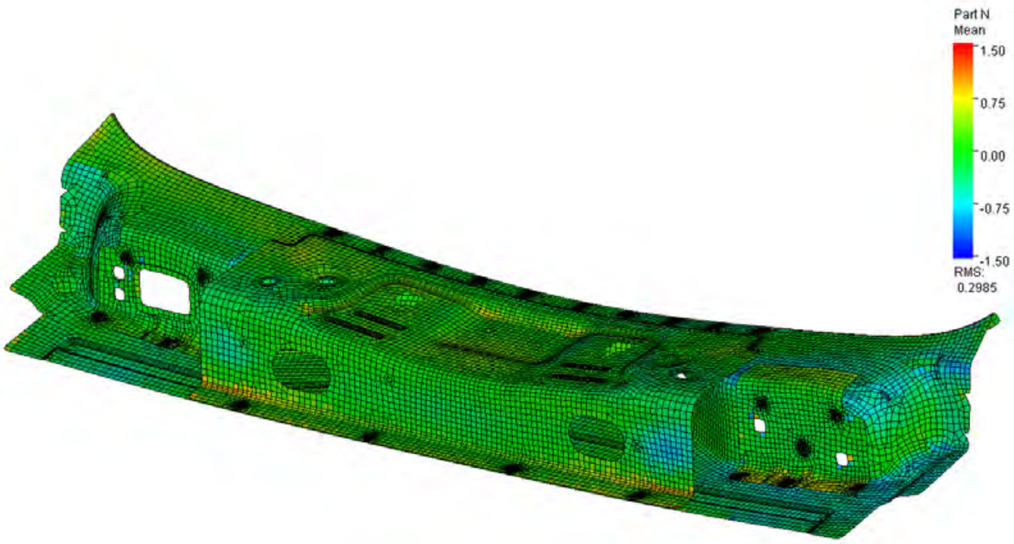


**Figure 4.11:** Deviation plot for the verification model.

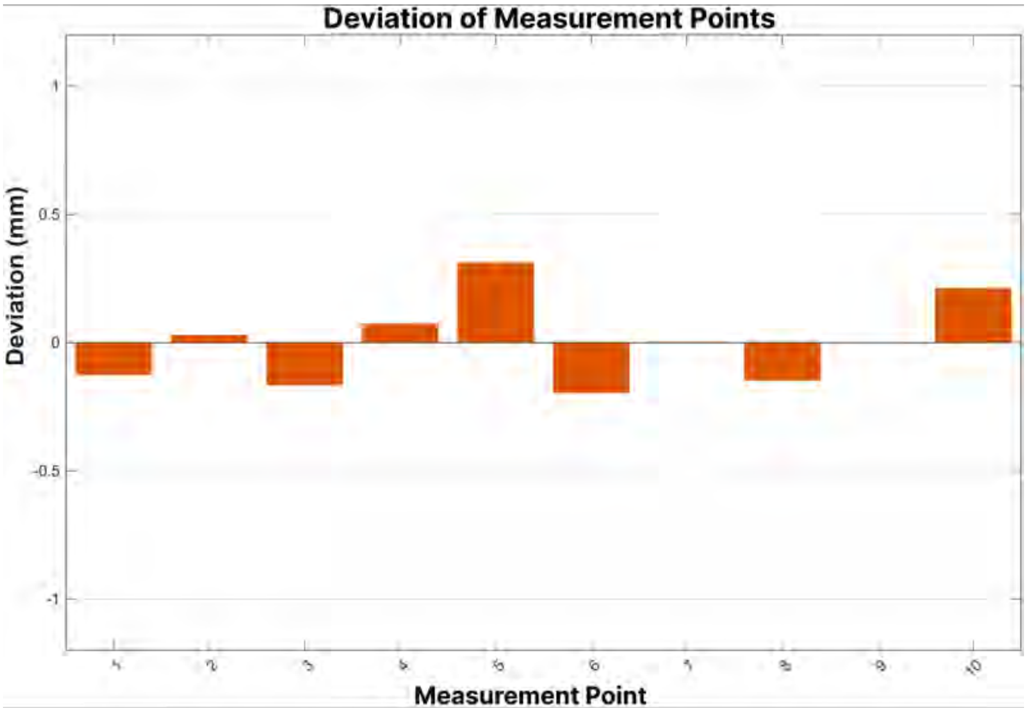


**Figure 4.12:** Mean shift of every measurement point for the verification model.

### 4.4.4 Synthesized Data Model

The synthesized data model showed a part RMS of 0.7960 in normal direction. Figure 4.13 illustrates the color plot for the simulation. It shows large areas of deviation in positive direction.

The results from the measurement points is illustrated in Figure 4.14 and Figure 4.15. In Figure 4.14 the mean shift displays the same pattern as the verification model but with bigger amplification. In Figure 4.15 it can be seen that the variation is significantly reduced in measurement points 2., 4., 7., and 9..

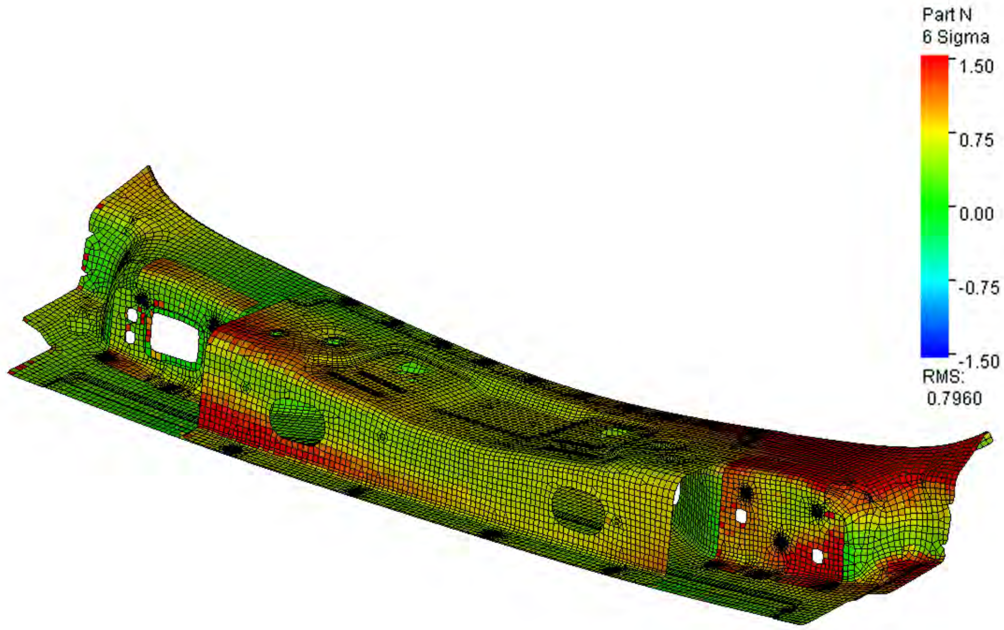


**Figure 4.13:** Deviation plot for synthesized data as input.

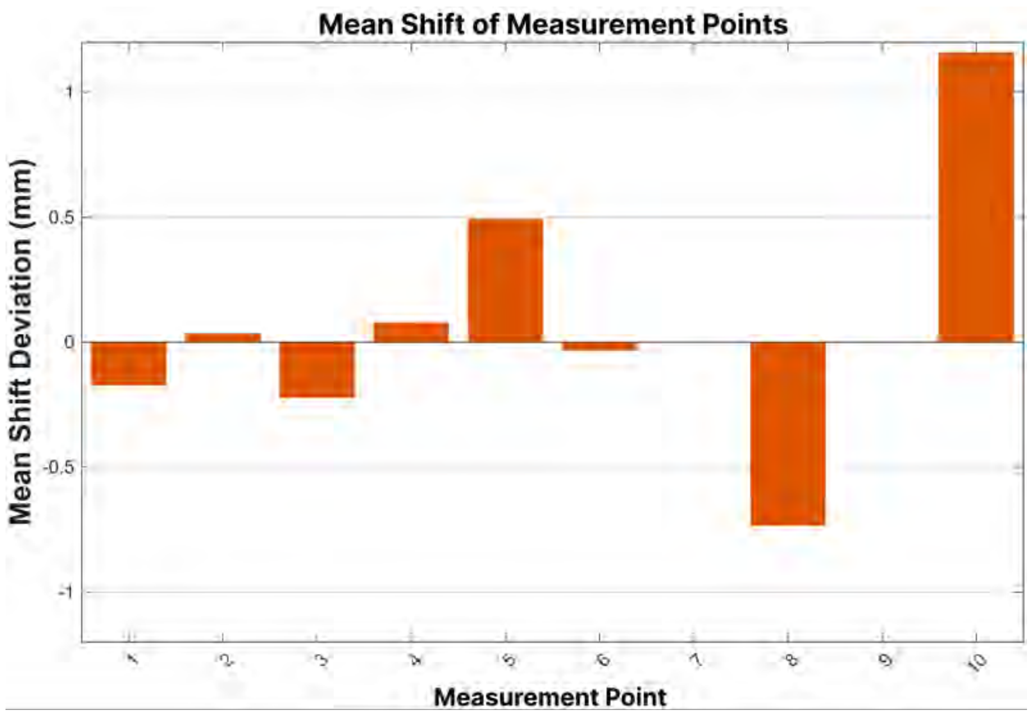


**Figure 4.14:** Mean shift of every measurement point for the model with synthesized data.

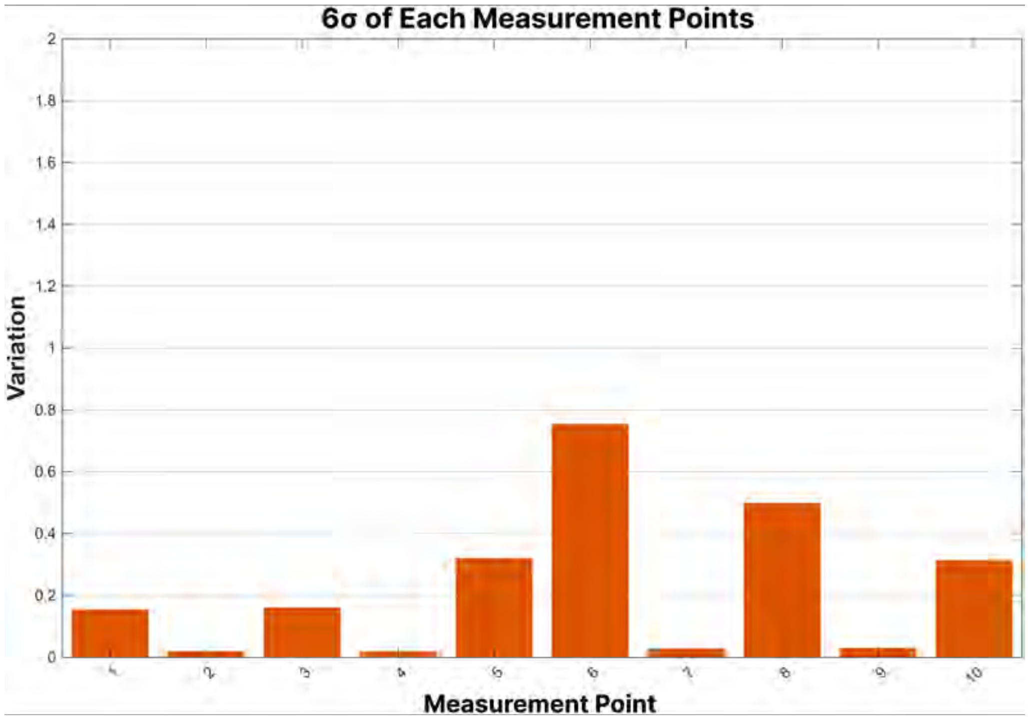


**Figure 4.15:** Variation in each measurement point for the model with synthesized data.

## 4.5 Simulation Influences

In order to verify possible influences on the simulation model, two verifications were ran. The first verification was gravity influence, since it is a compliant part which can deform due to gravity. The second verification was heat influence, since sheet metal can show heat influenced deformation. The two verifications are disclosed in under this section.

### 4.5.1 Gravity Influence

When applying gravity to the model with scan data as input, the RMS decreased by 0.041 mm in normal direction. Compared to the RMS of the model without gravity that is 0.299 mm in normal direction, it results in a 14% decrease. This is a significant change in the RMS, but not a significant enough to explain the deviation from the validation model. Since the verification model consists of one instance of input data, no variation is generated. Therefore, no variation plot is constructed for this case. The results from the measurement points is illustrated in Figure 4.18 displays without gravity influence and Figure 4.19 displays with gravity influence. The model influenced with gravity shows a slight positive movement in the measurement points that measure along the Z-axis and in normal direction from the surface (Z-axis, 8. and 10. N-direction, 5. and 6.). However, this amplitude is so small that it is not visible with the current scale. The biggest change occurred in the measurement point 10. with a value of 0.3 mm.

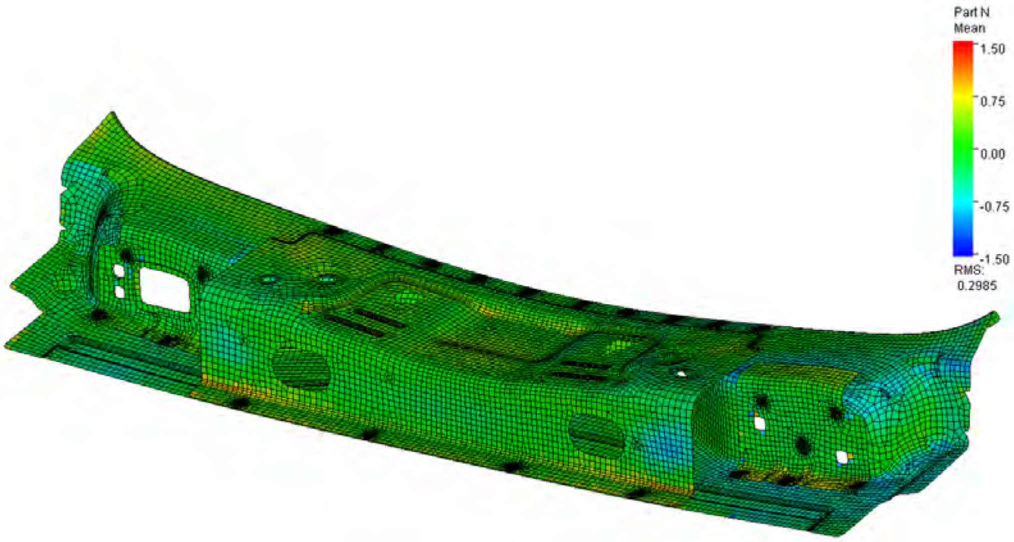


**Figure 4.16:** Deviation plot of the verification model.

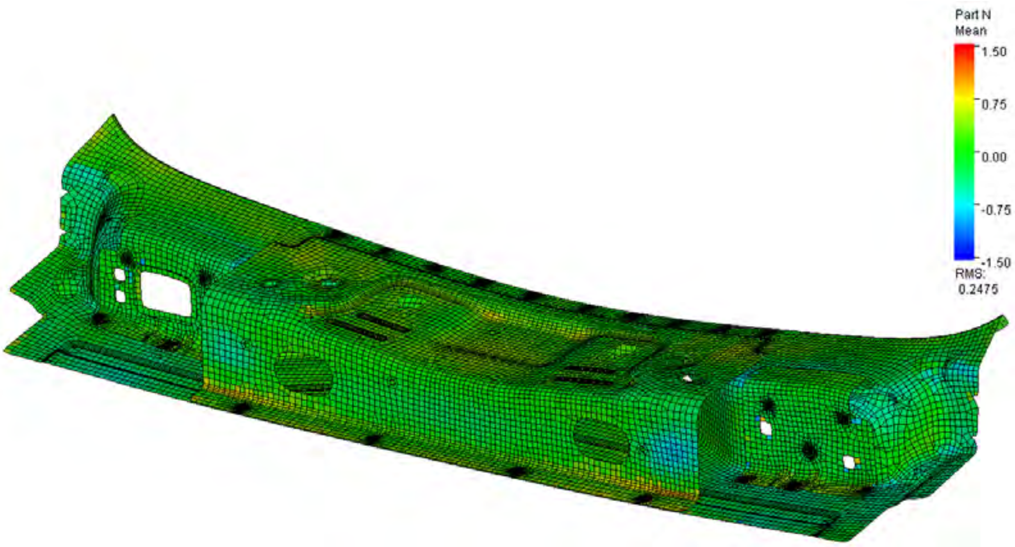


**Figure 4.17:** Deviation plot of the verification model under gravity influence.

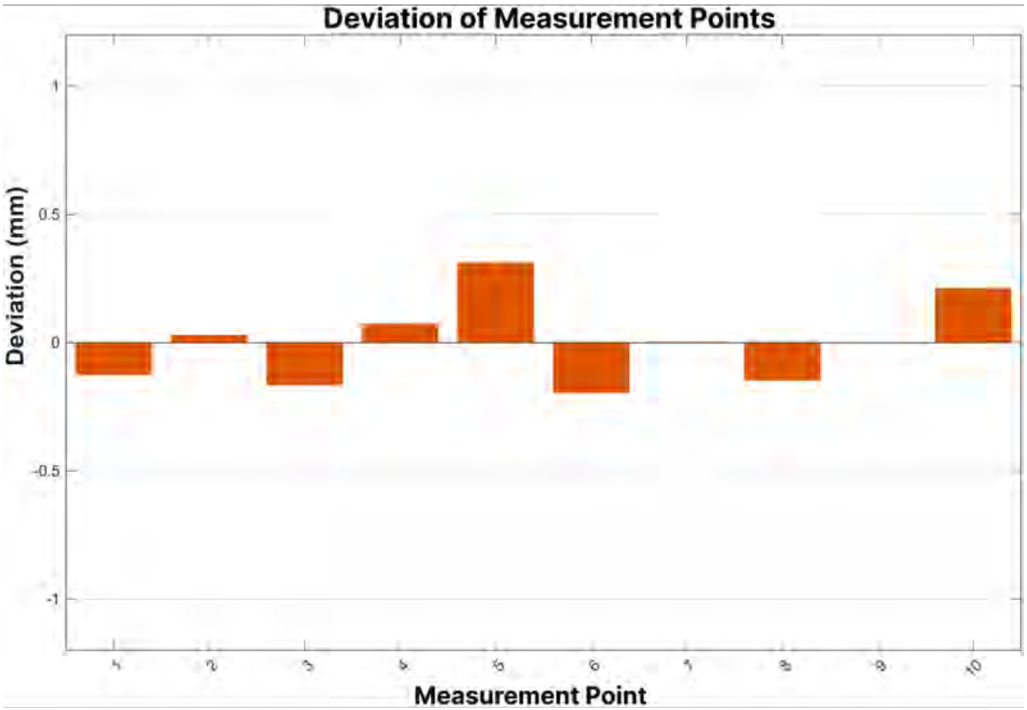


**Figure 4.18:** Deviation without gravity influence.

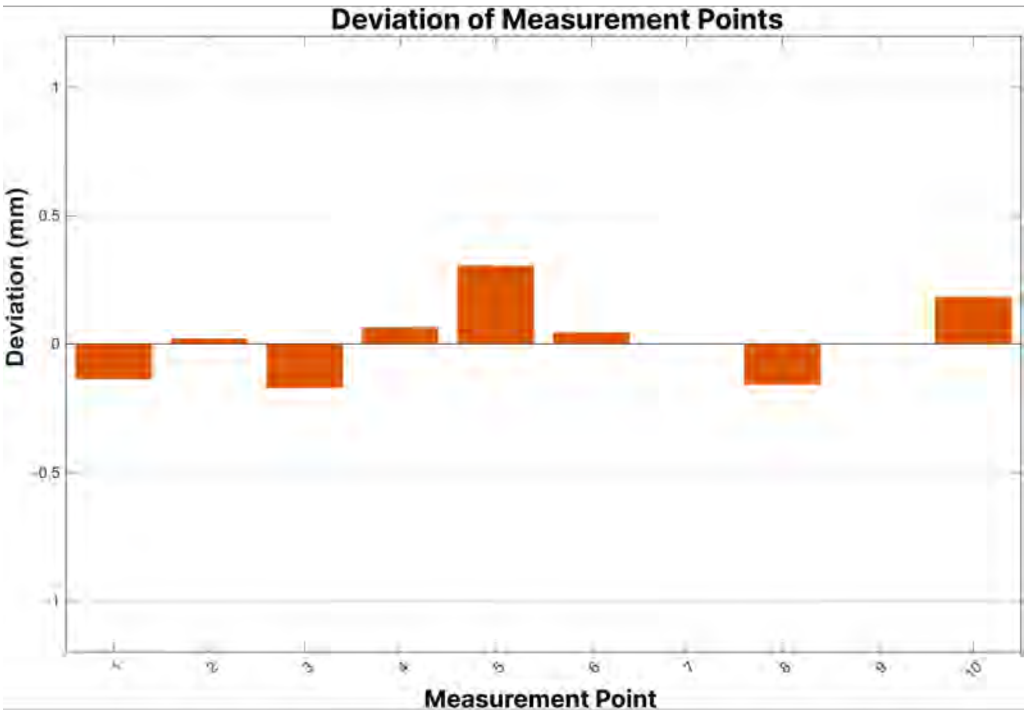


**Figure 4.19:** Deviation plot for the verification model with gravity influence.

### 4.5.2 Heat Influence

A heat influence analysis was conducted on the verification model. The heat influence generates a part deformation simulation, therefore no mean shift values could be extracted from the measurement points. With the influence of heat it showed a RMS of 0.071 mm in normal direction, illustrated in figure 4.20. Compared to the RMS of the verification model that shows a value of 0.2985 mm in normal direction, illustrated in Figure 4.11. The color map displays that most of the deviation occurs on the left side of the 600 part. With both the part RMS and color plot in consideration it can be deemed that heat influence is not a relevant contributor for this assembly.

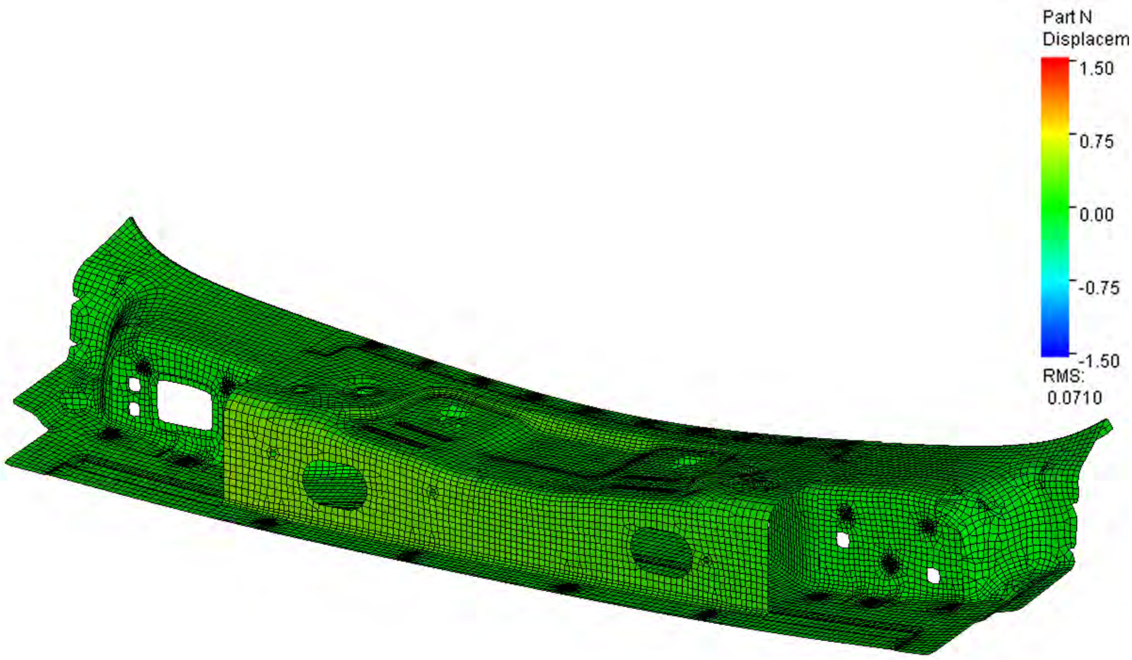


**Figure 4.20:** Deviation plot of simulation model with heat influence.

### 4.5.3 Contact Point Influence

A max contact point test was conducted on the verification model. With max contact points it shows a RMS of 0.2999 mm in normal direction, illustrated in Figure 4.21. Compared to the RMS of the verification model that shows a value of 0.2985 mm in normal direction, illustrated in Figure 4.11. The difference is is small enough to be considered as not a relevant influence over the simulation accuracy.

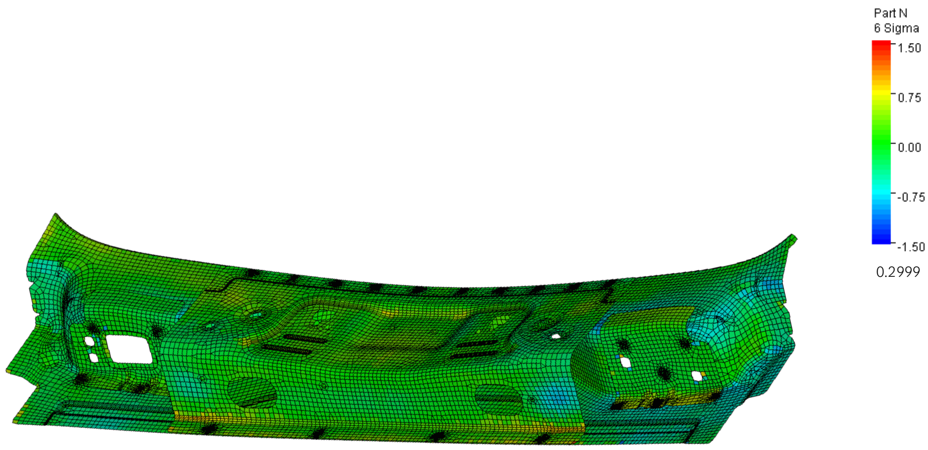


**Figure 4.21:** Deviation plot of simulation with max contact point test.

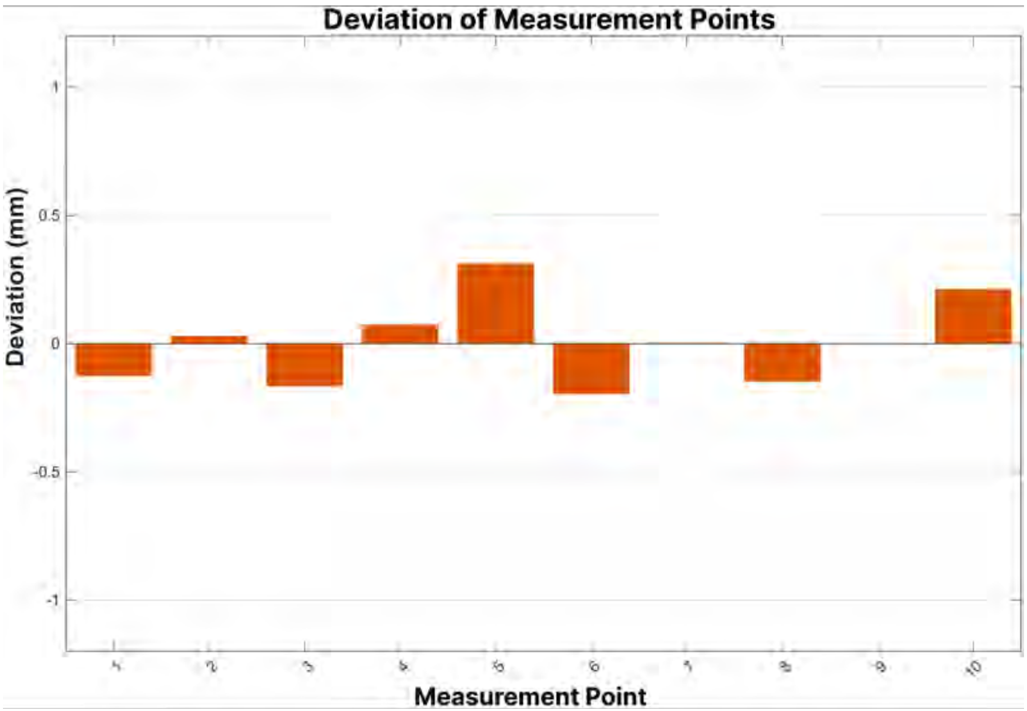


**Figure 4.22:** Mean shift of every measurement point during max contact point test.

## 4.6 Sensitivity Analysis

In this section the results from the sensitivity analysis is presented. First for the shimming and then for the weld sequence.

### 4.6.1 Shimming Sensitivity

The shimming sensitivity started by investigating the most feasible shimming points for the assembly. After running the script that scored all the different shimming points based on their global and local geometrical influence, the results showed that the baseline global deviation measure was $J$=0.029559. Furthermore, shim points 1, 2, 3, 4, and 5 (renamed for clarification purposes) showed the highest improvement potential and were therefore selected for the next step. Among these, shim point 1 gave the largest reduction in the global deviation measure, with an improvement of 0.010006 in the +2 mm direction. Shim point 2 showed a smaller global improvement, but improved the largest number of measurement points overall, improving 8 points while worsening only 2. The results of the five best shimming points can be seen in Table 4.1.

**Table 4.1:** Top five shimming points selected from the screening study.

| Shim point | Best direction | $J_{\text{best}}$ | Improvement $I_j$ | Improved points | Worsened points |
|---|---|---|---|---|---|
| 1 | +2 | 0.019553 | 0.010006 | 7 | 3 |
| 2 | +2 | 0.021363 | 0.008197 | 5 | 5 |
| 3 | -2 | 0.021378 | 0.008182 | 4 | 6 |
| 4 | -2 | 0.023452 | 0.006108 | 8 | 2 |
| 5 | +2 | 0.025931 | 0.003628 | 7 | 3 |

The five best shimming points can also be seen placed on the assembly in Figure 4.23. The points are named according to Table 4.1 above.

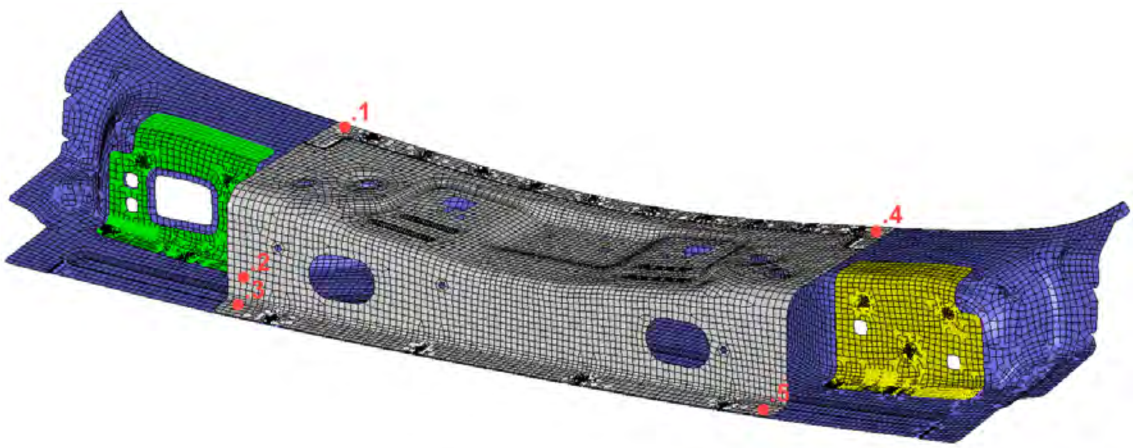


**Figure 4.23:** Shimming points location

After choosing the most feasible shimming points, the next step was to determine whether the assembly is sensitive to shimming or not based on the chosen shimming points and the range. The highest RMS value of the 3125 shimming combinations was 0.161632 and the lowest was 0.032211. Using these two values in Equation 3.4, the result is that the assembly's sensitivity towards shimming is 80.07%.

### 4.6.2 Weld Sequence Sensitivity

The welding sequence optimization was conducted through an internal optimization algorithm within RD&T. Using the Equation 3.4 we can conclude that the sensitivity to welding sequence for the verification model is 31.58% and for the nominal model 50%. The scanned data weld sequence can be seen in Figure 4.24 and nominal model weld sequence in Figure 4.25. The optimized weld sequence is illustrated in Figure 4.26.

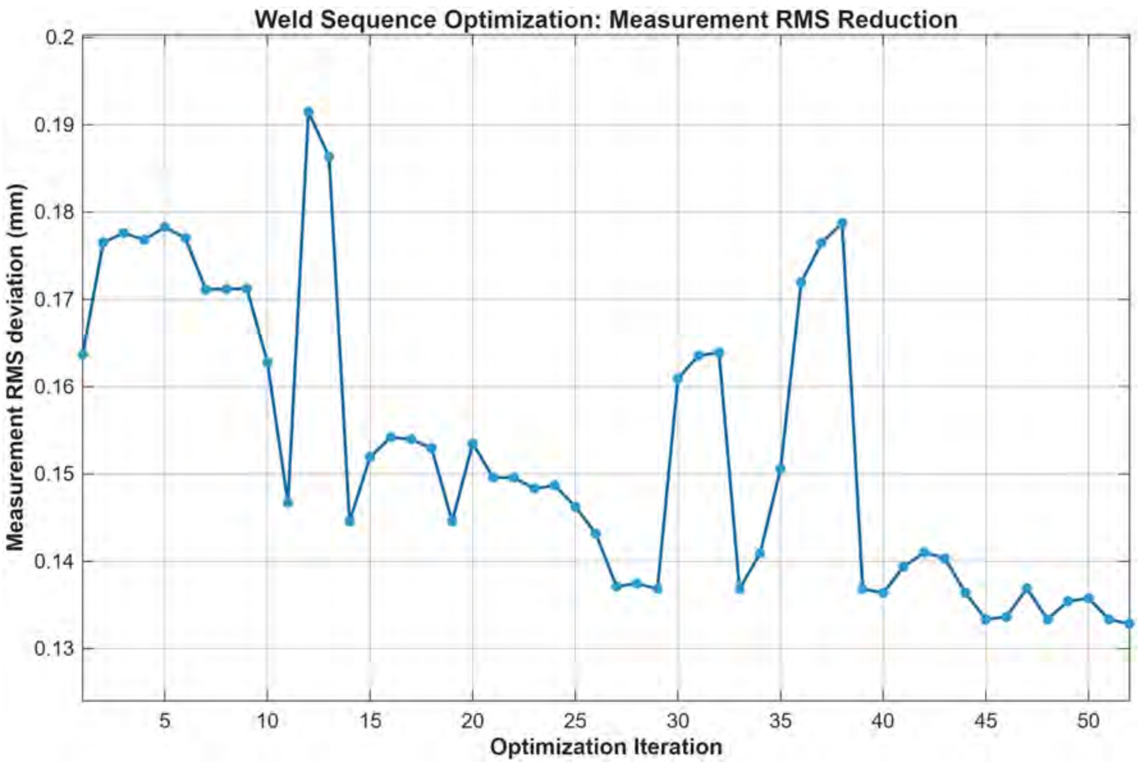


**Figure 4.24:** Weld sequence sensitivity for the model with scan data as input.

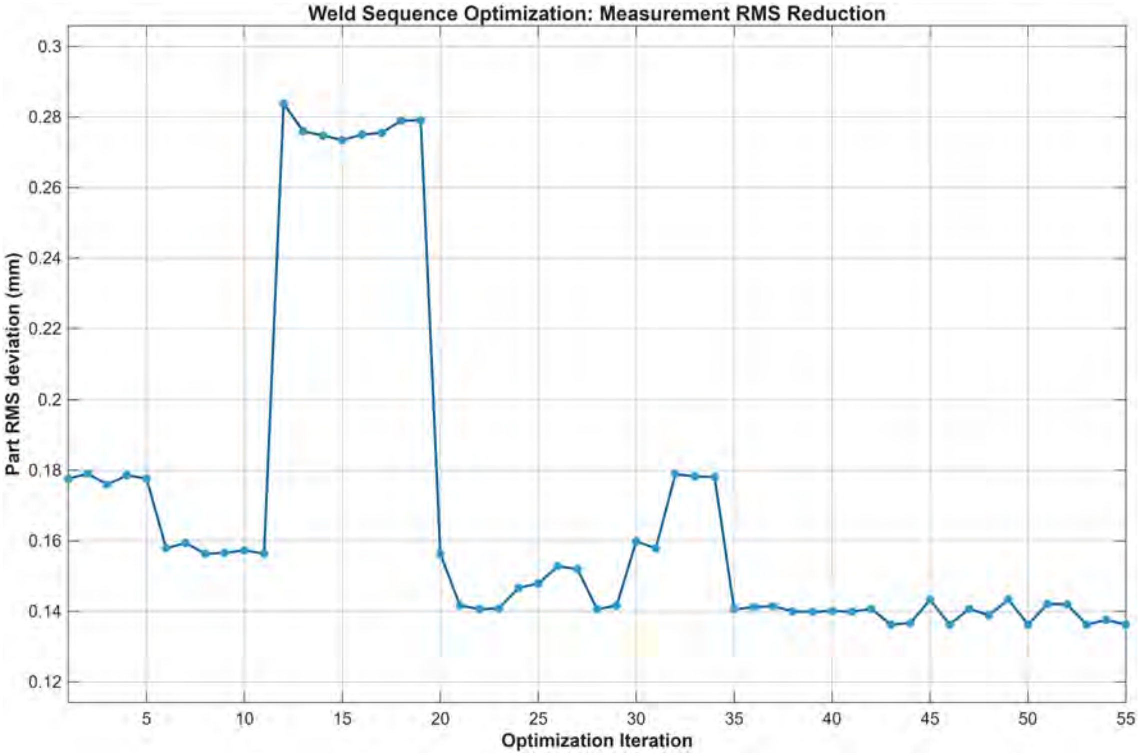


**Figure 4.25:** Weld sequence sensitivity for the nominal model with tolerances.

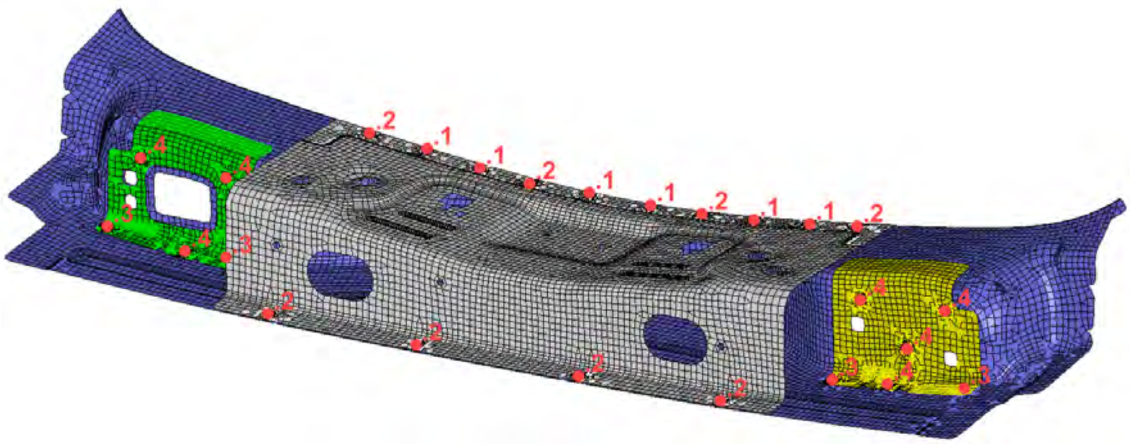

**Figure 4.26:** Optimized welding sequence.

## 4.7 Machine Learning

This section will present the results from the ML study. The results are divided into the prepared datasets, the quantile-based regression model, the PCA-based calibration model, comparison of the models and then the model selection.

### 4.7.1 Prepared Data for ML modeling

After preprocessing the measurement and simulation data, they were structured into a common format as shown in section 3.11.3 where each row represents one measurement point and each column represents one sample.

For the given assembly, there were a total of 10 common and individual measurement points. These points are shown in section 3.6. For each measurement point there was a total of 70 sample values from the measurement data. For the simulation, 100 sample values were gathered from the software RD&T. Furthermore, one case assembly was gathered with one set of measured single parts and one measured assembled assembly from the same single parts. The measures contained a scan and offset values in the 10 measurement points. The data is showcased below in Table 4.2

**Table 4.2:** Prepared data for ML modelling

| Dataset | Source | Nr. of measurement points | Nr. of samples | Use |
|---|---:|---:|---:|---:|
| Simulation data | RD&T variation simulation | 10 | 100 | Model input |
| Measured data | Physical assembly measurement | 10 | 70 | Calibration target |
| Scanned simulation case | RD&T with scan input | 10 | 1 | Case evaluation |
| Scanned assembly | Physical scan | 10 | 1 | Case evaluation |

The preprocessing also enabled newly exported CAT simulation result files to be converted into the same structure as the original simulation input table. This made it possible to apply the trained model to new simulation data using the same workflow.

### 4.7.2 Results from the Quantile-Based Regression Model

From the quantile-based regression model, both numerical and visual results were derived. In Table 4.3, the total RMSE and MAE for both the training and testing phase, is showcased. As seen, both the testing RMSE and MAE are higher than the training RMSE and MAE. It is also important to mention that the RMSE and MAE are based of the measurement points and not the overall RMS of the model.
Since the comparison is based on distribution, the improvement shows how well the predicted distributions match the measured distributions at point level on the measurement

**Table 4.3:** Training and testing performance of the quantile-based regression model

| Metric | Training | Testing |
|---|---|---|
| RMSE | 0.0011 | 0.0530 |
| MAE | 0.0008 | 0.0252 |

points. This means that it should not be interpreted as a complete case specific validation.

Furthermore, the RMSE for both the simulated and the predicted cases were derived. Comparing these, an improvement percentage based on the target was also calculated, to make it easier to interpret. This was done for each measurement point and can be seen in Table 4.4. The overall improvement based on calibration towards the target measures, was 90.22%, where all measurement points were improved. For the visual results, a his-

**Table 4.4:** RMSE and improvement results for the quantile-based model

| Measure | RMSE Simulation | RMSE Prediction | Improvement [%] |
|---|---|---|---|
| 1 | 0.20489 | 0.00613 | 97.009 |
| 2 | 0.28139 | 0.04275 | 84.808 |
| 3 | 0.16401 | 0.02296 | 85.999 |
| 4 | 0.13193 | 0.02304 | 82.534 |
| 5 | 0.25194 | 0.02353 | 90.660 |
| 6 | 0.31325 | 0.04126 | 86.829 |
| 7 | 0.16014 | 0.01133 | 92.926 |
| 8 | 0.28948 | 0.00907 | 96.867 |
| 9 | 0.08714 | 0.01109 | 87.273 |
| 10 | 0.41384 | 0.01102 | 97.336 |

togram plot with a Gaussian smoothed curve was derived for each measurement point. An example of these plots can be seen in Figure 4.27, where the results for measurement point 9 is shown. The plot showcases the percentage of values in different offset ranges. This is shown with a an overlaying histogram for the simulated, measured and predicted values. For further clarifications, a mean line for each dataset is also included. The visual results show that simulated values are calibrated towards the measured values. The rest of the result plots can be seen in Appendix C.1.

Furthermore, to visualize only the training and prediction results another plot from the same measurement point can be seen in Figure 4.28. The plot showcases each quantiles value for the simulated, measured and predicted dataset. In the plot, there are deviating points from the predicted dataset, that are not calibrated as close to the measure values like the rest. The plots for the other nine measurement points can be seen in Appendix C.1.

Lastly, to describe how the model operates, two separate workflow charts were created. One chart based of the training phase and one chart based of the prediction phase. The

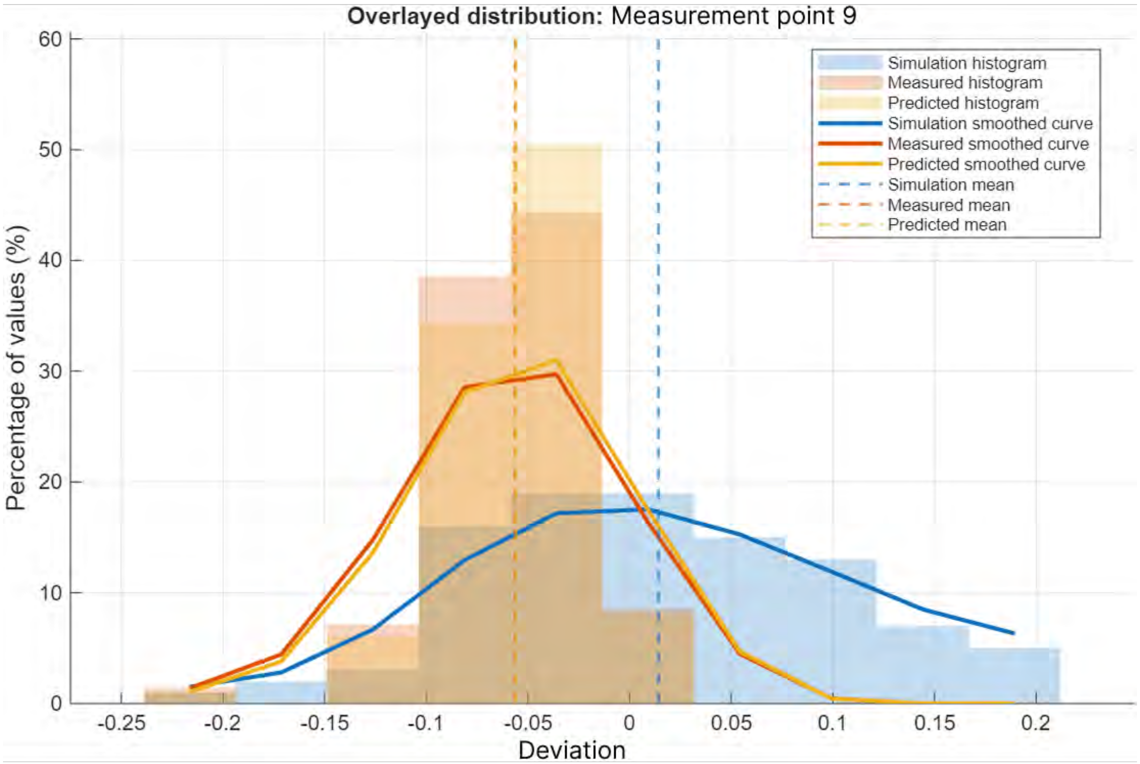


**Figure 4.27:** Histogram comparison on measurement point 9 in Y direction, for quantile-based model

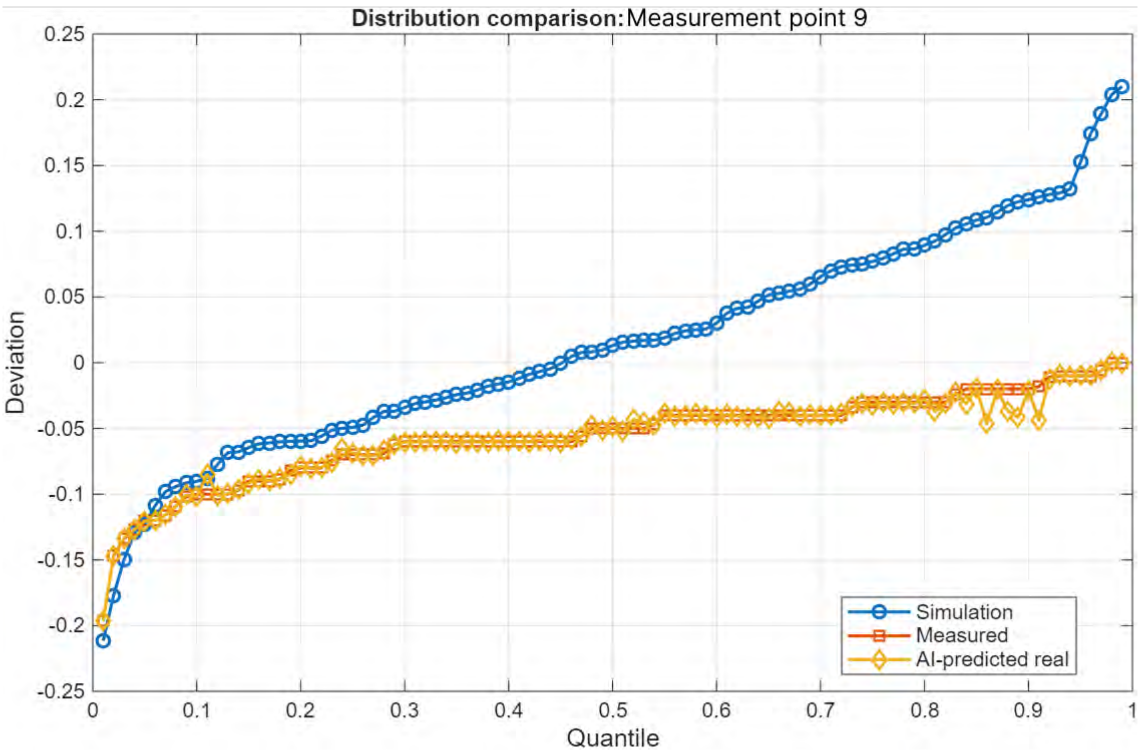


**Figure 4.28:** Quantile-based regression training and prediction in measurement point 9, Y direction

training phase chart can be seen in Figure 4.29. The workflow starts by showcasing simulation and measured data feature extraction based of the quantile grid that then trains and creates the regression model used in this case.

The chart for the prediction phase can be seen in Figure 4.30. This workflow showcases how new simulated data is used in the trained calibration model to predict the distribution and offsets.

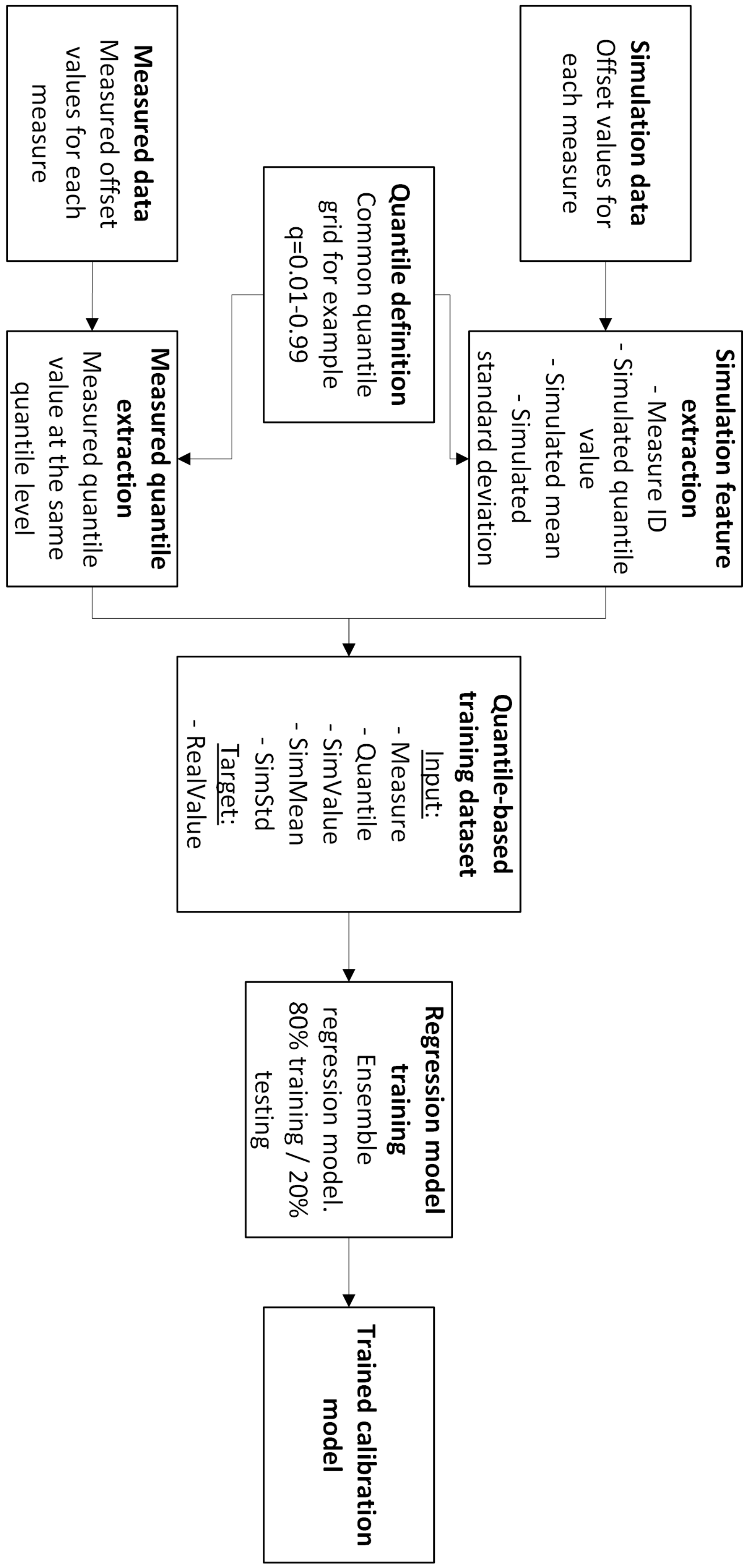


**Figure 4.29:** Quantile-based regression model workflow during training

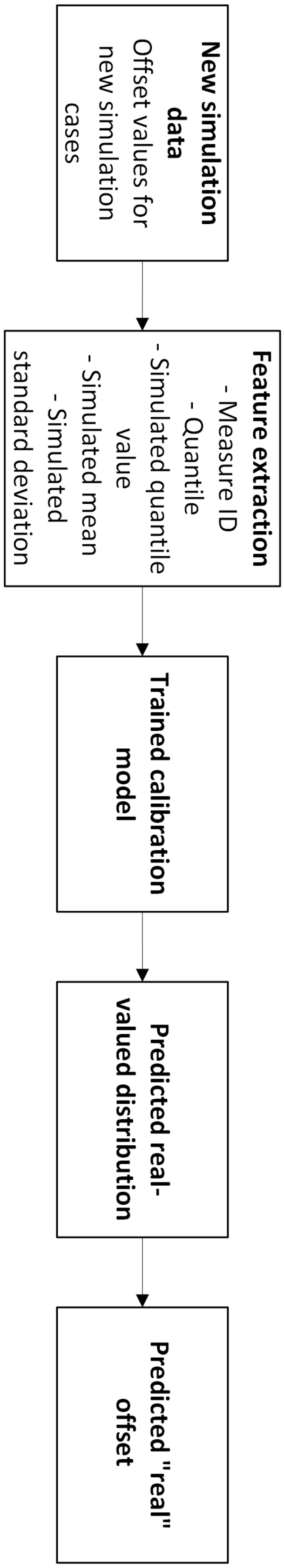


**Figure 4.30:** Quantile-based regression model workflow during prediction

### 4.7.3 Results from the PCA-Based State Calibration Model

The PCA analysis was first evaluated by studying how much variation was captured by each principal component. The first principal component captured 35.3656% of the total simulated variation, while the first six principal components together captured more than 90%. Therefore, six principal components were retained in the PCA-based model. The captured variation and cumulative captured variation from PC1 to PC10 can be seen in Table 4.5

**Table 4.5:** Variation captured by each principal component

| Principal Component | Variation Captured [%] | Cumulative Variation Captured [%] |
|---|---:|---:|
| PC1 | 35.3656 | 35.3656 |
| PC2 | 21.0625 | 56.4281 |
| PC3 | 11.5873 | 68.0154 |
| PC4 | 8.7004 | 76.7158 |
| PC5 | 7.8913 | 84.6071 |
| PC6 | 6.5829 | 91.1900 |
| PC7 | 3.1129 | 94.3029 |
| PC8 | 2.6252 | 96.9281 |
| PC9 | 2.2632 | 99.1913 |
| PC10 | 0.8087 | 100.0000 |

The six retained principal components were then used in the calibration model training. The RMSE and MAE in testing and prediction, for the corresponding principal component can be seen in Table 4.6. The training and testing errors varied between the principal components, indicating that the regression performance differed between the different variation modes.

**Table 4.6:** Training and testing performance for the PCA-based regression models

| PC | RMSE Training | MAE Training | RMSE Testing | MAE Testing |
|---|---:|---:|---:|---:|
| PC1 | 0.08112 | 0.02033 | 0.00616 | 0.00512 |
| PC2 | 0.02994 | 0.00863 | 0.05368 | 0.02979 |
| PC3 | 0.02219 | 0.00672 | 0.01355 | 0.00764 |
| PC4 | 0.04423 | 0.00968 | 0.05631 | 0.02838 |
| PC5 | 0.02096 | 0.00559 | 0.01961 | 0.01090 |
| PC6 | 0.01174 | 0.00356 | 0.02410 | 0.01389 |

After calibration in the PCA space, the predicted PC scores were reconstructed back to the original measurement point space. This made it possible to evaluate the PCA-based model using the same measurement points as the quantile-based model. The PCA-based model achieved a mean improvement of 42.94% across the measurement points. However, the improvement varied between measurement points, from 80.457% down to -18.226%. All the RMSE values and corresponding calibration improvement can be seen in Table 4.7.

**Table 4.7:** RMSE and improvement results for the PCA-based model

| Measure | RMSE Simulation | RMSE Prediction | Improvement [%] |
|---|---|---|---|
| 1 | 0.20489 | 0.06693 | 67.335 |
| 2 | 0.28139 | 0.06966 | 75.244 |
| 3 | 0.16401 | 0.03205 | 80.457 |
| 4 | 0.13193 | 0.07061 | 46.477 |
| 5 | 0.25194 | 0.04978 | 80.243 |
| 6 | 0.31325 | 0.09702 | 69.028 |
| 7 | 0.16014 | 0.18932 | -18.226 |
| 8 | 0.28948 | 0.24266 | 16.174 |
| 9 | 0.08714 | 0.07408 | 14.983 |
| 10 | 0.41384 | 0.42338 | -2.305 |

The result was then visualized the same way as for the quantile-model, in order to be comparable. A histogram plot corresponding to the same measurement point as for the quantile-based model can be seen in Figure 4.31. The figure shows that for this measurement point, it was not able to calibrate the input values. The histogram plots for the remaining measurement points can be seen in Appendix C.2.

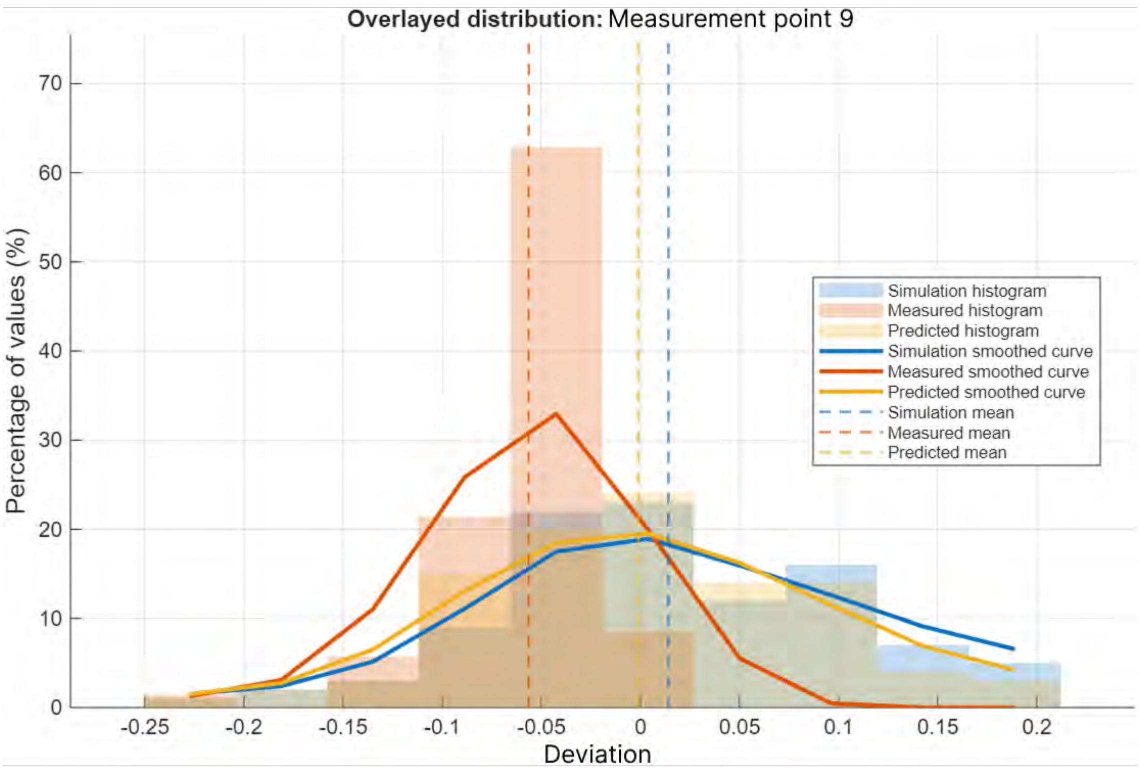


**Figure 4.31:** Histogram comparison on measurement point 9 in Y direction, for PCA-based model

Furthermore, a plot showing the quantile values for the simulation, prediction and measured cases is showed in Figure 4.32. This plot also shows that the PCA-based calibration model was not able to calibrate the simulated input values. The plots for the remaining measurement points can be seen in Appendix C.2.

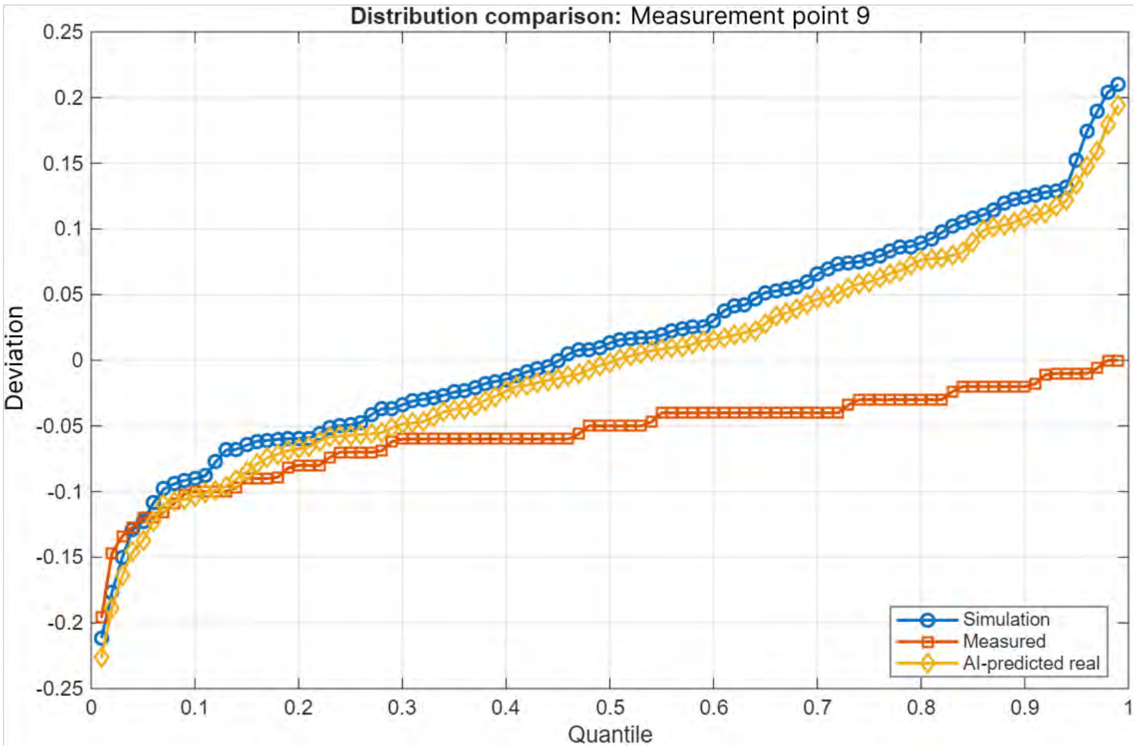


**Figure 4.32:** PCA-based regression training and prediction in measurement point 9, Y direction

Lastly, to describe how the model operates, two separate workflow charts were created. One chart based of the training phase and one chart based of the prediction phase. The training phase chart can be seen in Figure 4.33. The workflow starts by showcasing how simulation data is reconstructed into a PCA state space and how the measured data is projected into the same state space. Afterwards, the datasets are used as input and target to train a regression calibration model.

The prediction phase workflow chart can be seen in Figure 4.34. The workflow shows how new simulated data is projected into a PCA state space which is used as the input for the trained calibration model. The model then calibrate the PC scores and reconstruct it back to represent the measurement points.

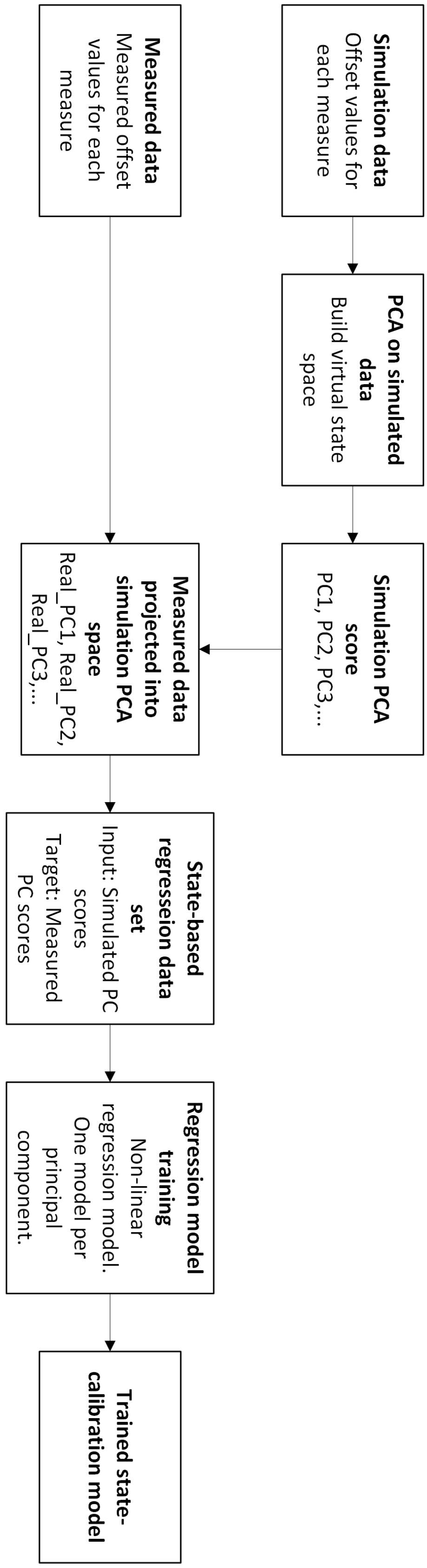


**Figure 4.33:** PCA-based regression model workflow during training

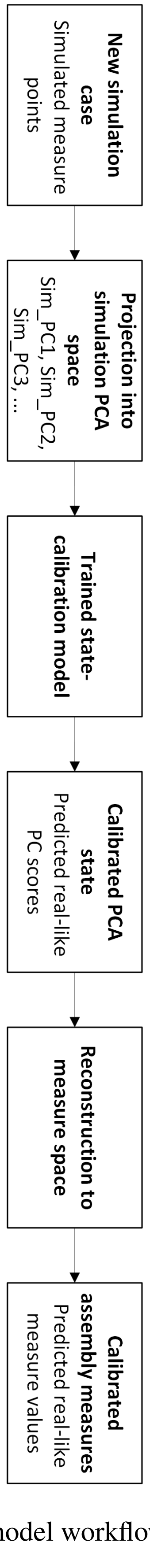


**Figure 4.34:** PCA-based regression model workflow during prediction

### 4.7.4 Comparison of Model Candidates

The model candidates were compared based on compatibility with available data, predictive performance, interpretability, data requirements and relevance for a digital twin workflow. The comparison was structured into a table that is showcased in Table 4.8, where each ML model is compared to every criterion. The comparison shows that the quantile-based model was most compatible with the available simulation and measurement data. The PCA-based model was more compatible to a digital twin with the state representation, but less consistent performance wise. The digital twin model was considered the most compatible to a digital twin as it's only conceptual, but unable to be constructed with the available data.

**Table 4.8:** Comparison of ML model candidates

| Criterion | Quantile-based model | PCA-based model | Future case-based DT model |
|---|---|---|---|
| Works with current data | Yes | Yes | No |
| Requires 1–1 case mapping | No | No | Yes |
| Main output | Calibrated measure distributions | Calibrated geometric state reconstructed to measures | Case-specific assembly prediction |
| Predictive performance | Best / most consistent | Mixed / less consistent | Not evaluated |
| Digital twin relevance | Calibration layer | State representation | Full DT concept |
| Interpretability | High | Medium | Depends on implementation |
| Data requirement | Moderate | Moderate | High |

### 4.7.5 Selected ML Model for the Proposed Workflow

The outcome of the model comparison resulted in the selection of the quantile-based regression model, as the ML model for the proposed workflow. It matched the available data structure, since it did not require traceable one-to-one cases between simulation and measurement. It also provided direct measurement-point-level calibration and was easier to integrate with new CAT simulation outputs.

The selected model should therefore be seen as a simulation-to-measurement calibration model. It improves the simulation output by learning distribution-level differences between simulated and measured data. However, it does not yet result in a full digital twin model. A full digital twin-based model would require traceable scanned single part data before assembly, measured assembly data after assembly, and process parameters such as shimming, locators and weld sequence.

## 4.8 Identified Gaps and Method Requirements

The identified gaps from the exploratory case study were translated into requirements for the construction of the proposed method and workflow. These identified gaps, their impact on the geometry assurance process, and the resulting requirements are detailed in Table 4.9.

**Table 4.9:** Identified gaps and the resulting requirements for the proposed method.

| Identified Gap | Impact on the Geometry Assurance Process | Method Requirement |
|---|---|---|
| **Data Breaks** Shimming and welding adjustments in production are not fed back into the PDM system. | Input data for simulations rely on nominal data, not actual process parameters reducing accuracy | **Closed-Loop** The method should showcase a feedback loop to highlight the need to update process parameters for simulations. |
| **Rigid & Non-Rigid Workflow** Rigid & non-rigid simulations conducted in separate workflows | Detached workflow, rigid simulations fails to capture physical deformation. | **Compliant Simulation:** The method must utilize non-rigid variation simulations as the standard analytical tool for sheet metal. |
| **Simulation Outcome Storage** Results from simulations are stored in .pdf or .ppx formats for decision making. | Creates a disconnected data loop for reuse of result data. | **Data storage and Loop:** The result data should be stored in supported file formats so it can be used in ML or CAT integration. |
| **Traceable Scan Data Between Single Parts and Assembly** To enable a digital twin-based workflow, traceable data is required. | Cannot tell exactly which factor leads to which deformation, leading to assumed optimizations. | **Scanned Single Parts and Assemblies:** The workflow must incorporate linked scanned data between single parts and assemblies to enable a digital twin-based workflow. |

## 4.9 Proposed Geometry Assurance Workflow

From the exploratory cases study, gaps, and method requirements a proposed geometry assurance workflow was constructed. The overview of the workflow showcases how the simulation workflow connects to the ML model which also connects to the physical process, and how this data flow can create a bi-loop for the process. This overview is illustrated in figure 4.35. The important highlights is connected to the first and fourth requirement, that showcases how the process optimizations are traceable and links back to the simulation workflow and ML calibration model. Furthermore, it displays a data flow for the traceable scan data that trains the is used within the ML calibration model and feeds back to the non rigid simulation workflow through it.

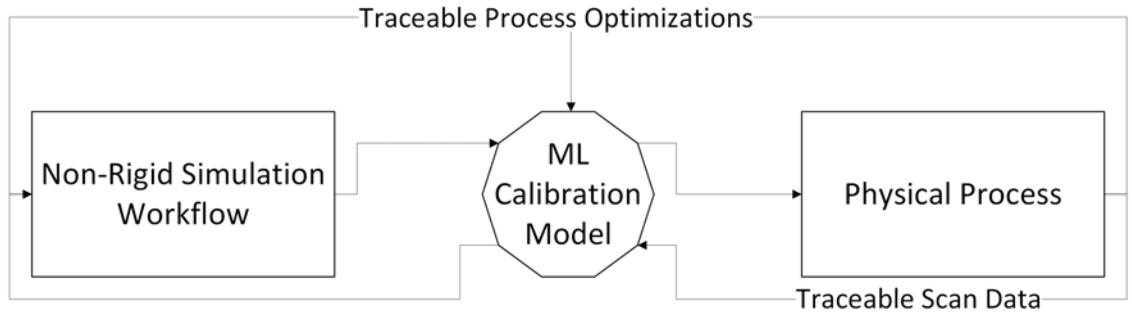


**Figure 4.35:** Overview of the proposed geometry assurance workflow.

The details of the data traceability and process optimizations are illustrated in figure 4.36. The top row showcases the geometry assurance process and the three columns describe the ML model, real process, and the simulation process. With this traceability of scan data that both trains the ML and is used as input in the simulation, and the traceability of the process optimizations — enables a digital twin-based geometry assurance workflow. The black arrows showcases how the data moves in between the different processes and supports them. Furthermore, the arrows showcases how the scanned assembly after the optimization feeds back to the start to iteratively improve the physical process using the digital representation.

The proposed non-rigid simulation workflow is illustrated in figure 4.37. The workflow details the necessary steps in order to enable a digital twin-based non-rigid simulation workflow. It starts with input data gathering and ends with storage of result data. The verification of the simulation model requires decision based on available data. A decision tree for this step can be seen in Appendix B.

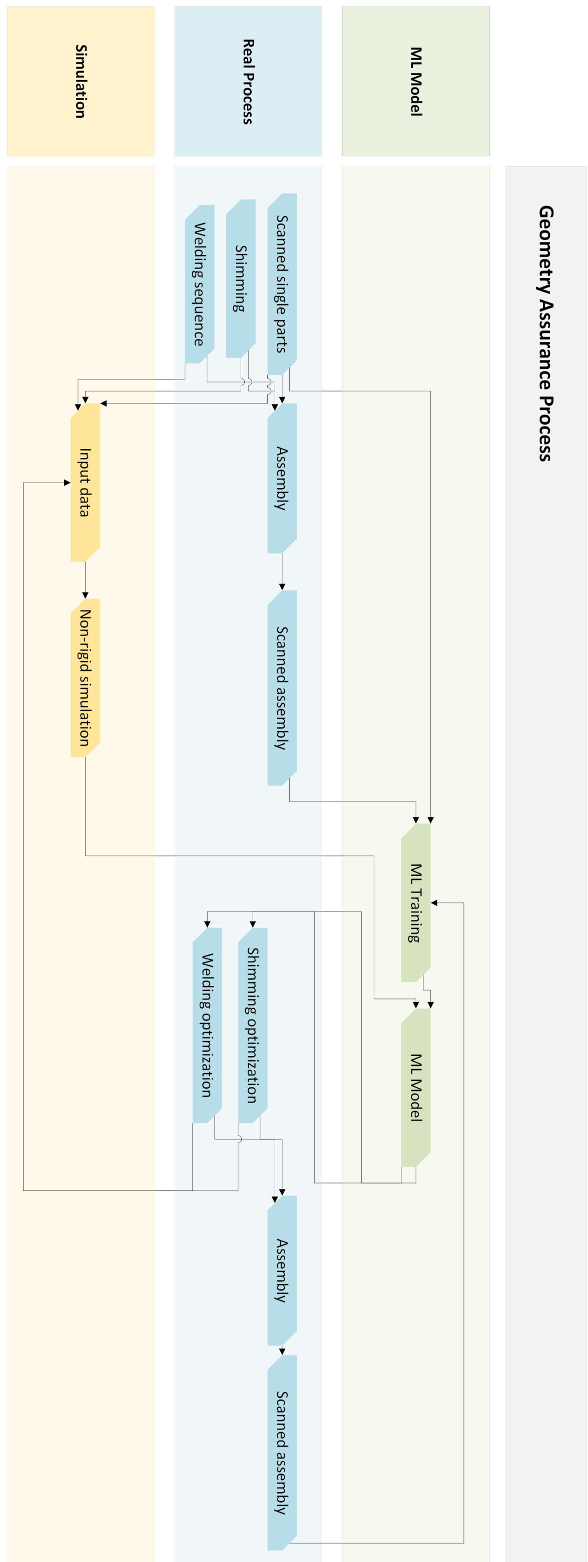


**Figure 4.36:** Data flow that enables a digital twin-based geometry assurance process.

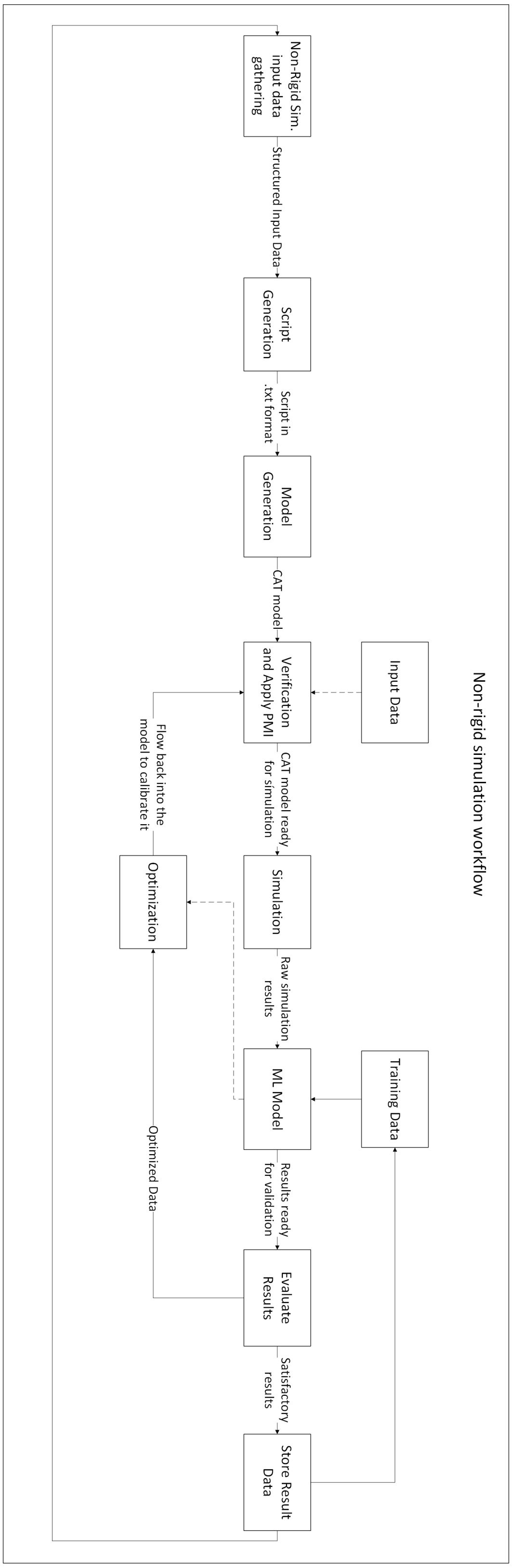


**Figure 4.37:** Proposed non-rigid simulation workflow.

# 4.10 Method Evaluation

This section presents the findings from the rear roof frame case study. The case study showed partial agreement between the simulated and physical outcomes, while differences remained in both magnitude and location. Furthermore, despite the previously identified breaks in the data flow, the integration of optimization analyses and an ML calibration model demonstrates significant potential for establishing a robust, digital twin-based geometry assurance framework.

## 4.10.1 Scanned Assembly

The verification assembly consists of a scanned assembly, with a traceability link to its single parts. The deviation the assembly shows from nominal geometry is illustrated in a color plot, which can be seen in figure 4.38. Furthermore, the assembly was measured according to the measurement points. The mean shift of each measurement point is illustrated in figure 4.39.

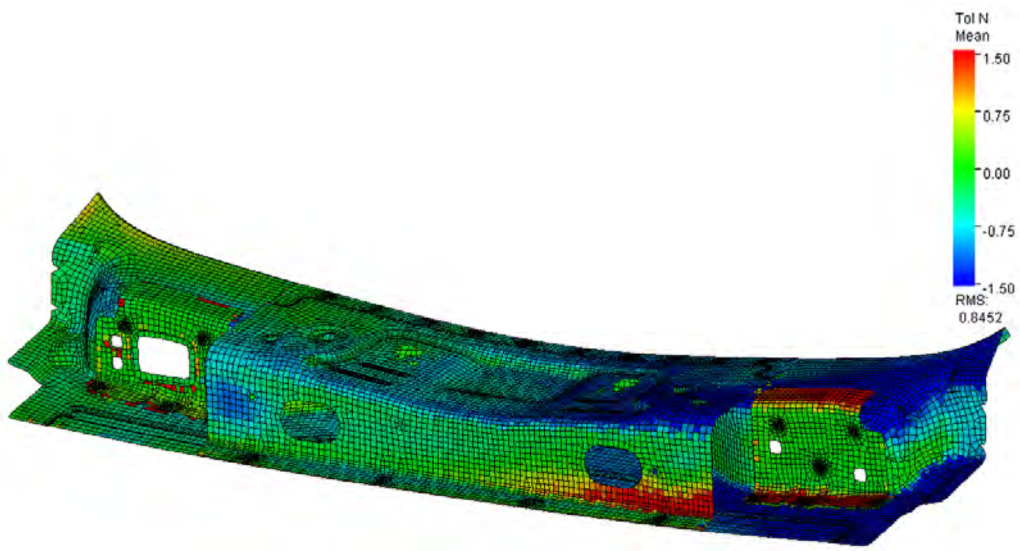


**Figure 4.38:** Deviation in normal direction of the scanned assembly compared to nominal geometry.

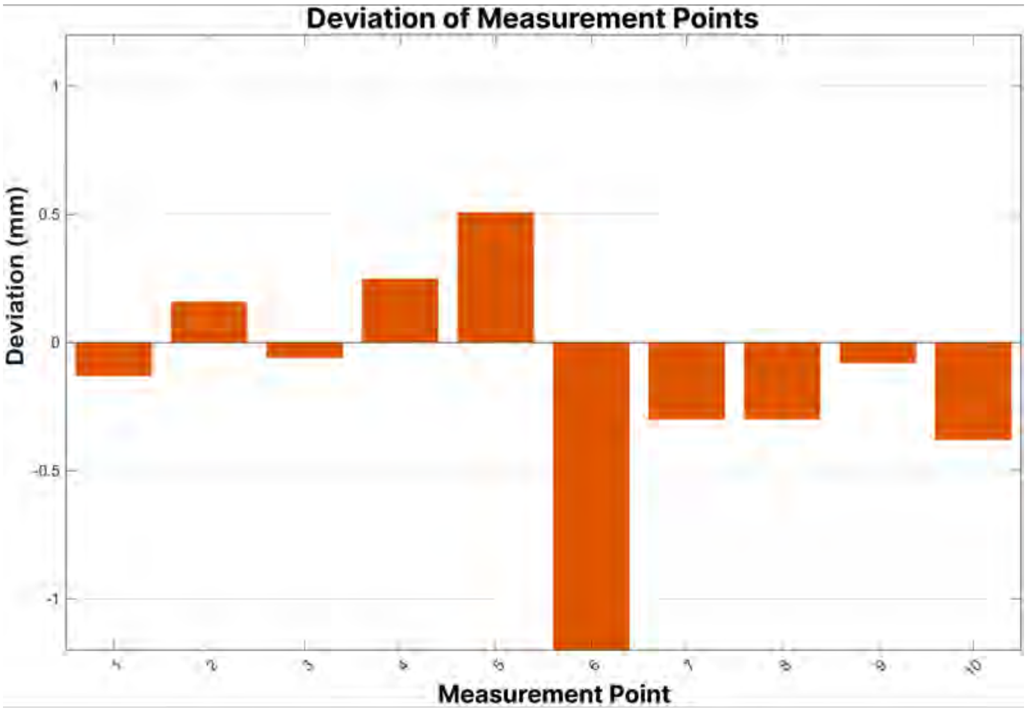


**Figure 4.39:** Deviation of every measurement point of the scanned assembly.

### 4.10.2 Evaluation Inputs and Physical Baseline

The 3D scans of the single parts (before assembly) yielded the input data required for the workflow. It was digitalized as STL files. The 3D scans together with nominal meshes marked the data gathering phase as complete.

### 4.10.3 Initial Simulation Model

The initial simulation model was constructed using the meshes based on nominal CAD geometry, with input data in the form of the STL scan data of the single parts. Referring to the decision tree for verifying the simulation model in Appendix B, B.1, the decision tree provided a sufficient guide to verify and finalize the simulation model.

### 4.10.4 ML Implementation

The variation analysis results based on the scanned single parts were then used in the trainedML model to predict the outcome of the measurement points offsets. As stated before, the quantile-based regression calibration model was the chosen model for the workflow. Furthermore, the scanned assembly measurements were used as the reference for this case in order to compare the outcome.

For each of the 10 measurement points, the input value from the scanned simulation was processed through the trained quantile-based regression model. The input values were then calibrated with the model, predicting new offset values intended to represent the real outcome. The calibrated predicted values were compared with measurement values for both the scanned single part simulation and the scanned assembly, which can be seen in Figure 4.40. The plot also contains the improvement for each measurement point.

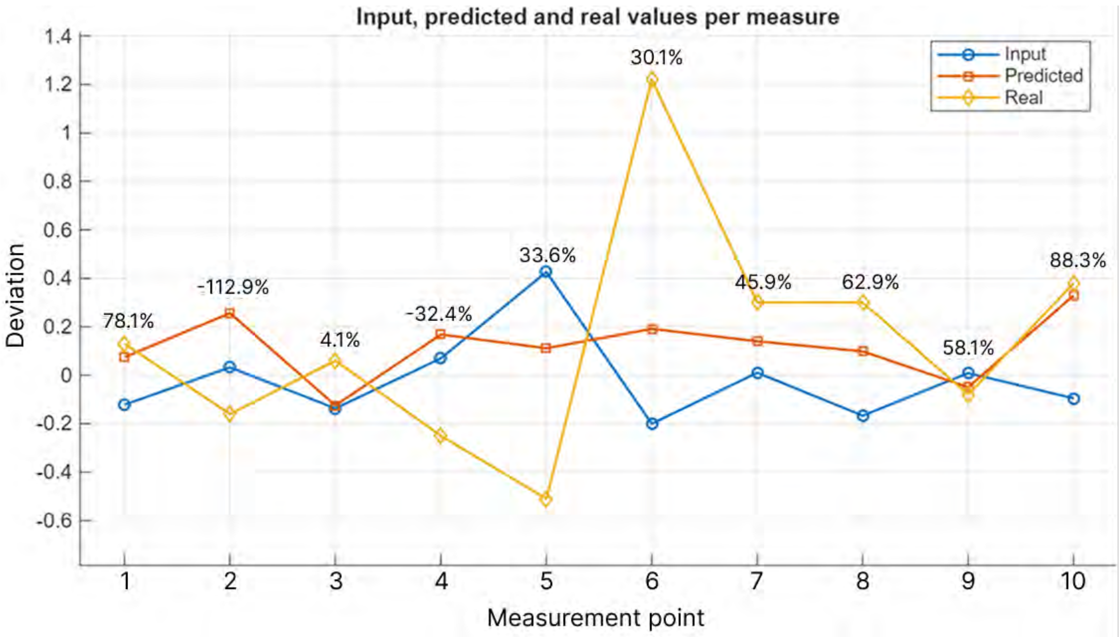


**Figure 4.40:** Prediction outcome of scanned simulation

The result for each measurement point is shown in Table 4.10. Since the case study contains one value per measurement point, the measurement error is presented as absolute error. The overall RMSE and MAE values are instead calculated across all ten measurement points. The results show that eight out of ten measurement points were improved after ML calibration, while two measurement points were shifted further away from the measured assembly value.

**Table 4.10:** Measurement point results for the selected ML model on the scanned simulation case

| Measure | Input Value | Predicted Value | Real Value | Input Error | Prediction Error | Improvement [%] |
|---|---|---|---|---|---|---|
| 1 | -0.12200 | 0.07488 | 0.13000 | 0.25200 | 0.05512 | 78.128 |
| 2 | 0.03240 | 0.24968 | -0.16000 | 0.19240 | 0.40968 | -112.930 |
| 3 | -0.13700 | -0.12898 | 0.06000 | 0.19700 | 0.18898 | 4.069 |
| 4 | 0.06960 | 0.17329 | -0.25000 | 0.31960 | 0.42329 | -32.445 |
| 5 | 0.42600 | 0.11110 | -0.51000 | 0.93600 | 0.62110 | 33.643 |
| 6 | -0.20000 | 0.22744 | 1.22000 | 1.42000 | 0.99256 | 30.101 |
| 7 | 0.01030 | 0.14338 | 0.30000 | 0.28970 | 0.15662 | 45.938 |
| 8 | -0.16700 | 0.12687 | 0.30000 | 0.46700 | 0.17313 | 62.928 |
| 9 | 0.00874 | -0.04281 | -0.08000 | 0.08874 | 0.03719 | 58.095 |
| 10 | -0.09550 | 0.32456 | 0.38000 | 0.47550 | 0.05544 | 88.341 |

Lastly, the RMSE and MAE was calculated across the 10 measurement points. The result is shown in Table 4.11. The result shows that both the MAE and RMSE decreases with the ML calibration with an improvement of 32.88% in MAE and 29.66% in RMSE.

**Table 4.11:** Overall results of the selected ML model on the scanned simulation case

| Metric | Before ML calibration | After ML calibration | Improvement [%] |
|---|---|---|---|
| MAE | 0.46379 | 0.31131 | 32.88 |
| RMSE | 0.60580 | 0.42611 | 29.66 |

### 4.10.5 Shimming Sensitivty Analysis

After the ML prediction, the results were saved and used to investigate what amount of shimming that would be best fitted. The shimming points were directly based of the 5 shimming points chosen earlier. The results can be seen in Figure 4.41. As seen in the plot, only one measurement point was located outside the acceptable limits before the shimming, but was moved due to the shimming.

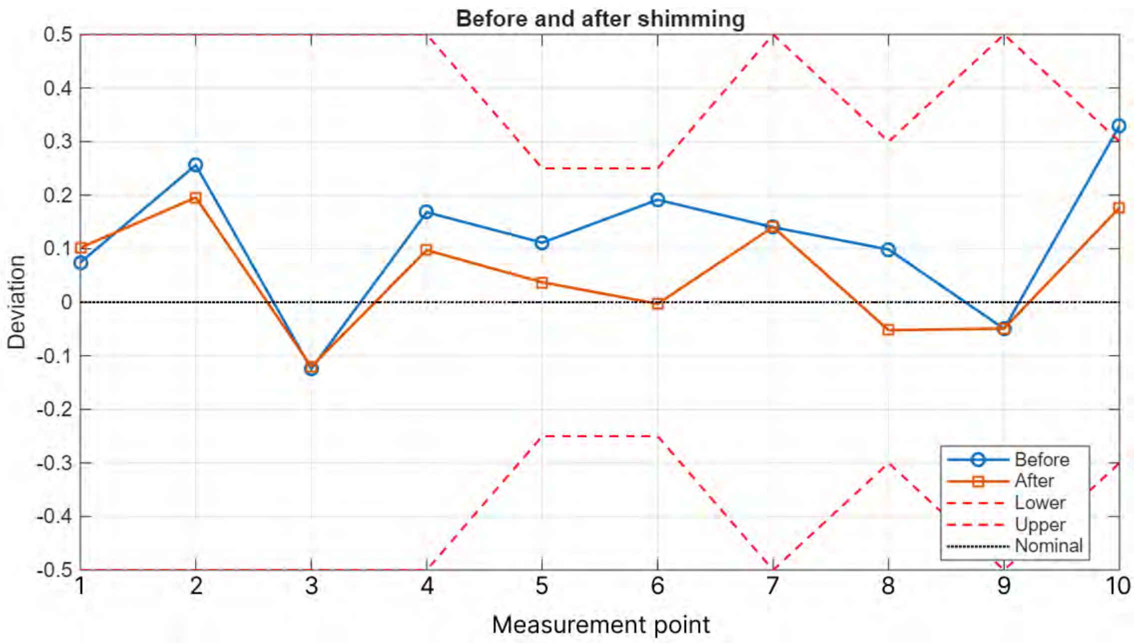


**Figure 4.41:** Deviation before and after shimming

The results on how much each shimming points should be deviated in order to generate the plot in Figure 4.41, can be seen in Table 4.12.

**Table 4.12:** Shimming values for each shimming point

| Shimming point | Shim value [mm] |
|---|---|
| Shim 1 | -1 |
| Shim 2 | -2 |
| Shim 3 | 2 |
| Shim 4 | 1 |
| Shim 5 | 2 |

The scoring results for the top five shimming combinations can be seen in Table 4.13. As seen in the results, the five top contenders had no points outside the limits, which made centering the ranking factor.

**Table 4.13:** Top five shimming candidates based on the AI-predicted target

| Case ID | Shim 1 [mm] | Shim 2 [mm] | Shim 3 [mm] | Shim 4 [mm] | Shim 5 [mm] | OutCount | ViolationScore | CenteringScore |
|---|---|---|---|---|---|---|---|---|
| 2617 | -1 | -2 | 2 | 1 | 2 | 0 | 0 | 0.97877 |
| 2623 | 0 | -2 | 2 | 2 | 2 | 0 | 0 | 0.97892 |
| 2622 | -1 | -2 | 2 | 2 | 2 | 0 | 0 | 0.98347 |
| 2611 | -2 | -2 | 2 | 0 | 2 | 0 | 0 | 0.99829 |
| 2616 | -2 | -2 | 2 | 1 | 2 | 0 | 0 | 1.02170 |

As most of the measurement points deviation in the ML predicted values, were located inside acceptable tolerance limits, a test with the scanned assembly values was also conducted. The results can be seen in Figure 4.42. In this plot, only one out of three measurement points was able to be shimmed and moved into acceptable tolerance limits. This suggests that the shim is too low or the shimming points location are flawed.

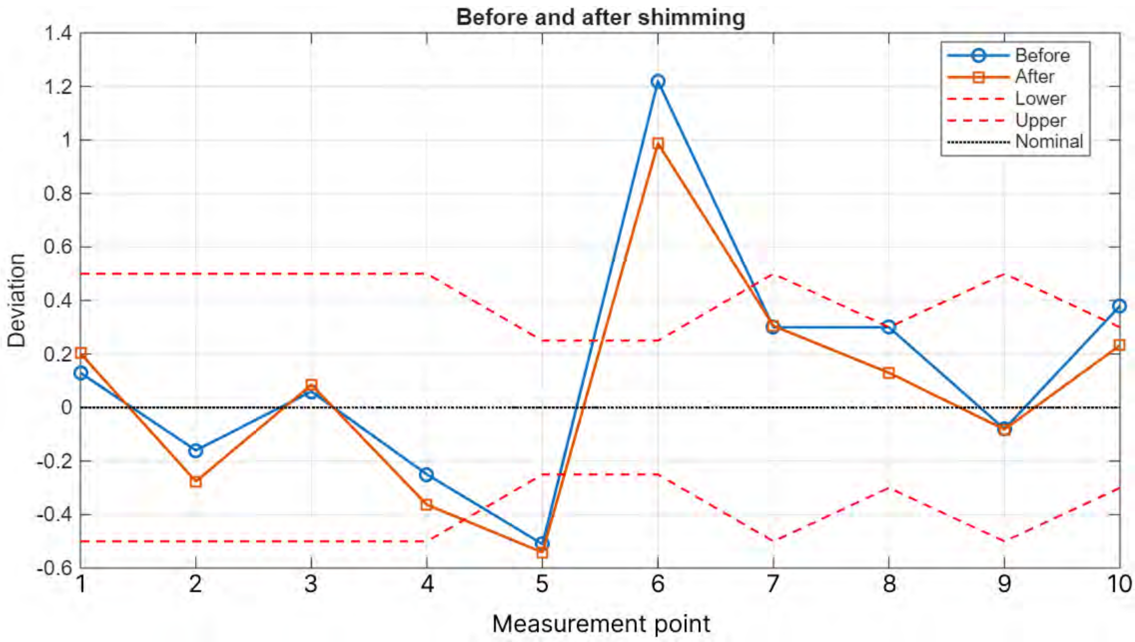


**Figure 4.42:** Deviation before and after shimming with scanned assembly

The results on how much each shimming points should be deviated in order to generate the plot in Figure 4.42, can be seen in Table 4.14.

**Table 4.14:** Shimming values for each shimming points in scanned assembly

| Shimming point | Shim value [mm] |
|---|---|
| Shim 1 | -2 |
| Shim 2 | -2 |
| Shim 3 | 2 |
| Shim 4 | -2 |
| Shim 5 | 2 |

The suggested shimming was used as an input in the verification simulation model. The color plot with the optimized shimming as input is illustrated in Figure 4.43 and the deviation values in Figure 4.44. The color plot shows promising results, showing the same deviation pattern as the scanned assembly, with just a few inconsistencies. The measurement point deviation plot shows the same pattern as the scanned assembly, but with less magnitude. Since the model consists of a single instance of input data, no variation is generated. Therefore, no variation plot is constructed for this case.

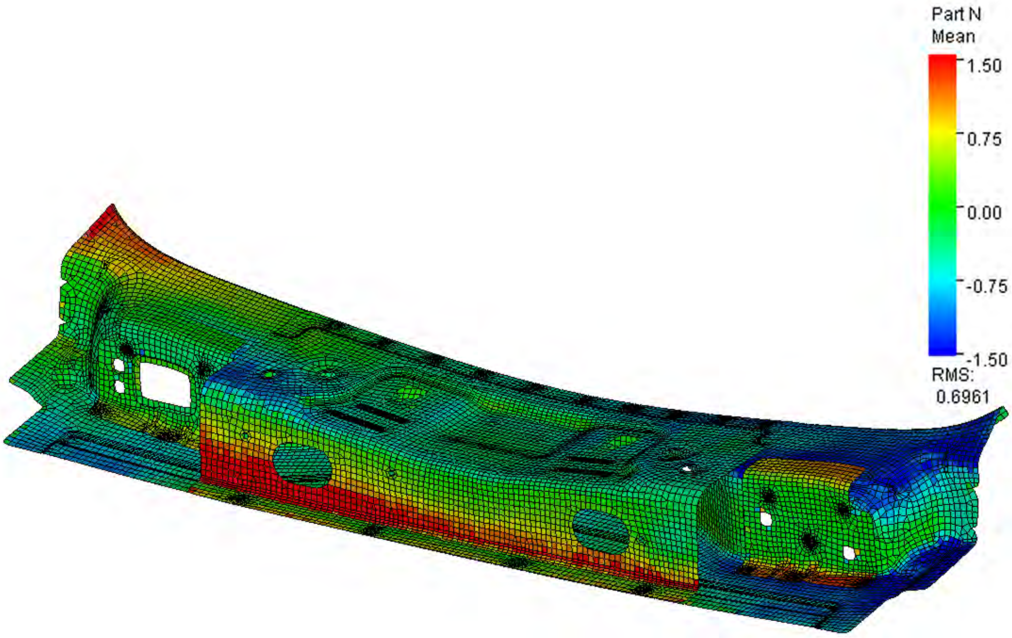


**Figure 4.43:** Deviation plot of the verification model with shimming optimizations applied to the shimming points.

A visual analysis of the physical assembly revealed a geometric offset at the flange connection between part 11600 and part 11700, illustrated in figure 4.46. When comparing to the non-rigid simulation output, illustrated in Figure 4.45 — the model replicated a deformation of the same magnitude and local geometry at a similar joint. However, the joint is located on the mirrored side of the assembly. Despite this mirrored scenario, the replication of the localized deformation indicates that the simulation is capable of replicating the shimming process.

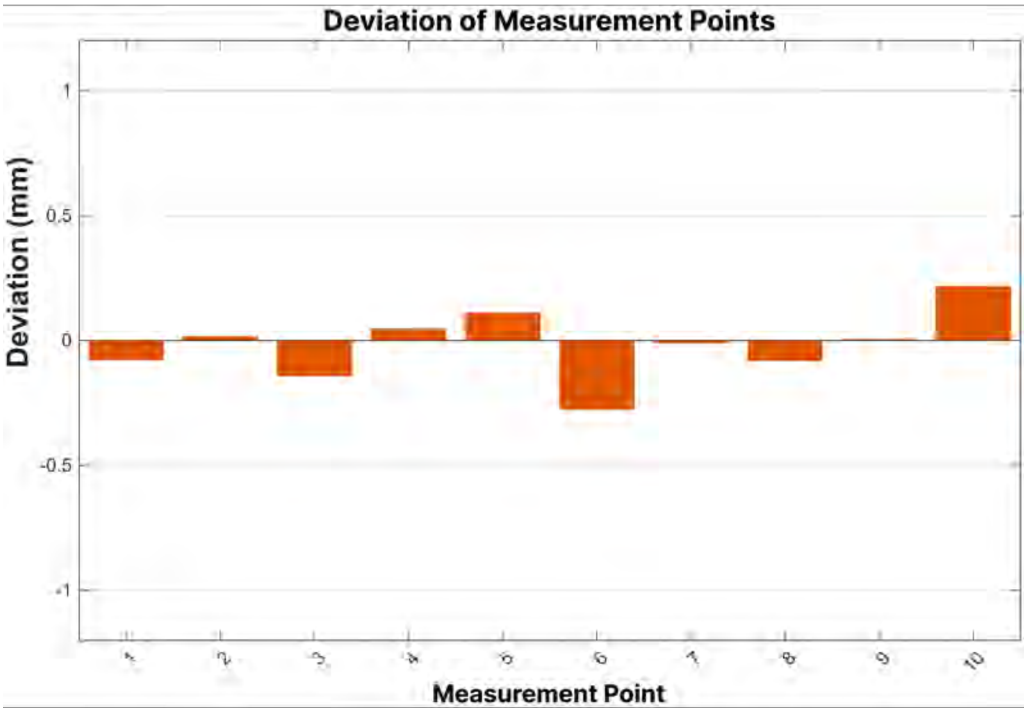


**Figure 4.44:** Deviation for every measurement point for the verification model with shimming optimizations.

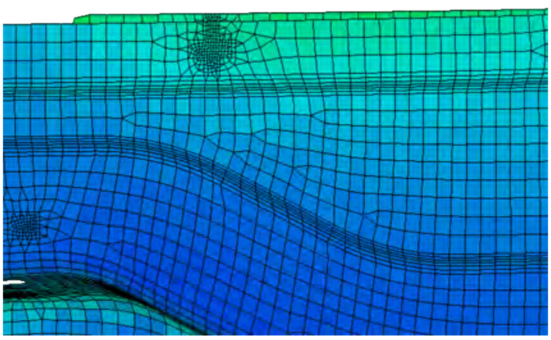

**Figure 4.45:** Closeup of the digital assembly showcasing a mismatch between the flanges at a joining location.

**Figure 4.46:** Closeup of the physical assembly showcasing a mismatch between the flanges at a joining location.

# 5
# Discussion

The purpose of this chapter is to interpret the results in relation to the four research questions and to evaluate the relevance, limitations, and industrial applicability of the proposed workflow. The discussion is based on the data mapping, simulation studies, sensitivity analyses, ML calibration results, and the case-based comparison with the physical assembly.

The results indicate that data continuity and traceability are central requirements for digital twin-based geometry assurance. The case study also showed similarities between the simulated and physical deformation patterns. However, differences in magnitude and location remained, and only one traceable physical case was available. The findings should therefore be interpreted as an initial evaluation of the proposed workflow rather than a complete validation.

## 5.1 What Tools and Data are Needed for a Sheet Metal Geometry Assurance Assembly Simulation?

The study showed that a non-rigid sheet metal assembly simulation requires more detailed input data than a rigid simulation. In addition to nominal geometry, tolerances, locating schemes, and measurement points, the compliant model also requires FE meshes, material properties, support points, joining information, contact definitions, and process sequence data.

However, the main limitation was not the absence of tools or information. Most of the required data existed within the industrial environment, but was distributed across PLM/PDM systems, internal standards, measurement databases, and process knowledge. Some information also differed from the physical process. For example, the stored welding sequence did not fully correspond to the sequence used at the assembly station, while shimming adjustments were not consistently recorded. This means that a simulation can be technically correct while still not representing the actual assembly conditions.

The results therefore indicate that data quality, consistency, and traceability are more important than simply increasing the amount of model input. The influence studies also showed that additional model detail does not always justify the increased computational effort. Heat and increased contact-point density had a limited influence in relation to their computational cost, while shimming and welding sequence had a considerably larger impact. The required level of detail should therefore be selected according to the purpose of the simulation and the sensitivity of the assembly.

The results further showed that including shimming information improved the agreement between the simulated outcome and the scanned assembly. Similar local deformation behavior was also observed around the flange regions. Although differences in magnitude and location remained, the result emphasizes the importance of representing actual process adjustments consistently in the simulation input.

Furthermore, the synthesized data model showed that a larger number of input samples does not necessarily result in a more representative simulation. Although 1000 shapes were generated, the data were based on a limited physical foundation and did not produce the variation observed in the measured data. This shows that having representative and varied data is more important than having a large number of samples.

The semi-automated model building process also reduced manual work, but it did not remove the need for engineering judgement. Locating schemes, weld definitions, tolerances, and measurement points still required manual verification or completion. Automation should therefore support, rather than replace, technical model verification.

The necessary tools include CAD and meshing software, CAT software, PLM/PDM systems, measurement and scanning equipment, and scripting tools for data processing and automation. These tools are already largely available. The more significant challenge is connecting them through structured and machine-readable data. Simulation inputs and outputs should therefore be stored in reusable formats rather than only as plots, PDF files, or presentation documents.

Overall, the findings show that the technical tools required for non-rigid geometry assurance simulations are available, but their effective use depends on reliable and traceable data. A digital twin-based workflow therefore requires greater consistency between stored product data, actual process parameters, simulation inputs, and physical assembly outcomes.

## 5.2 How can Simulation, Measure, and Process Data be Integrated into Different Product Development Phases?

The results indicate that the same geometry assurance workflow can support several product development phases, but its purpose and reliability depend on the maturity of the available data. Early simulations are mainly suitable for comparing concepts, while later stages provide better conditions for representing the physical process through measurement, scan, and process data. The workflow should therefore be adapted to the available data rather than applied with the same level of detail throughout the process.

The main limitation was not the amount of generated data, but the lack of continuity between systems and activities. Shimming adjustments and changes to the welding sequence were not consistently stored or linked to the corresponding simulation model. Therefore, the digital representation could be based on nominal or outdated process conditions, even when the physical process had already been modified. This limits both the accuracy of the simulation and the ability to explain differences between simulated and measured outcomes.

The results also showed that storing information is not sufficient if the format prevents reuse. Simulation outputs stored as plots, PDF files, or presentation material support communication, but cannot be directly used in later simulations or ML calibration. Both input and output data therefore need to be structured, machine-readable, and connected to the relevant product and physical assembly case.

The proposed workflow addresses these limitations by treating measurement results and process adjustments as feedback to the digital representation. However, a closed-loop workflow requires clear traceability between product data, simulation inputs, process settings, and physical outcomes. Without this connection, the workflow remains one-directional and cannot support a complete digital twin-based geometry assurance process.

Integration also requires case specific traceability. Scanned single part data, process parameters, simulation inputs, and the resulting assembly measurements must be connected through a common case ID. Otherwise, the information may be stored but cannot be reliably attributed to a specific physical outcome or reused for case-based model development.

The proposed workflow illustrates how this connection could be structured, but it was evaluated using only one traceable physical case and was not implemented throughout the complete product development process. Its applicability across the different phases should therefore be interpreted as a proposed framework rather than a fully demonstrated industrial workflow.

Overall, integration across product development phases is possible if the simulation purpose is adapted to data maturity and if process changes and results are stored in reusable formats. The central requirement is therefore not an additional simulation tool, but a consistent and traceable data structure that enables information to be updated and reused throughout the development process.

## 5.3 What Verification and Evaluation Processes are Required to Ensure that the Simulation Outcome is Relevant and Sufficient?

The results show that verification and evaluation must address different aspects of the simulation. Verification concerns whether the model is correctly implemented and reacts reasonably to changes in its assumptions and input parameters. Evaluation concerns whether the simulation and the proposed workflow are sufficiently useful for the intended geometry assurance purpose. A comparison with physical data may support validation, but the single traceable case used in this study is not sufficient for full statistical validation.

The influence analyses showed that model detail should be selected according to its relevance. Gravity, heat, and contact definitions affected the outcome, but their influence was limited compared with shimming and welding sequence. At the same time, some of these analyses significantly increased the computational effort. This indicates that verification should not only confirm that an effect can be modeled, but also determine whether its influence is large enough to justify its inclusion.

The high shimming sensitivity of 80.07% and the weld-sequence sensitivity of 31.58% for the scan-based model demonstrate that process parameters can strongly affect the geometrical outcome. These results do not prove that the simulation is correct, but they identify which parameters must be accurately represented and traced. If the physical process uses different shimming values or welding sequences than those stored in the digital model, a meaningful comparison between simulation and reality becomes difficult.

The comparison with the physical assembly showed similarities in deformation pattern, but differences remained in magnitude and location. This suggests that the simulation captured parts of the physical behavior, while incomplete process data and modeling simplifications still limited the agreement. The result should therefore be interpreted as an initial case-based evaluation rather than a complete validation.

Overall, a sufficient assessment requires a combination of technical model verification, influence and sensitivity analysis, and comparison with traceable physical data. The level of required agreement should also depend on the intended application, since concept comparison, process optimization, and case-specific prediction place different demands on simulation accuracy.

## 5.4 How can the Simulation Results be Improved with the help of ML Approaches?

The results indicate that ML can improve simulation outcomes by acting as a calibration layer between simulated and measured data. The purpose is therefore not to replace the physics-based simulation, but to compensate for systematic differences between the digital and physical outcomes.

The quantile-based model was most suitable for the available data because it did not require one-to-one traceability between simulated and measured cases. It achieved a mean distribution-level improvement of 90.22%, compared with 42.94% for the PCA-based model. The PCA model captured the main global variation patterns, but its reconstruction produced less consistent results at individual measurement points. This suggests that representing the assembly as a reduced global state may remove local behavior that remains important for geometry assurance. This may partly be explained by the model being based only on a limited number of measurement points rather than full geometric data. Therefore, the PCA representation may capture the dominant global relationships between the selected points while overlooking localized deformation patterns in the surrounding geometry.

When applied to the scanned case, the selected quantile-based model reduced the overall RMSE by 29.66%. However, two of the ten measurement points were shifted further away from the physical values. The difference between the strong distribution-level performance and the lower case-specific improvement shows that calibration of unpaired distributions does not ensure accurate prediction of an individual assembly.

The main limitation is therefore the structure of the available data. The model was trained on unpaired simulation and measurement distributions and could not learn how specific incoming parts and process conditions resulted in a particular assembly outcome. In addition, the model can correct predicted values but cannot identify whether an error originates from part variation, shimming, fixture conditions, or welding sequence.

Another limitation was the amount and coverage of the available training data. The models were developed using 100 simulated values and 70 measured values for each measurement point. Although these data were sufficient to construct the distribution-based models, they may not represent the full range of variation occurring in the physical process.

This limitation became apparent when the quantile-based model was applied to the scanned case. Two measurement points were predicted further away from the physical target, and the model showed lower accuracy for deviations located far from the nominal values. This suggests that these regions were insufficiently represented in the training distributions or that the scanned case differed from the relationships learned from the available data. Additional data covering a wider range of physical variation would therefore be required to assess whether the model can generalize more reliably to previously unseen assembly cases.

Another limitation is that the trained model is geometry specific. Since the model was developed using data from one assembly, it learned relationships associated with that geometry, locating scheme, joining process, and set of measurement points. Therefore, it cannot be assumed to provide reliable predictions for a different assembly without additional training data and model retraining. The model may have greater potential for use in derivative projects where the geometry and assembly process remain similar. In such cases, legacy data from the previous product could potentially be used as an initial training basis and supplemented with data from the new derivative. However, this transferability was not evaluated in the present study and would need to be investigated before the model could be reused.

Overall, ML can improve the agreement between simulation and measurement data, but the current model should be considered a calibration layer rather than a complete digital twin model. Case-specific prediction would require traceable data connecting single-part geometry, process parameters, and the resulting physical assembly outcome.

# 6

# Conclusion and Future Work

The aim of this thesis was to develop and evaluate a method for digital twin-based geometry assurance of non-rigid sheet metal assemblies. The resulting workflow connects data collection, compliant variation simulation, model verification, ML-based calibration, process optimization, and feedback of simulation and measurement data. The workflow was developed and evaluated through an industrial case study of a rear roof frame assembly.

Regarding the first research question, the study showed that a non-rigid geometry assurance simulation requires more detailed information than a rigid simulation. In addition to nominal geometry, tolerances, locating schemes, and measurement points, the compliant model requires FE meshes, material properties, support points, joining definitions, contact conditions, and process-sequence data. The required tools and much of the necessary information were available, but the data were distributed across several systems, documents, and sources of process knowledge. The main limitation was therefore not the absence of data, but insufficient consistency, traceability, and physical representativeness. The synthesized data study further showed that increasing the number of samples does not necessarily produce a more representative model. Semi-automated model generation can reduce manual work, but it does not replace engineering verification.

Regarding the second research question, the proposed workflow can support several product development phases, although its purpose and expected accuracy depend on the maturity of the available data. Early phases primarily support concept comparison using nominal and legacy data, whereas later phases can include scan, measurement, and process data. A digital twin-based workflow requires process adjustments, simulation inputs, and physical outcomes to be stored in structured and reusable formats and connected to the corresponding physical case. The proposed workflow illustrates how such integration could be structured, but it was evaluated using only one traceable case and was not implemented throughout the complete industrial development process.

Regarding the third research question, the relevance of a simulation outcome cannot be assessed through one activity or metric alone. Technical model verification should be combined with influence and sensitivity analyses and comparison with traceable physical data. The investigated assembly showed a shimming sensitivity of 80.07% and a weld-sequence sensitivity of 31.58% for the scanned model, demonstrating that these process parameters should be represented consistently in the digital model. Gravity, heat, and contact definitions also influenced the results, but their relevance must be considered in relation to computational cost and the intended simulation purpose. The physical comparison showed similarities in deformation behaviour, while differences remained in magnitude and location. The result should therefore be interpreted as an initial evaluation rather than a full statistical validation.

Regarding the fourth research question, the results showed that ML can improve simulation outcomes by acting as a calibration layer between simulated and measured data. The quantile-based regression model was selected because it was compatible with the available unpaired datasets and achieved a mean distribution improvement of 90.22%, compared with 42.94% for the PCA-based model. When applied to the scanned case, the selected model reduced the overall RMSE by 29.66%. However, two measurement points were predicted further away from the physical values, showing that strong distribution calibration does not ensure accurate prediction of an individual assembly. The model is also specific to the investigated geometry and cannot be assumed to generalize directly to other assemblies without additional data and retraining.

Overall, the study indicates that a digital twin-based geometry assurance workflow for non-rigid sheet metal assemblies is feasible as a methodological framework. Its successful industrial implementation is, however, dependent on structured and traceable data, recorded process parameters, representative physical cases, and continuous feedback between the physical and digital processes. The proposed method therefore provides a foundation for further development rather than a fully implemented or statistically validated digital twin.

## 6.1 Future Work

The proposed workflow provides a foundation for digital twin-based geometry assurance, but further development is required before it can be implemented and evaluated as a complete industrial digital twin workflow.

The first priority is to collect additional traceable physical cases. Each case should include scanned geometry of the individual parts before assembly, identification of the parts used in the assembly, recorded process parameters, and measurement and scan data from the final assembly. Since the present study included only one traceable physical case, additional cases are required to evaluate repeatability, statistical validity, and the ability of the workflow to represent production variation.

Process parameters should also be stored in a structured and reusable form. The results showed that shimming and welding sequence had an influence on the geometrical outcome. Future implementations should therefore record shimming values and locations, locator adjustments, clamping conditions, welding sequence, and other relevant process changes. These parameters should be connected to the corresponding physical assembly case and fed back into the simulation model. This would reduce the identified data breaks and improve the correspondence between the physical process and its digital representation.

The ML implementation should be further developed from distribution-based calibration toward case-based prediction. The current quantile-based model was suitable for the available non-paired datasets, but it could not determine the outcome of a specific assembly based on its individual incoming parts and process settings. With additional traceable data, a supervised case-based model could instead use single-part geometry and process parameters as inputs and predict the final assembly outcome. Such a model could also be investigated as a decision support tool for suggesting adjustments to controllable parameters, such as shimming or welding sequence.

Further work should also evaluate the proposed workflow on additional sheet metal assemblies. The current case study was limited to one rear roof frame assembly, and its results cannot be assumed to represent assemblies with different geometries, stiffnesses, locating schemes, or joining processes. Applying the workflow to several assemblies would make it possible to assess its generalizability and identify which parts of the method can be standardized and which require case-specific adaptation.

# Bibliography


[1] Mercedes-Benz AG. *MB E-Class Estate 2024*. 2024.

[2] R. Söderberg, L. Lindkvist, and J. Carlsson. "Virtual Geometry Assurance for Effective Product Realization". In: *NordPLM*. 2006.

[3] J. Camelio et al. "Impact of Fixture Design on Sheet Metal Assembly Variation". In: *Journal of Manufacturing Systems* 23.3 (2004).

[4] R. Sadeghi Tabar et al. "Digital Twin-Based Clamping Sequence Analysis and Optimization for Improved Geometric Quality". In: *Applied Sciences* 14.2 (2024).

[5] R. Sadeghi Tabar et al. "Augmented Geometry Assurance Digital Twin with Physics-Based Incremental Learning". In: *CIRP annals - Manufacturing Technology* 74.1 (2025).

[6] R. Sadeghi Tabar et al. "Critical joint identification for efficient sequencing". In: *Journal of intelligent Manufacturing* 32(3) (2021), pp. 769–780.

[7] R. Sadeghi Tabar et al. "Enhancing Welding Geometric Precision: Analyzing the Impact of Weld Path Directions, Sequences and Locating Schemes on Displacement". In: *Applied Sciences* 14.23 (2024).

[8] R. Söderberg et al. "Virtual geometry assurance process and toolbox". In: *Procedia Cirp* (2016), pp. 3–12.

[9] R. Söderberg et al. "Toward a Digital Twin for real-time geometry assurance in individualized production". In: *CIRP annals* 66(1) (2017), pp. 137–140.

[10] M. David and F. Rowe. "What does PLMS (product lifecycle management systems) manage: Data or documents? Complementarity and contingency for SMEs". In: *Computers in Industry* 75 (2016), pp. 140–150. DOI: 10.1016/j.compind.2015.05.005.

[11] K. Ulrich, S. Eppinger, and M. Yang. *Product design and development*. McGraw-Hill Education, 2020.

[12] H. Zheng. "Combine Dimensional Management and Manufacturing Process Simulation for Automotive Parts". PhD thesis. Universität der Bundeswehr München, 2022.

[13] F. Litwa. "Entwicklung eines integrierten Ansatzes zur Optimierung von dünnwandigen Blechbauteilen im Karosserierohbau mithilfe von Toleranzsimulationen". PhD thesis. Universität des Saarlandes, 2018.

[14] A. Saaksvuori and A. Immonen. *Product Lifecycle Management*. Springer, 2008.

[15] M. Roth et al. "Linking Model-Based Definition and Non-Intrusive Finite Element Analysis for Automated Variation Simulation". In: *Computer Aided Design* 191 (2026).

[16] M. Roth et al. “Closing gaps in the digital thread with the Quality Information Framework (QIF) standard for a seamless geometry assurance process”. In: *Computer-Aided Design* 182 (2025), p. 103860. DOI: 10.1016/j.cad.2025.103860.

[17] B. Schleich et al. “Geometrical Variations Management 4.0: towards next Generation Geometry Assurance”. In: *The 15th CIRP Conference on Computer Aided Tolerancing* (2018).

[18] M. Hallmann, S. Goetz, and B. Schleich. “Mapping of GD&T information and PMI between 3D product models in the STEP and STL format”. In: *Computer-Aided Design* 115 (2019), pp. 293–306. DOI: 10.1016/j.cad.2019.06.006.

[19] M. Bohn and K. Hetsch. *Toleranzmanagement im Automobilbau*. Hanser Verlag GmbH & Co. KG, 2013.

[20] R. Sadeghi Tabar. “JOINING SEQUENCE OPTIMIZATION IN COMPLIANT VARIATION SIMULATION”. Licentiate thesis. Chalmers University of Technology, 2019.

[21] P. Kurowski. *Finite Element Analysis for Design Engineers*. eISBN: 978-0-7680-5310-4. Warrendale, PA: SAE International, 2004. ISBN: 0-7680-1140-X.

[22] DIN Deutsches Institut für Normung e. V. *DIN EN ISO 5459:2025-12 Geometrical product specifications (GPS) – Geometrical tolerancing – Datums and datum systems (ISO 5459:2024)*. DIN EN ISO 5459:2025-12. Standard. English translation of DIN EN ISO 5459:2025-12. DIN Deutsches Institut für Normung e. V. Dec. 2025.

[23] E. Morse et al. “Tolerancing: Managing uncertainty from conceptual design to final product”. In: *CIRP Annals - Manufacturing Technology* 67 (2018).

[24] ISO 1101:2017. *Geometrical product specifications (GPS) - Geometrical tolerancing - Tolerances of form, orientation, location and run-out*. European Committee for Standardization. 2017.

[25] W. Sun and Y. Gao. “The Rule-based Specification of the Datum-based Model for Geometric Dimensioning & Tolerancing”. In: *Procedia CIRP* 114 (2022), pp. 189–196. DOI: 10.1016/j.procir.2022.10.026.

[26] J. Kassim, R. Ramli, and A. Hadi Azman. “A Review on Geometrical Tolerance Applications in The Automotive Industry”. In: *Jurnal Kejuruteraan* (2018), pp. 41–48. DOI: 10.17576/jkukm-2018-si1(6)-06.

[27] R. Sadeghi Tabar et al. “Contact Search Using a Kd-Tree for Non-Rigid Variation Simulation”. In: *Proceedings of the ASME 2022 International Mechanical Engineering Congress and Exposition (IMECE2022)*. Columbus, Ohio, USA, 2022, V02BT02A069. DOI: 10.1115/IMECE2022-94989.

[28] R. S. Tabar. “Joining Sequence Analysis and Optimization for Improved Geometrical Quality.” PhD thesis. Chalmers University of Technology, 2021.

[29] Robust Design Tolerancing. *Robustness evaluation and tolerance analysis: Software Manual*. Software Manual. Version 1.23. Mar. 8, 2022.

[30] M. Rosenqvist et al. “Variation Analysis considering manual assembly complexity in a CAT tool”. In: *Procedia CIRP* 43 (2016), pp. 94–99. DOI: 10.1016/j.procir.2016.02.020.

[31] J. S. Carlson and R. Söderberg. “Assembly Root Cause Analysis: A Way to Reduce Dimensional Variation in Assembled Products”. In: *The International Journal of Flexible Manufacturing Systems* 15 (2003).

[32] E. VanDerHorn and S. Mahadevan. “Digital Twin: Generalization, characterization and implementation”. In: *Decision Support Systems* 145.113524 (2021).

[33] Trevor Hastie, Robert Tibshirani, and Jerome Friedman. *The Elements of Statistical Learning: Data Mining, Inference, and Prediction*. 2nd ed. Springer, 2009. DOI: 10.1007/978-0-387-84858-7.

[34] Alex J. Cannon, Stephen R. Sobie, and Trevor Q. Murdock. “Bias Correction of GCM Precipitation by Quantile Mapping: How Well Do Methods Preserve Changes in Quantiles and Extremes?” In: *Journal of Climate* 28.17 (2015), pp. 6938–6959. DOI: 10.1175/JCLI-D-14-00754.1.

[35] Hervé Abdi and Lynne J. Williams. “Principal Component Analysis”. In: *WIREs Computational Statistics* 2.4 (2010), pp. 433–459. DOI: 10.1002/wics.101.

[36] Meriam Library. *Evaluating Information: Applying the CRAAP Test*. Information sheet. Licensed under Creative Commons Attribution 4.0 International. California State University, Chico, Sept. 17, 2010.

# A

# Appendix: Data Collection

## A.1 Data Formats

**Table A.1:** Table displaying necessary input parameters for a non-rigid sheet metal assembly simulation, their corresponding formats, sources, and compatible formats to RD&T.

| Input Parameter | Source System | Native Format (from study) | Compatible Formats (RD&T) |
|---|---|---|---|
| Tolerances | PDM system | .pdf, .pptx, 3D PMI (Native CAD visual) | manual entry |
| Mesh | CAE pre-processor | .inp, .nas, .inpnas | .inp, .nas |
| Material data | | | |
| Sheet metal thickness | PDM system | .inp, .nas, .inpnas, .plmxml | .inp, .nas, .txt |
| Thermal properties | PDM system | .mat | .mat |
| Young's modulus | PDM system | .plmxml | manual entry |
| Poisson ratio | PDM system | .plmxml | manual entry |
| Density | PDM system | .plmxml | manual entry |
| Measure points | PDM system | .xml | manual entry |
| Locating scheme & support points | PDM system | .xml | .txt |
| Welding points | PDM system | .xml | .txt |
| Assembly sequence & clamping sequence | PLM system | .pdf, .ppx | manual entry |

# B

# Appendix: Decision Trees Proposed Method

## B.1 Verify Simulation Model Decision Tree

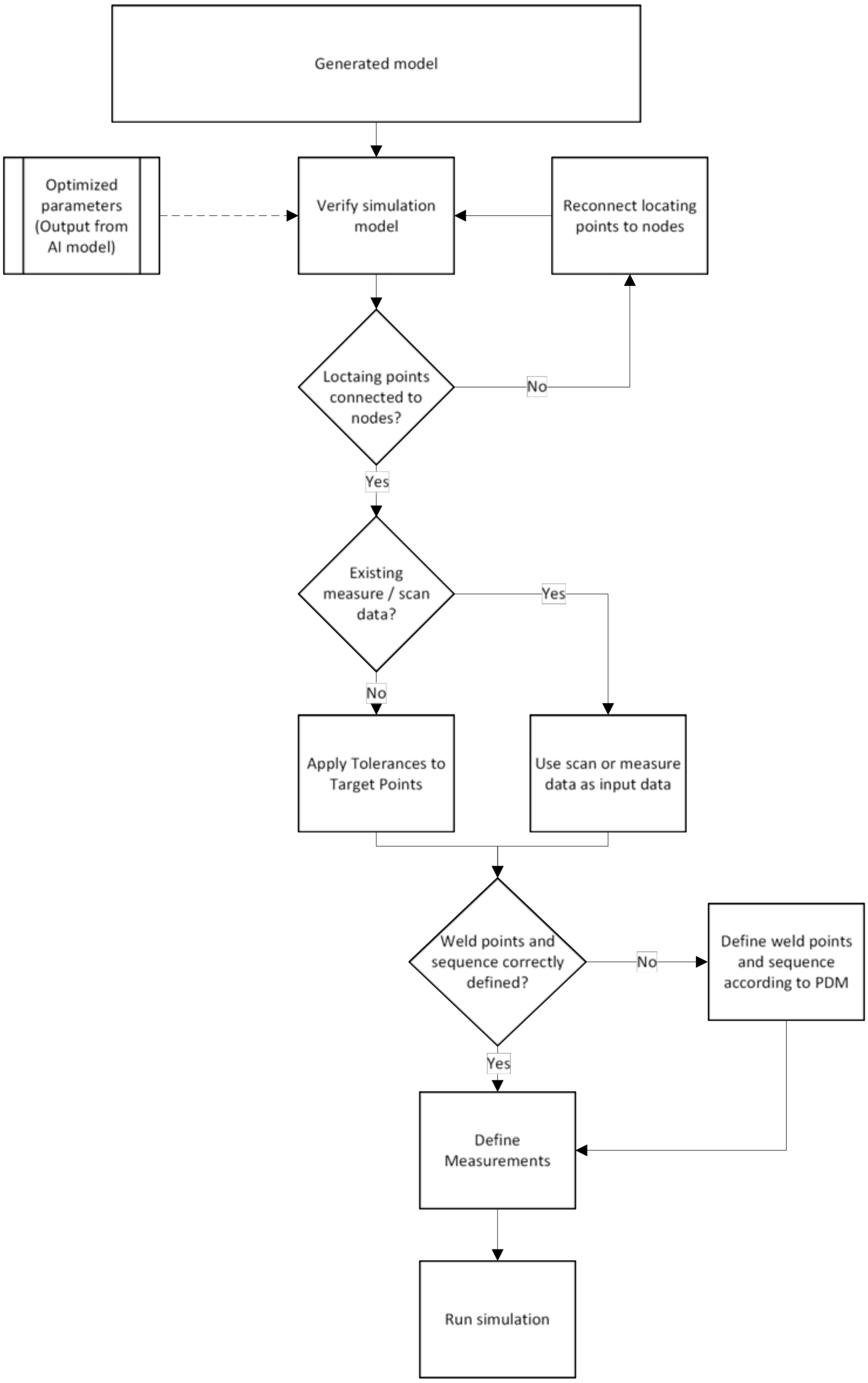


**Figure B.1:** Decision tree for verifying simulation model.

# C

# Appendix: Additional ML Model Plots

## C.1 Selected Quantile-Based Model Plots

This section presents selected representative plots for the quantile-based regression model. The examples include one well-performing measurement point, one typical measurement point, and one measurement point with larger prediction deviations.

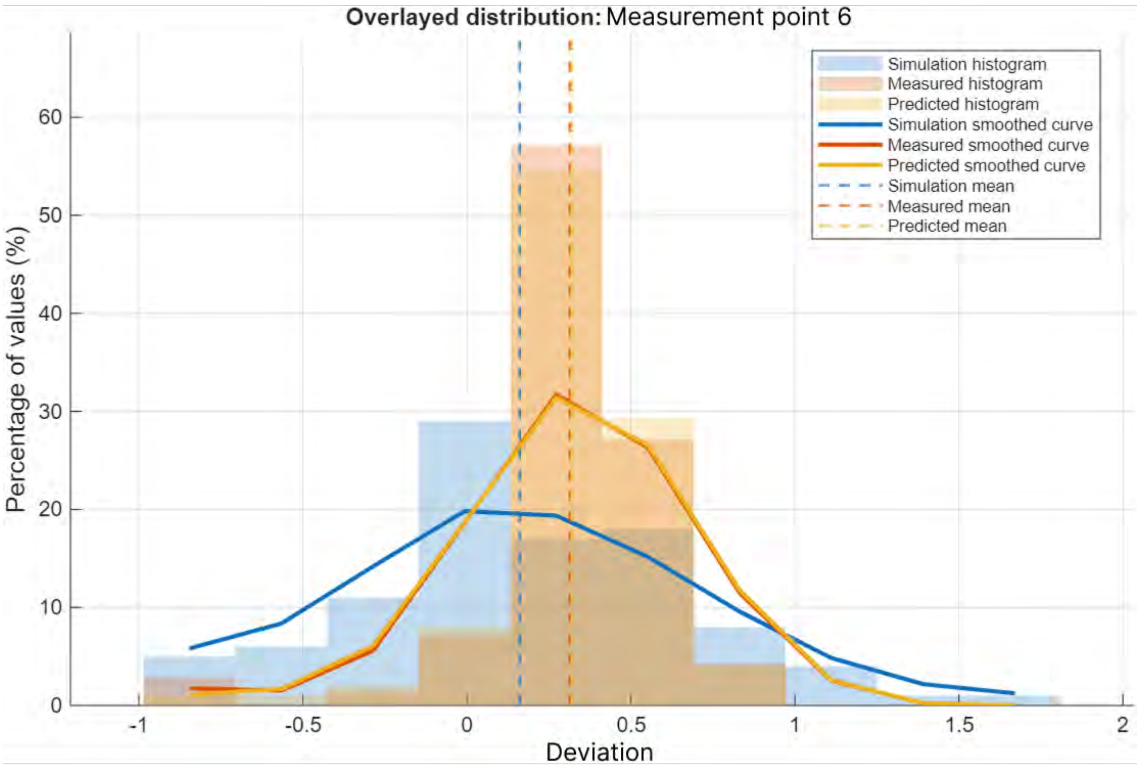


**Figure C.1:** Histogram of quantile-based model evaluation on measurement point 6

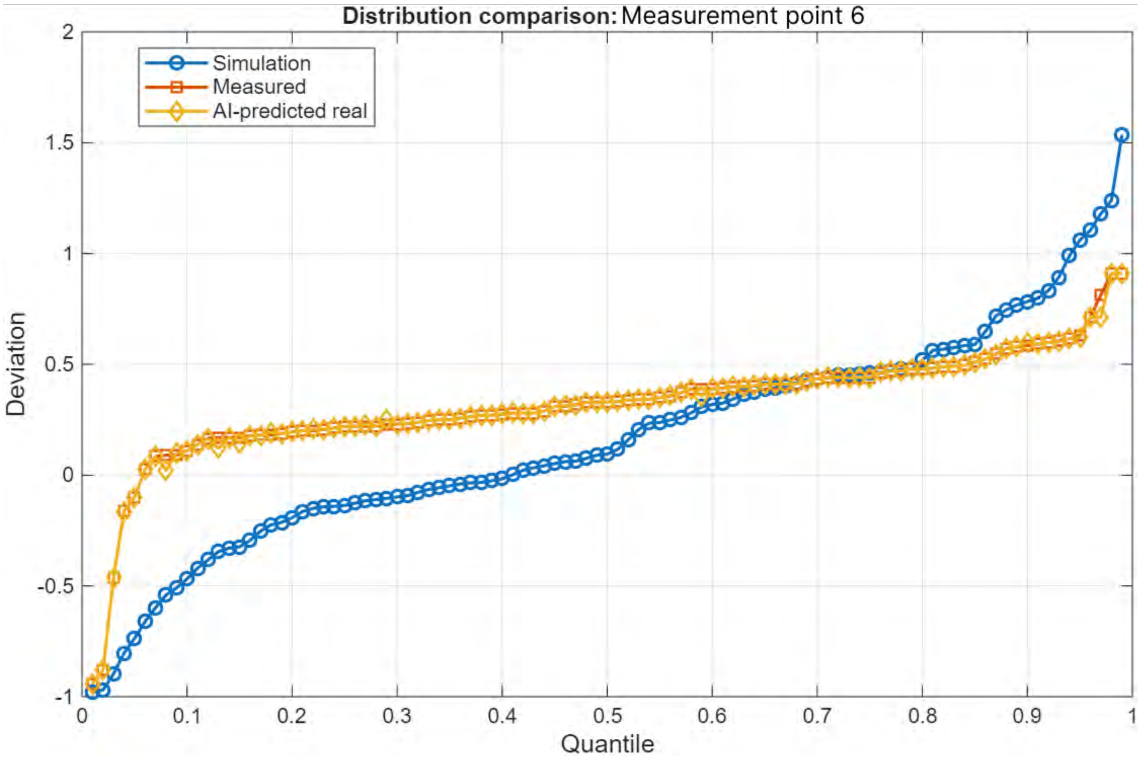


**Figure C.2:** Calibration plot of quantile-based model evaluation on measurement point 6

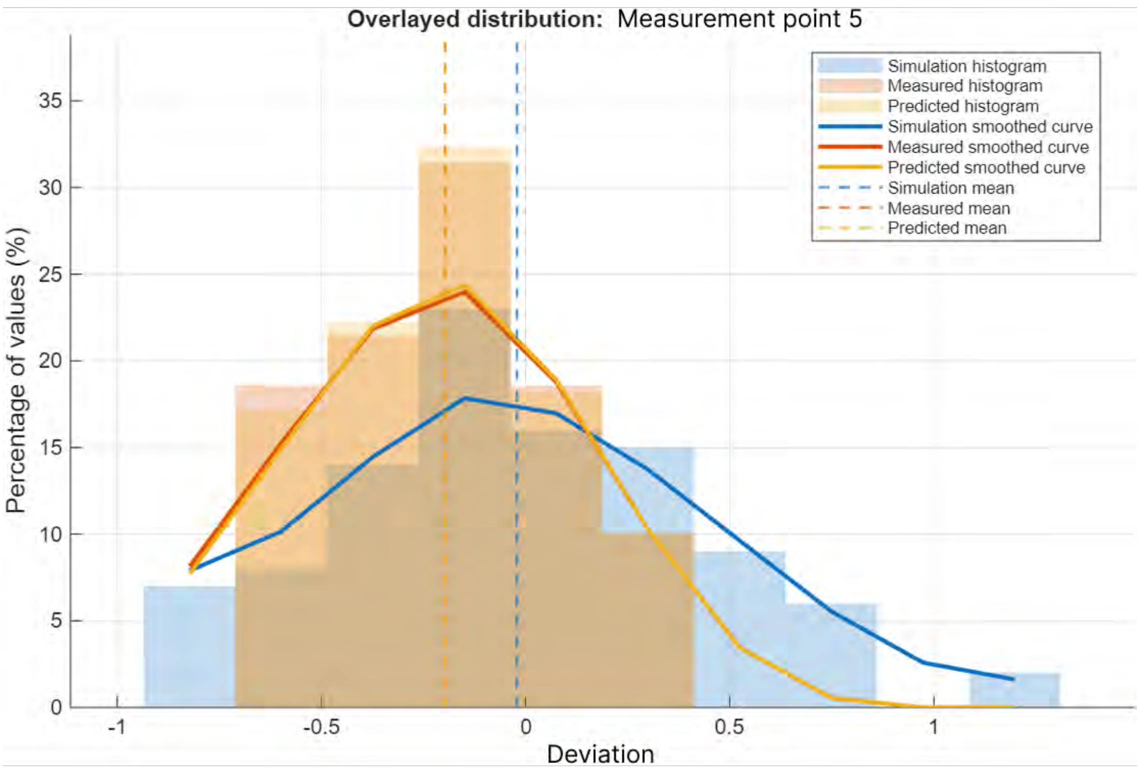


**Figure C.3:** Histogram of quantile-based model evaluation on measurement point 5

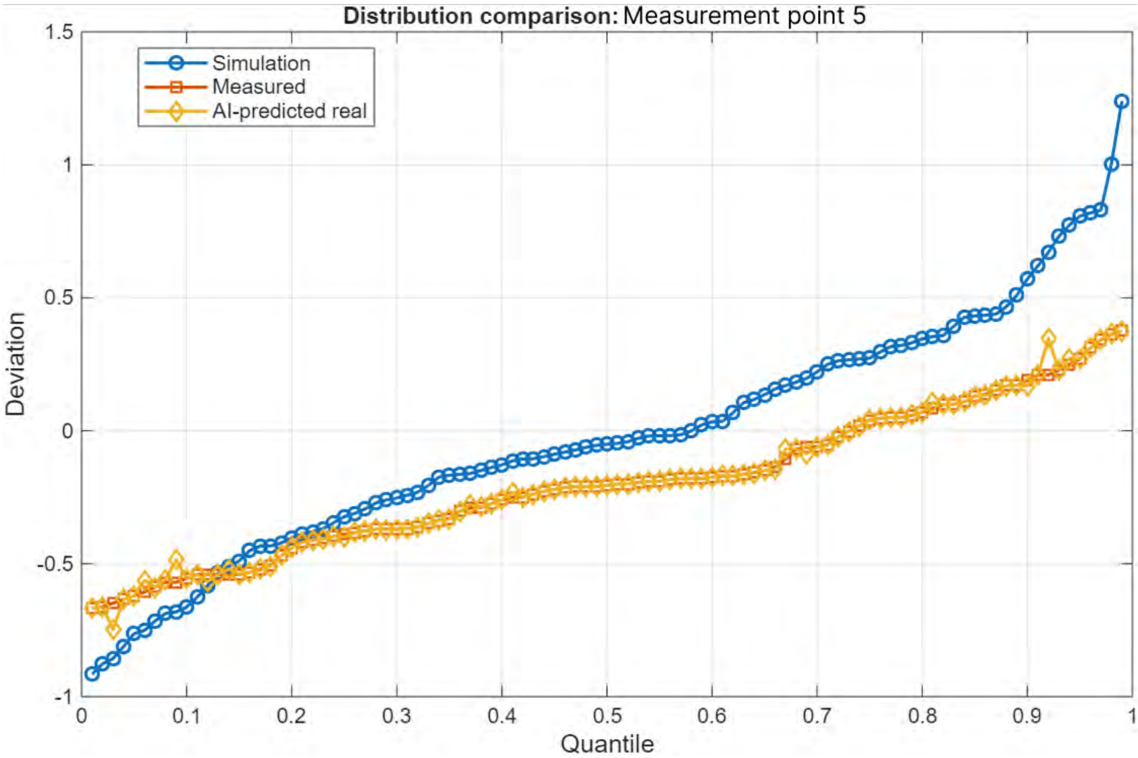


**Figure C.4:** Calibration plot of quantile-based model evaluation on measurement point 5

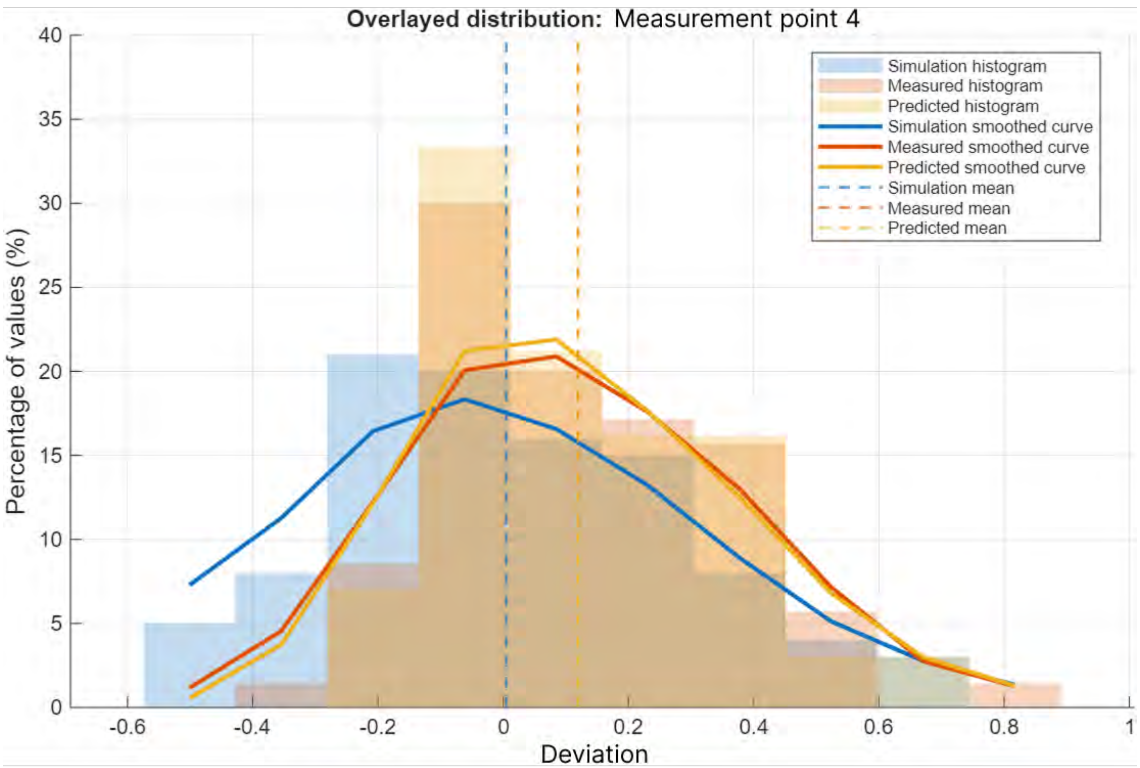


**Figure C.5:** Histogram of quantile-based model evaluation on measurement point 4

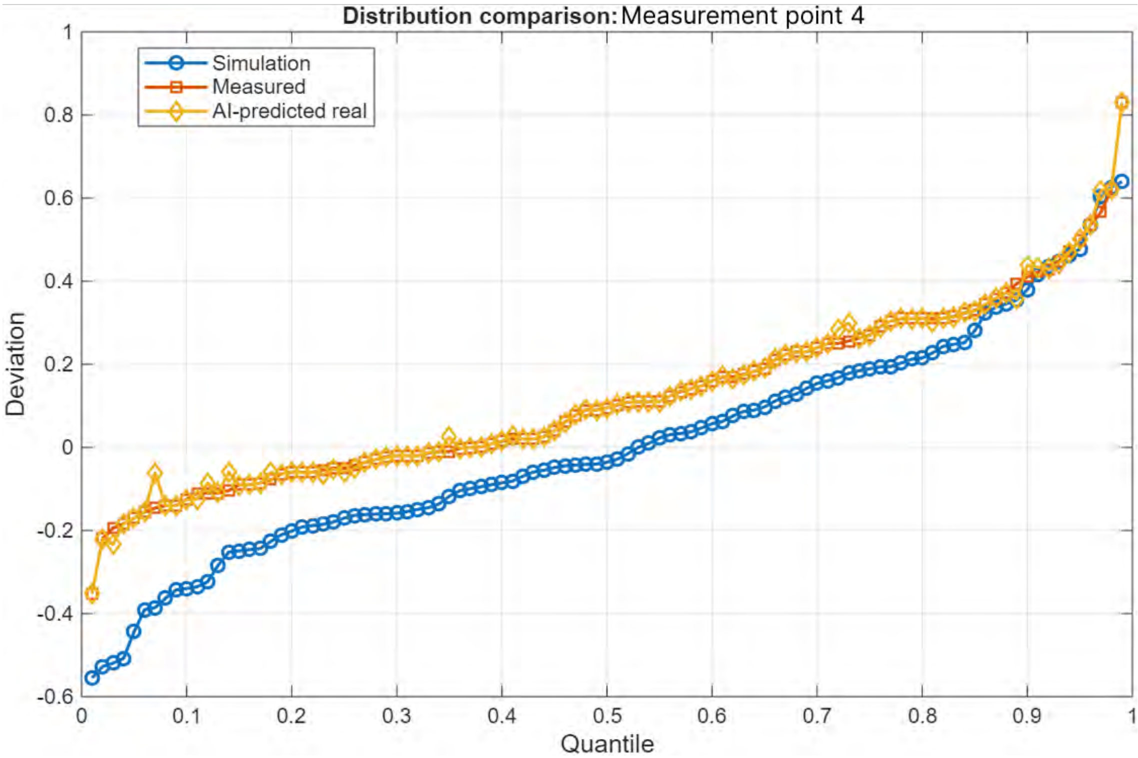


**Figure C.6:** Calibration plot of quantile-based model evaluation on measurement point 4

## C.2 Selected PCA-Based Model Plots

This section presents selected representative plots for the PCA-based state calibration model. The examples include one well-performing measurement point, one typical measurement point, and one measurement point where the prediction was less accurate.

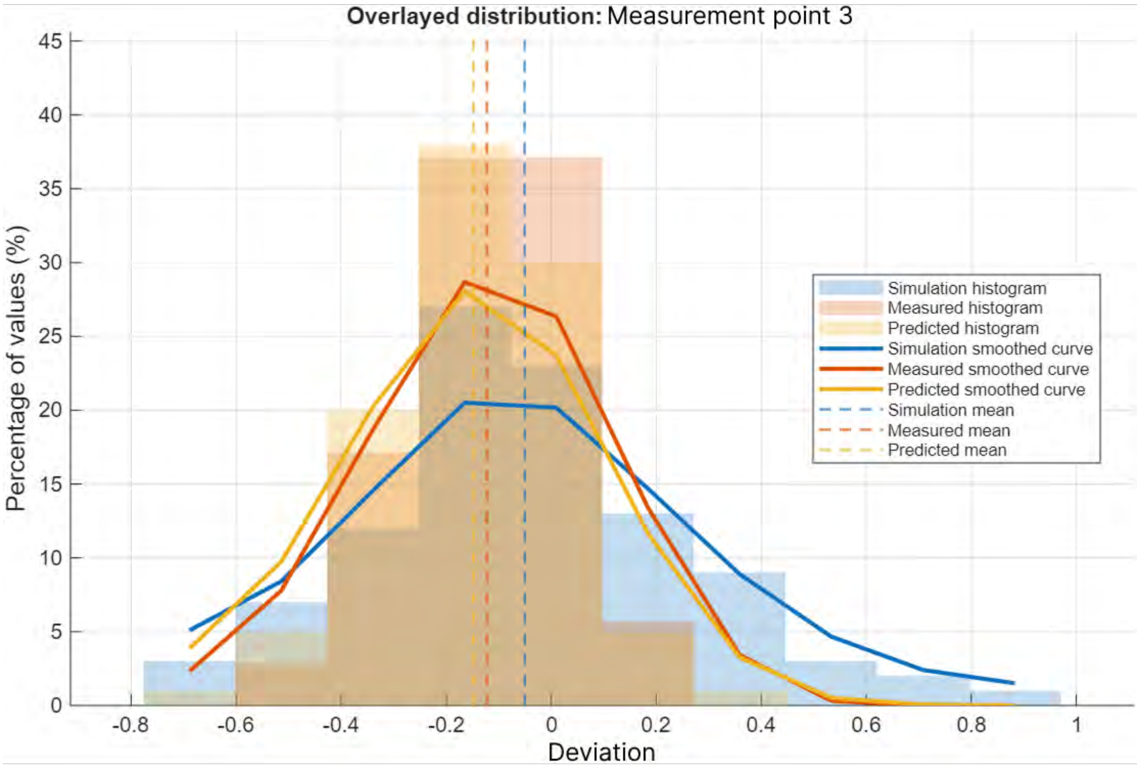


**Figure C.7:** Histogram of PCA-based model evaluation on measurement point 3

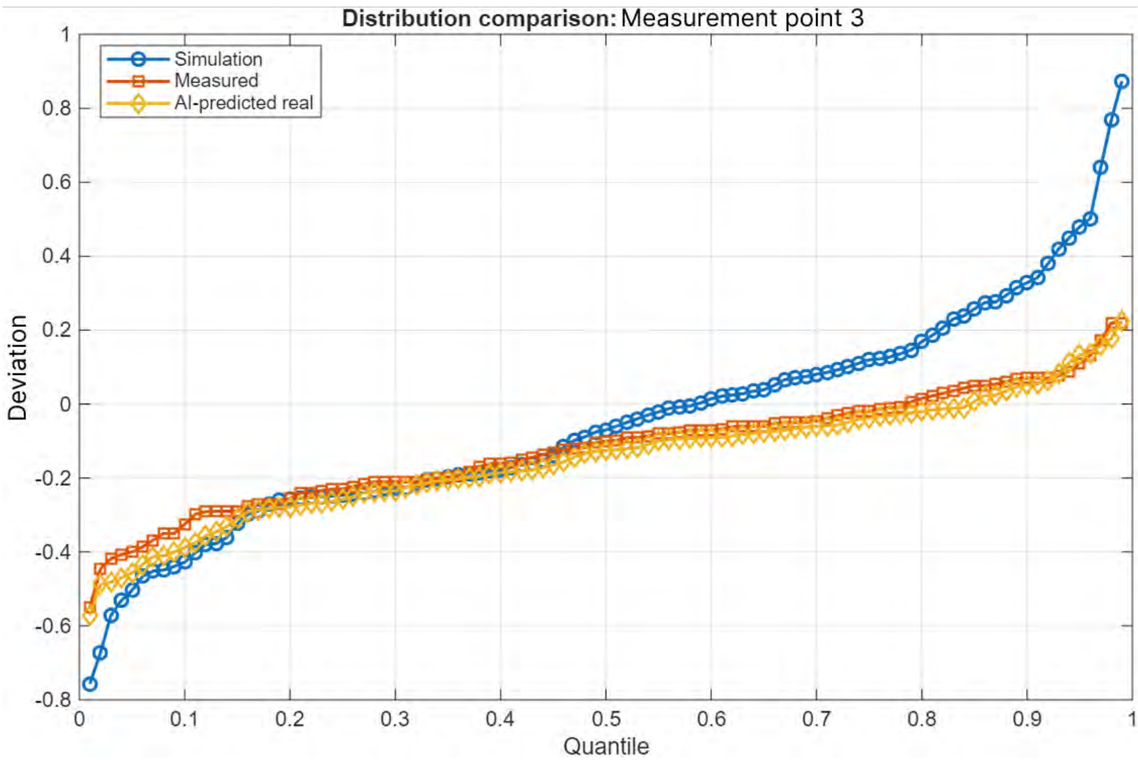


**Figure C.8:** Calibration plot of PCA-based model evaluation on measurement point 3

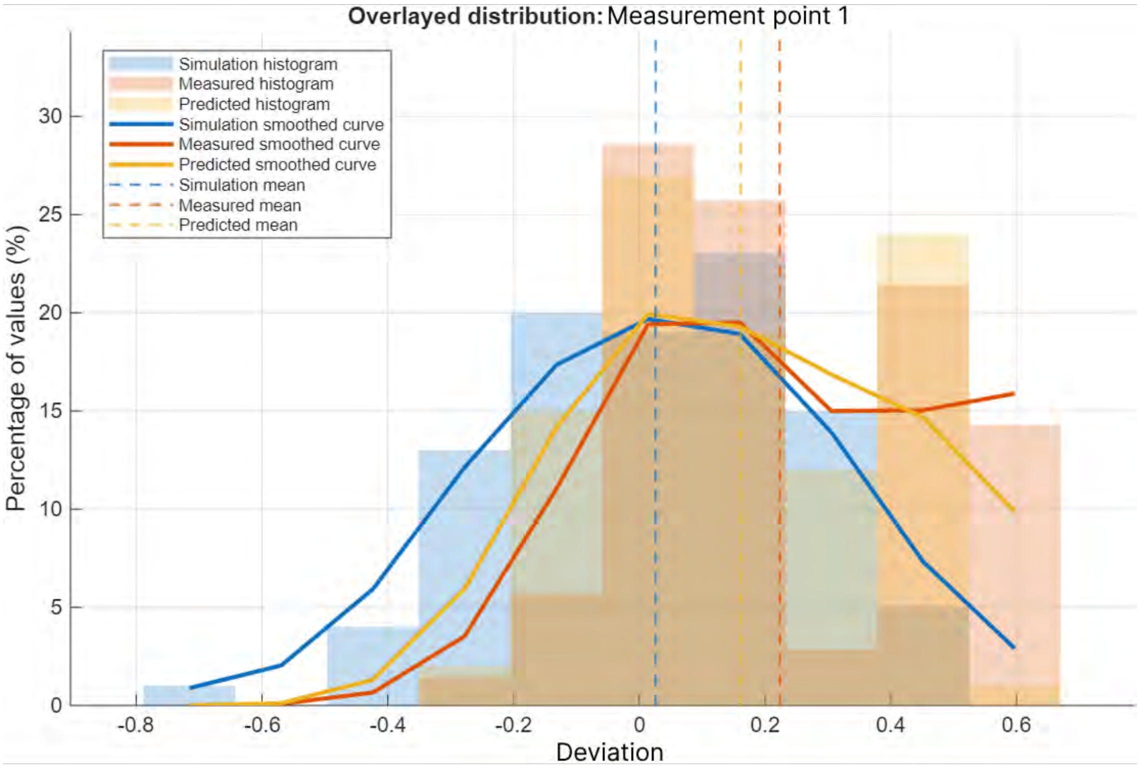


**Figure C.9:** Histogram of PCA-based model evaluation on measurement point 1

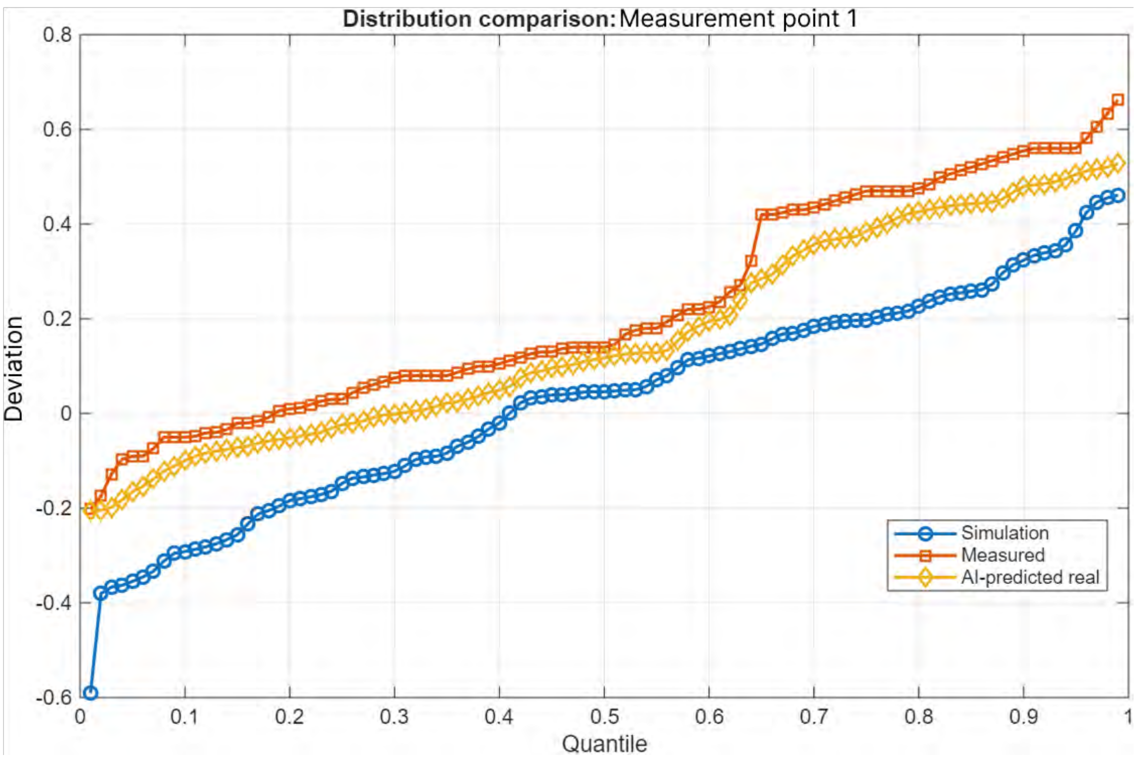


**Figure C.10:** Calibration plot of PCA-based model evaluation on measurement point 1

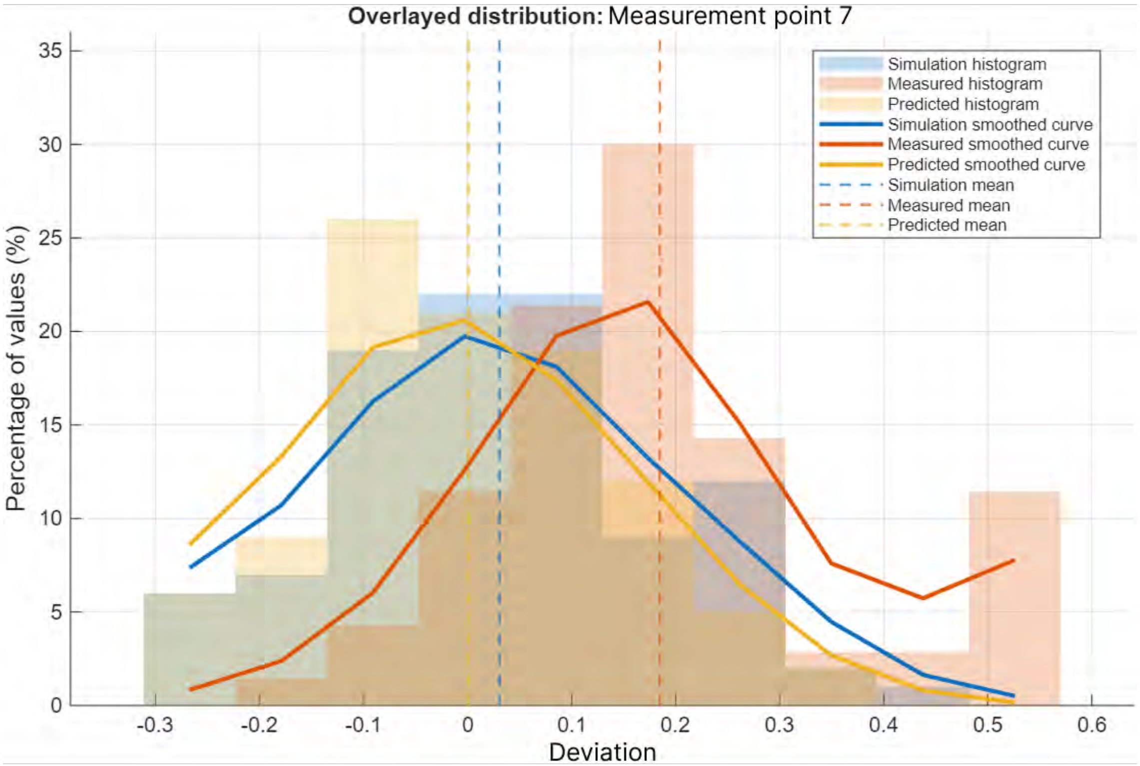


**Figure C.11:** Histogram of PCA-based model evaluation on measurement point 7

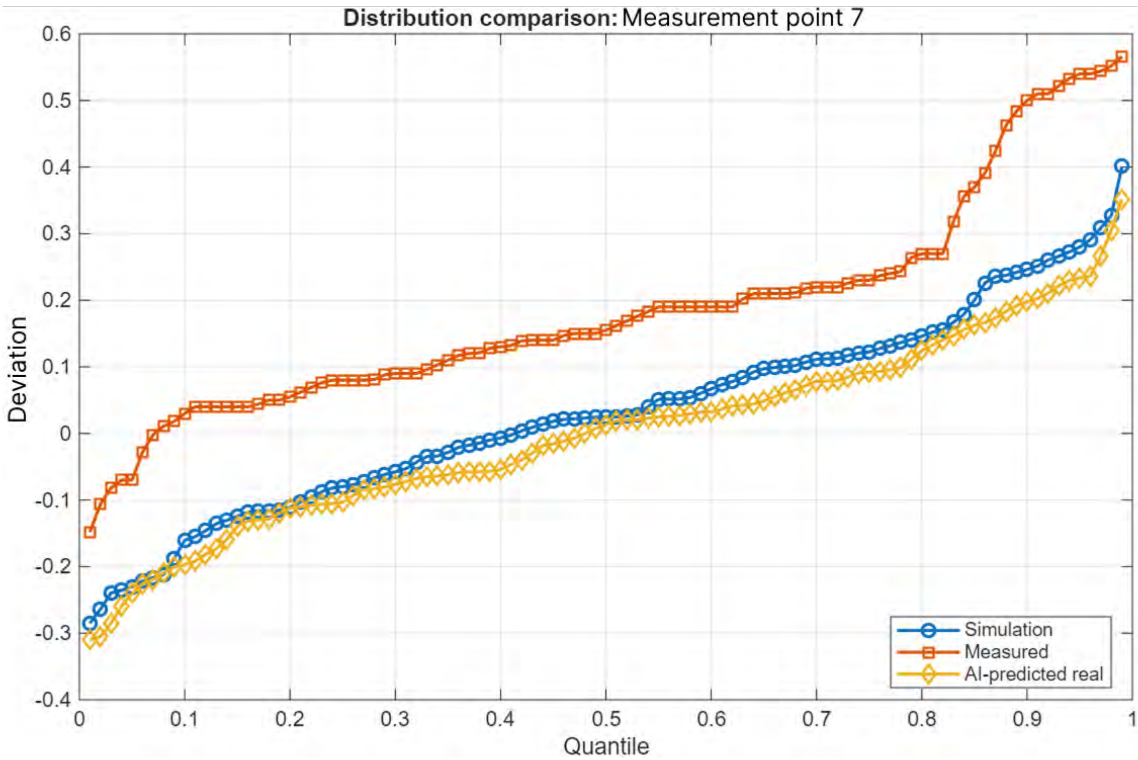


**Figure C.12:** Calibration plot of PCA-based model evaluation on measurement point 7

**DEPARTMENT OF INDUSTRIAL AND MATERIALS SCIENCE**
**CHALMERS UNIVERSITY OF TECHNOLOGY**
Gothenburg, Sweden
www.chalmers.se

CHALMERS
UNIVERSITY OF TECHNOLOGY